DISSERTATION / DOCTORAL THESIS

Titel der Dissertation /Title of the Doctoral Thesis

„Towards Quantum Experiments on Gravitating Objects"

verfasst von / submitted by

Mag. rer. nat. Philipp Köhler

angestrebter akademischer Grad / in partial fulfilment of the requirements for the degree of

Doktor der Naturwissenschaften (Dr. rer. nat.)

Wien, 2021 / Vienna 2021

To Mandy, her family and my family for being with me through this journey.

ACKNOWLEDGMENTS

What a journey! I turns out that writing an acknowledgment is as hard as it is easy. Hard, because of the voice in your head that you might forget to mention someone. Easy, because it takes you down memory lane, which is always rose tinted.

To begin, I will always be grateful for the time spent working on this PhD and it wouldn't have started without my supervisor Markus, who always had and has an infectious enthusiasm for science. I also can't go without mentioning all my colleagues who I worked with over the years. Especially my office buddies, Ralf, Hans, Mathias, Jeremias (thanks for the coffee!) and the old guard, Tom and Claus. There is a lot of unforgettable memories here. From my early times in the group I still remember long drives to one of our retreats with Jason either as driver or on navigation sharing great insights about physics or just life in general as well as just fun moments and lots of positive energy. These moments will always stay with me. Tom, who always made being in the office very entertaining with an infinite well of Monster energy drinks (I still don't know how that many could fit inside a drawer, maybe he took the bottom out...?). Claus, who I share a wonderful friendship with since the first moment we met and who kept me sane throughout most of this journey, thank you for your friendship and I hope there will be a lot more crazy adventures in the future (thanks for the best birthday ever)!

I also want to thank my experimentalist colleagues. Jonas, Ramon and Uros (Kaiserschmarrn!), who gave me a warm welcome into the group when I started out. Sebastian, a fellow theorist, helping with his Mathematica knowledge and fun discussions. Josh, our canadian postdoc, always there when needed. David, for his level headedness. Nikolai, for always being available for discussions and interesting little factoids.

And of course, I cannot forget all the people behind the scenes encouraging me, and being there for me when I needed it. My parents, thank you for making my life better every minute. My grandparents, always believing in me. My brother and his girlfriend, Daniel and Artemis, for a lot of fun dinners and evenings. My friend, Clemens, getting the gains together. And of course Peter, for the best of friendships, trips and sushi nights! On that note, it was for Peter that I met my girlfriend Mandy. My rock and my partner in crime, what a boring life it would be without you!

I am sure there is people I missed, so also a general thank you to everyone who was a part of my life in the last eight years and hopefully continues to be for the adventures to come.

ABSTRACT

This thesis presents an overview of experiments to test novel decoherence phenomena and their theoretical foundations. The decoherence phenomena studied here have different origins, be it due to general relativistic effects or modifications of quantum mechanics. Multiple avenues for such experiments have been explored in the literature. We first focus on phenomena related to general relativity. We will give an overview over the interactions of a quantum state and an external gravitational field with general relativistic properties. Decoherence can arise from proper time differences in the degrees of freedom of a quantum state. These proper time differences lead to a coupling of internal degrees of freedom within a quantum state. These couplings allow for the generation of which path information. Another source of decoherence analyzed in the literature is due to a gravitational wave background. This stochastic background interacts with every quantum state and leads to decoherence. We will then analyze modifications of quantum mechanics. Initially, these models originated from the desire to shed light unto the quantum to classical transition. It was discovered early on that such modifications have to be done with great care as to not run into contradictions with relativistic principles. Nevertheless, nonlinear Schrödinger equations were analyzed as a possible intermediate solution for the transition of a system with quantum properties to a system with classical ones. To circumvent some of the relativistic constraints, the Schrödinger equation can also be modified with a nonlinearity counterbalanced with a stochastic part. This stochastic property is necessary to prevent superluminal signaling within the theory. We analyze some of the theoretical efforts in this direction and review experimental constraints of the parameter space of such theories. We also describe a new set of experiments to test such stochastic models (collapse models) with photonic crystals and the advantages of using these systems to constrain the parameter space defined by the theory. Last, we will give a new experimental approach to test possible fifth-force contributions in measurements of gravity between small masses.

ZUSAMMENFASSUNG

Diese Arbeit gibt einen Überblick über Experimente zum Testen neuartiger Dekohärenzphänomene und ihrer theoretischen Grundlagen. Die hier untersuchten Dekohärenzphänomene haben unterschiedliche zu Grunde liegende Mechanismen, sei es durch relativistische Effekte oder Modifikationen der Quantenmechanik. In der Literatur wurden mehrere Ansätze für solche Experimente untersucht. Wir konzentrieren uns zunächst auf Phänomene im Zusammenhang mit der Allgemeinen Relativitätstheorie. Wir geben einen Überblick über die Wechselwirkungen eines Quantenzustands und eines externen Gravitationsfeldes mit relativistischen Eigenschaften. Dekohärenz kann aus Eigenzeitunterschieden in den Freiheitsgraden eines Quantenzustands entstehen. Diese Eigenzeitunterschiede führen zu einer Kopplung interner Freiheitsgrade innerhalb eines Quantenzustands. Diese Kopplungen ermöglichen die Generierung von „Welcher-Weg"-Information. Eine weitere in der Literatur analysierte Dekohärenzquelle ist auf einen Gravitationswellenhintergrund zurückzuführen. Dieser stochastische Hintergrund interagiert mit jedem Quantenzustand und führt zu Dekohärenz. Desweiteren werden wir Modifikationen der Quantenmechanik analysieren. Ursprünglich entstanden diese Modelle aus dem Wunsch, den Übergang von Quantensystemen zu klassischen Systemen zu beleuchten. Schon früh wurde erkannt, dass solche Modifikationen mit großer Sorgfalt vorgenommen werden müssen, um nicht in Widersprüche mit relativistischen Prinzipien zu geraten. Dennoch wurden nichtlineare Schrödinger-Gleichungen als mögliche Zwischenlösung für den Übergang eines Systems mit Quanteneigenschaften in ein System mit klassischen Eigenschaften analysiert. Um einige der relativistischen Einschränkungen zu umgehen, kann die Schrödinger-Gleichung auch mit einer Nichtlinearität modifiziert werden, die mit einem stochastischen Teil ausgeglichen wird. Diese stochastische Ergänzung ist notwendig, um überlichtschnelle Signale innerhalb der Theorie zu verhindern. Wir werden einige der theoretischen Ansätze in dieser Richtung analysieren und experimentelle Beschränkungen des Parameterraums solcher Theorien überprüfen. Wir beschreiben auch eine neue Reihe von Experimenten zum Testen solcher stochastischer Modelle (Kollapsmodelle) mit photonischen Kristallen und die Vorteile der Verwendung dieser Systeme, um den von der Theorie definierten Parameterraum einzuschränken. Zuletzt werden wir einen neuen experimentellen Ansatz vorstellen, um mögliche Beiträge einer weiteren (fünften) Kraft bei Messungen der Gravitationskraft zwischen kleinen Massen zu testen.

CONTENTS

INTRODUCTION

Quantum mechanics and its foundational concepts have been successfully applied to most aspects of modern physics. From the description of atoms and fields, quantum mechanics has revolutionized our understanding of particle physics and beyond. On the other hand, general relativity, describing gravitational fields and interactions, has furthered our understanding of cosmological phenomena as well as revolutionized our understanding of time and space. However, it is only formulated as a classical field theory so far. Considerable effort has been expended to find a quantum theory of gravity, leading to string theory and loop quantum gravity (among others), candidates for a canonically quantized description of gravity. So far, no unified field theory has been found.

The description of the gravitational field is given by the Einstein equations, describing the coupling of space-time to the energy momentum tensor. However, in the standard description the energy momentum tensor is assumed to be a classical quantity. In contrast, quantum mechanics taught us that momentum, energy and in general every degree of freedom should be connected to an operator description in order to adhere to the quantum mechanical framework. Indeed, every experiment not involving gravity but other forces, like the electromagnetic field, show a quantization of its degrees of freedom in experiments. Incorporating quantization into the description of these forces has led us to quantum electrodynamics, quantum field theory and the standard model of particle physics. The incorporation of gravity into experiments probing quantum effects is notoriously difficult, because of the very small interaction strength. So far only experiments testing an external gravitational field in a quantum setting have been carried out.

General relativity also has a remarkable history of experimental success in describing cosmological phenomena, not least the recent detection of gravitational waves as well as phenomena like gravitational lensing, the Lense-Thirring effect or the description of black holes.

One interesting test bed that arises is the regime were the two theories should supposedly meet, a regime were we still have a small enough size to be able to prepare a coherent quantum state as well as large enough to measure a gravitational influence originating from the prepared state. There are several obstacles that make this a difficult endeavor. One of them is decoherence, the interaction of the quantum state with its environment. This diminishes the control over the purity of the state, and subsequently leads to a loss of quantum properties

like entanglement or superposition and leading to a quasi-classical description of the remaining state. Precise control of the environment becomes a key obstacle to increase the mass of a test system needed to detect its gravitational field, and several solutions to this conundrum have been proposed. However, so far no experiment has reached a regime were a genuine gravitational field of a mass in superposition could have been detected.

Theoretical proposals of experiments exist for general relativistic effects in quantum systems. These could shed light on the incorporation of gravity into the framework of quantum mechanics by analyzing the effect of time dilation on the coherence of quantum states. Other conceptual ideas include the incorporation of a gravitational wave background, which should show as an additional decoherence in quantum systems, ultimately limiting the preparation of large quantum superposition.

From a theorist point of view, another question seems to be pressing. How can we mend the apparent disconnect of Einstein's equations and their classical nature and the operator description of quantum mechanics. Two possible solutions come to mind: The quantization of the gravitational field, leading to quantum gravity. Or to find a representation of the energy momentum tensor that is inherently classical (at least in an intermediate regime).

The conundrum of finding a quantized description of the Einstein tensor has also led to proposals of keeping the classical properties of gravity and finding a modification of quantum mechanics that effectively eliminates the need for quantization for all practical purposes. Although such proposals cannot be ruled out with certainty at this point, it leads to multiple conceptual problems. For one, nonlinear modifications of quantum mechanics lead to contradictions of relativistic principles, potentially allowing superluminal signaling. Also, when analyzing proposals like the replacement of the energy momentum tensor with an expectation value of a quantum state, the source of the gravitational field becomes tied to the probability of the wave function. This creates a peculiar disconnect of the gravitational field and the position of its source mass when considering a superposition. Interestingly, these modifications might still be useful to determine regimes in which experiments could give new insights into the interplay of quantum mechanics and gravity, even when a full description of gravity will be a quantized theory.

To this effect we will review the concept of collapse models, an approach to describe the collapse of the wave function through an objective mechanism directly integrated into the Schrodinger equation. This modified Schrödinger equation leads to several effects testable in experiments. We will propose such a setup, making use of photonic crystals to probe for an intrinsic heating effect. Our approach has mul-

tiple advantages regarding the limits of the model and can potentially reach a parameter space of the model previously unprobed.

We will also simulate possible fifth force candidates in gravitational force experiments. We will analyze a torsion pendulum experiment to detect gravity of small source masses and potential additional forces from scalar chameleon fields.

This work contains six major chapters. Chapter two will focus on the theoretical description of phenomena that are linked to gravity and lead to decoherence in experiments. Specifically, we will analyze decoherence from general relativity, decoherence from a gravitational wave background and decoherence from nonlinear modifications of quantum mechanics. We will also describe additional scalar fields within the standard model, so called chameleon fields.

In chapter three we will give an overview of experiments aiming to detect such decoherence effects, focusing on experiments connected to the theoretical descriptions given in chapter one.

In chapter four, we will give an analysis of a new way to test CSL collapse models, using photonic crystals acting as a waveguide for optical photons and mechanical phonons. We will describe the modifications needed to calculate the heating effect of collapse models within such structures and how it influences the phonon occupation number. We will also describe the setup used to detect a possible heating effect and possible new bounds arising from the experiment.

In chapter five, we will analyze an experimental setup to test chameleon field theories introducing a potential fifth force. We will do a full numerical analysis of the setup to quantify possible influences of the chameleon field on the experimentally measured gravitational force.

We will sum up our findings in chapter six, the Conclusions & Outlook section.

THEORY BACKGROUND, DECOHERENCE

2.1 DECOHERENCE

We will start out the theory chapter with a basic introduction to decoherence as a tool to analyze the transition to macroscopic systems and interactions with the environment. We will use the tools introduced here to analyze experiments and to show possible ways of detecting gravity in quantum systems.

We will begin with a simple model [88]. Imagine a system with two degrees of freedom and its environment $\mathcal{H} = \mathcal{H}_S + \mathcal{H}_E$. The interaction is given by

$$\mathcal{H}_{int} = \frac{1}{2}\sigma_z \otimes \sum_{i=1}^{N} g_i \sigma_z^{(i)} \tag{2.1}$$

This Hamiltonian is already diagonal, giving us the eigenbasis $\{|n\rangle\} = \{|0\rangle, |1\rangle\}$ as preferred basis of the system. The eigenstates of $\mathcal{H}_{int}$ are all tensor product combinations of the basis states $|n\rangle$ with dimension N (giving $2^N - 1$ combinations). For an initially uncorrelated state

$$|\psi\rangle = (a|0\rangle + b|1\rangle) \otimes \sum_{i=1}^{2^N-1} c_n|n\rangle \tag{2.2}$$

the time evolution given by $e^{-i\mathcal{H}_{int}t}$ creates an entangled state with the environment. The environmental components of the state are given by their evolution

$$|\mathcal{E}_0(t)\rangle = |\mathcal{E}_1(-t)\rangle = \sum_{i=1}^{2^N-1} c_n e^{-iE_n t/2}|n\rangle \tag{2.3}$$

Due to this entanglement we can gather information of the system by evaluating the environment. The more distinguishable the environment states are, the more information about the system state is available. This can be quantified by the overlap of the states

$$r(t) = \langle |\mathcal{E}_0(t)\rangle|\mathcal{E}_1(t)\rangle\rangle = \sum_{i=1}^{2^N-1} |c_n|^2 e^{iE_n t} \tag{2.4}$$

If the factor $r(t) \to 0$ then off diagonal elements in the density matrix $|\psi\rangle\langle\psi|$ will vanish. That means the environment can have a

dampening effect on the interference terms of the quantum state. If we consider a large amount of degrees of freedom in the environment, we have 2^N different state vectors with N large compared to the system dimension. All these vectors rotate with different frequencies E_n. The average sum over such rotating vectors follows a two dimensional random walk, giving us

$$\langle |r(t)|^2 \rangle = 2^{-N} \tag{2.5}$$

The overall dampening of interference terms scales with the environment size. The environment acts like a selector for a preferred basis, given by the eigenstates of its Hamiltonian. However, it is important to note that due to the cyclic nature of the time evolution and the finite degrees of freedom of the environment, the state will disentangle from the environment after a recurrence time $\tau = \prod_n 1/E_n$ (or earlier, if frequencies are multiples of each other). Another thing to note for this simple system is that there is no energy exchange between the environment and the system. Since the Hamiltonian only contains components of σ_z, it commutes with the state change operator σ_x, i.e. the populations are conserved. Decoherence can occur without dissipation.

To generalize the above decoherence and also incorporate possible dissipation (transfer of energy between the state and the environment) we will introduce the Master equation form used to describe decoherence processes. We are interested in a way to study the dynamics of the system at hand and changes of it due to the coupling to the environment. But we are not interested in an explicit description of the environment degrees of freedom. We introduce the reduced density matrix of the system

$$\rho_S(t) = Tr_\mathcal{E}\left(\rho(t)\right) = Tr_\mathcal{E}\left(\hat{U}(t)\rho(0)\hat{U}^\dagger(t)\right) \tag{2.6}$$

The unitary operators $\hat{U}(t)$ represent the time evolution of the combined system and environment. We want to avoid working with these operators. We instead define the time evolution of the system as given by

$$\rho_S(t) = V(t)\rho_S(0) \tag{2.7}$$

with $V(t)$ being called a dynamical map. This operator depends on the system-environment states and has to be defined through the properties of the environment and interaction.

We will restrict ourselves to linear, differential equations that are local in time. They take the form

$$\frac{d}{dt}\rho_S(t) = -i\left[H_S(t), \rho_S(t)\right] + \mathcal{D}\left[\rho_S(t)\right] \tag{2.8}$$

With a unitary term and a non unitary term containing decoherence and dissipation. In order to find a more tangible form of this equation we will apply the Born-Markov approximations. Two assumptions enter here:

1. Born approximation

   The environment is large compared to the system at hand, approximately constant in time and remain separable from the system:

$$\rho(t) = \rho_S(t) \otimes \rho_\mathcal{E} \tag{2.9}$$

2. Markov approximation

   Any self correlations within the environment are significantly shorter lived than the characteristic time scale of the system. There is no memory within the environment of the system evolution.

Imposing the Born approximation leads to a time evolution in the interaction picture

$$\frac{d}{dt}\rho_{S,I}(t) = -\int_0^t dt' \, Tr_\mathcal{E} \left[\mathcal{H}_{int}(t), \left[\mathcal{H}_{int}(t'), \rho_{S,I}(t') \otimes \rho_\mathcal{E}\right]\right] \tag{2.10}$$

with $\rho_{S,I}(t)$ given by the time evolution with respect to the system and environment without interaction. For the Markov approximation we will have a close look at the interaction Hamiltonian. We can write $\mathcal{H}_{int}(t)$ in its diagonal form

$$\mathcal{H}_{int}(t) = \sum_i S_i(t) \otimes \mathcal{E}_i(t) \tag{2.11}$$

When inserting into (2.10) we get (among others) terms of the form $Tr_\mathcal{E}\left[\mathcal{E}_i(t)\mathcal{E}_j(t')\rho_\mathcal{E}\right]$. If we assume that the environment is in a stationary state, the explicit time dependence drops out and we are left with only a relative time dependence

$$Tr_\mathcal{E}\left[\mathcal{E}_i(t-t')\mathcal{E}_j\rho_\mathcal{E}\right] \equiv c_{ij}(t-t') \tag{2.12}$$

.

Now we apply the Markov approximation by noticing that due to the time scale of correlations in the environment, the $C_{ij}(t-t')$ have to be sharply peaked around $t - t' = 0$. That implies that we can replace $\rho_{S,I}(t')$ with $\rho_{S,I}(t)$ since contributions at different times will vanish. Another change we can make is to the lower integration limit

by shifting it to $-\infty$. If we now shift back to the Schrödinger picture, we will arrive at the final form of our Born-Markov equation

$$\frac{d}{dt}\rho_S(t) = -i\left[\mathcal{H}_S, \rho_S(t)\right] - \sum_i \left([S_i, B_i\rho_S(t)] + [\rho_S(t)C_i, S_i]\right) \quad (2.13)$$

with

$$B_i = \int_0^\infty d\tau \sum_j c_{ij}(\tau)S_j(-\tau) \quad (2.14)$$

$$C_i = \int_0^\infty d\tau \sum_j c_{ji}(-\tau)S_j(-\tau) \quad (2.15)$$

One last aspect to mention here is that the resulting reduced density matrix $\rho_S(t)$ will not necessarily be positive at all times. We can write a more restrictive form, the Lindblad form, by demanding that $\langle\psi|\rho_S(t)|\psi\rangle \geq 0 \,\forall t$. The diagonalized form is

$$\frac{d}{dt}\rho_S(t) = -i\left[\mathcal{H}_S, \rho_S(t)\right] + \sum_i \kappa_i \left(L_i^\dagger L_i \rho_S(t) + \rho_S(t)L_i^\dagger L_i - 2L_i\rho_S(t)L_i^\dagger\right)$$

$$(2.16)$$

with the Lindblad operators L_i given by suitable linear combinations of the operators S_i. If the Lindblad operators are hermitian we can simplify (2.16) to

$$\frac{d}{dt}\rho_S(t) = -i\left[\mathcal{H}_S, \rho_S(t)\right] + \sum_i \kappa_i \left[L_i, [L_i, \rho_S(t)]\right] \quad (2.17)$$

One notable example of this Lindblad equation is the master equation for environmental scattering, with the Lindblad operators given by $L = x$ and $\mathcal{H}_S = p^2/2m$.

Modeling of many possible physical interactions to recover decoherence relations with arbitrary environments can be simplified in most cases. It turns out that by modeling the system in phase space with operators X, P and an environment given by a bath of harmonic oscillators is sufficient under many circumstances. (Or in the case of spin particles, spin description and spin-bath environments can be used) In particular, we want to have a closer look at the master equation for quantum brownian motion as it is of importance for later chapters.

We start with the Hamiltonian of the system

$$\mathcal{H} = \mathcal{H}_S + \mathcal{H}_\mathcal{E} + \mathcal{H}_{int} \quad (2.18)$$

with the interaction Hamiltonian

$$\mathcal{H}_{int} = x \otimes \sum_i c_i q_i^{(\mathcal{E})} \tag{2.19}$$

with x the position operator of the system and $q_i^{(\mathcal{E})}$ the position operators of the harmonic oscillators of the environment. The environment Hamiltonian is simply a sum of oscillator Hamiltonians

$$\mathcal{H}_{\mathcal{E}} = \sum_i \left(\frac{1}{2m_i} p_i^{(\mathcal{E})2} + \frac{1}{2} m_i \omega_i q_i^{(\mathcal{E})} \right) \tag{2.20}$$

First, we will calculate the self correlation function (2.12) for the environment

$$c(\tau) = \sum_i c_i^2 Tr \left(q_i^{(\mathcal{E})}(\tau) q_i^{(\mathcal{E})} \rho_{\mathcal{E}}(0) \right) \tag{2.21}$$

where we used that different oscillators of the environment are not interacting. To calculate $c(\tau)$ we can use the ladder operator representation and the well known time evolution of the operators $a_i, a_i^\dagger$ in the interaction picture to arrive at the expression

$$c(\tau) = \sum_i \frac{c_i^2}{2m_i \omega_i} \left(\coth \left(\frac{\hbar \omega_i}{2k_B T} \right) \cos(\omega_i \tau) - i \sin(\omega_i \tau) \right) \tag{2.22}$$

We have used the known relation for the mean occupation number $\langle a_i^\dagger a_i \rangle = (\exp(\hbar \omega_i / k_B T) - 1)^{-1}$. The self correlation function is often rewritten as

$$c(\tau) = \nu(\tau) - i\eta(\tau) \tag{2.23}$$

with

$$\nu(\tau) = \int_0^\infty d\omega J(\omega) \coth \left(\frac{\hbar \omega}{2k_B T} \right) \cos(\omega \tau) \tag{2.24}$$

$$\eta(\tau) = \int_0^\infty d\omega J(\omega) \sin(\omega \tau) \tag{2.25}$$

the decoherence and dissipation kernel respectively.
The function $J(\omega)$ is called the spectral density of the environment.

$$J(\omega) = \sum_i \frac{c_i^2}{2m_i \omega_i} \delta(\omega - \omega_i) \tag{2.26}$$

We can now use our prior knowledge from above to calculate all the components of the Born-Markov equation to get

$$\frac{d}{dt}\rho_S(t) = -i\left[\mathcal{H}_S, \rho_S(t)\right] - \int d\tau \left(\nu(\tau)\left[x, \left[x(-\tau), \rho_S(t)\right]\right]\right.$$
$$\left. -i\eta(\tau)\left[x, \{x(-\tau), \rho_S(t)\}\right]\right) \quad \text{(2.27)}$$

Where the decoherence and the dissipation with the environment is completely determined by the decoherence and dissipation kernel and the position operator of the system. In order to get explicit expression we assume that the system is also confined in a harmonic oscillator potential.

$$\mathcal{H}_S = \frac{1}{2M}p^2 + M\Omega^2 x^2 \quad \text{(2.28)}$$

Again using the interaction picture, the resulting master equation reads

$$\frac{d}{dt}\rho_S(t) = -i\left[\mathcal{H}_S + M\tilde{\Omega}^2 x^2, \rho_S(t)\right] - i\gamma\left[x, \{p, \rho_S(t)\}\right]$$
$$- D\left[x, \left[x, \rho_S(t)\right]\right] - f\left[x, \left[p, \rho_S(t)\right]\right] \quad \text{(2.29)}$$

with the four characteristic coefficients

$$\tilde{\Omega}^2 = -\frac{2}{M}\int_0^\infty d\tau \eta(\tau)\cos(\Omega\tau) \quad \text{(2.30)}$$

$$\gamma = \frac{1}{M\Omega}\int_0^\infty d\tau \eta(\tau)\sin(\Omega\tau) \quad \text{(2.31)}$$

$$D = \int_0^\infty d\tau \nu(\tau)\cos(\Omega\tau) \quad \text{(2.32)}$$

$$f = -\frac{1}{M\Omega}\int_0^\infty d\tau \nu(\tau)\sin(\Omega\tau) \quad \text{(2.33)}$$

The first term $\tilde{\Omega}^2$ represents a frequency shift of the system. γ is a momentum dampening constant, thus describing the diffusion of the system. D describes the decoherence of the system in the position basis and f is an anomalous diffusion coefficient. It is called anomalous because it has the form of diffusion but with respect to two different variables x and p. In a lot of systems this coefficient can be neglected.

Lastly, we want to introduce the high temperature limit $k_B T \gg \hbar\Lambda \gg \hbar\Omega$ of the above Born-Markov equation (2.29), the Caldera-Leggett equation. When considering the spectral density

$$J(\omega) = \frac{2M\gamma_0}{\pi}\omega \quad \text{(2.34)}$$

known as an ohmic bath, with a cutoff Λ such that

$$J(\omega) = \frac{2M\gamma_0}{\pi} \omega \frac{\Lambda^2}{\Lambda^2 + \omega^2} \tag{2.35}$$

which is known as the Lorenz-Drude form. The calculation of the four characteristic functions is straight forward. For D we simply have a double fourier cosine transform, which leaves even functions unchanged. We get

$$D = M\gamma_0\Omega \frac{\Lambda^2}{\Lambda^2 + \omega^2} \coth\left(\frac{\hbar\Omega}{2k_BT}\right) \approx 2M\gamma_0\Omega k_BT \tag{2.36}$$

Similarly, for the damping γ we have a double fourier sine transform, giving

$$\gamma = \gamma_0 \frac{\Lambda^2}{\Lambda^2 + \Omega^2} \approx \gamma_0 \tag{2.37}$$

The calculation of the other two functions needs an explicit evaluation of the double fourier transforms giving

$$\tilde{\Omega}^2 = -2\gamma_0 \frac{\Lambda^3}{\Lambda^2 + \Omega^2} \tag{2.38}$$

In the case of the anomalous diffusion coefficient an explicit evaluation is difficult due to the term $\coth(\hbar\Omega/k_BT)$ but using our approximation an explicit form can be given

$$f = \frac{2\gamma_0 k_BT}{\Lambda} \tag{2.39}$$

This term is typically negligible when compared to D and can be omitted. Using these coefficients we can now write down the Caldera-Leggett form of the master equation

$$\frac{d}{dt}\rho_S(t) = -i\left[\mathcal{H}_S + M\tilde{\Omega}^2 x^2, \rho_S(t)\right] - i\gamma_0\left[x, \{p, \rho_S(t)\}\right]$$
$$- 2M\gamma_0\Omega k_BT\left[x, [x, \rho_S(t)]\right] \tag{2.40}$$

Decoherence is a powerful tool in understanding the influence of an environment on a quantum system. It is often used as an explanation for the transition from quantum mechanics to our classical perception of macroscopic systems. Specifically, decoherence shines a light on the emergence of a preferred basis as an operational outcome of the system-environment interaction. However, the question of definite outcomes in an experiment from a superposition state is not directly

contained within the formalism. The state within the system might appear in a state in the measurement basis, but the superpositions with the environment are still intact, the unitarity of the combined system is upheld. This question of how to select a specific outcome is addressed in a variety of interpretations of quantum mechanics. Further discussion on the interpretations of quantum mechanics can be found in (quantum interpretations)

We are mostly interested here in including gravitational effects into quantum mechanical settings. First, we will look at gravity and general relativity effects as new sources of decoherence in quantum systems. Then we will look at the question of gravity as a classical field and the problems of coupling to quantum systems arising from it. In contrast, if gravity is a quantum field theory, one might not expect a transition region coming from a quantum-to-classical-transition. Instead, one might look at a region in which gravitational interactions become dominant. These two regimes are not mutually exclusive and have overlaps, giving us the opportunity to use them as test beds for unknown gravity effects independent of the properties of the gravitational field. Specifically, if there is a transition region between quantum mechanics and gravity, where would one look for such a transition and what would be the expected outcomes? We will address these questions by looking at possible modifications of quantum mechanics, such as the Schrödinger-Newton equation. This equation emerges from the Newtonian approximation of the Moller-Rosenfeld equation, an attempt to unify the operator form of the energy-momentum tensor with the Einstein tensor. We will also look at collapse models, specifically addressing the quantum-to-classical transition from the perspective of definite outcomes in quantum measurements and their tie-ins with gravity. A complete overview of interpretational problems from the perspective of collapse models can be found in [14, 15].

2.2   GRAVITY IN QUANTUM SYSTEMS

The interplay of gravity and quantum mechanics is a topic for theorists and experimentalists for a considerable amount of time. Since gravity should, like any other force have an impact on the phase of superposition states, this was one of the first test beds for gravitational effects in a quantum setting. The first experiment testing such phase shift was introduced by Colella, Overhauser and Werner, who showed such a phase shift in [28] using a neutron beam traveling through a silicon crystal interferometer [85]. The phase shift then depends on the height difference of the two paths through the interferometer. The

state after passing through the interferometer, but before recombining can be written as

$$|\phi\rangle = \frac{1}{\sqrt{2}} \left(i e^{-i\varphi_1} |\phi_1\rangle + e^{-i\varphi_2 + i\chi} |\phi_2\rangle \right) \tag{2.41}$$

with detection probabilities of

$$P_{1,2} = \frac{1}{2} \left(1 \pm \cos\left(\Delta\varphi + \chi\right) \right) \tag{2.42}$$

In the original paper [77] the phase shift is attributed to a Hamiltonian $H = p^2/2m + mgz$. The induced phase factors are proportional to the action $S_{1,2} = \int dt\, V_{1,2}$ along the respective path.

An important thing to note here is that the gravitational effect is only an external field acting on a quantum system. The effect is equivalent to the electric Aharanov-Bohm effect, where the vector potential of an electric field can create a phase difference in superposed paths through an interferometer. Any classical potential, such as a Newtonian potential can create this effect. A genuine relativistic effect would have to take into account a property of Einstein's theory of relativity that is not present in the Newtonian description. One such property is time dilation, which leads to an additional effect if the proper time states (acting as clocks) of the particles traversing the interferometer are taken into account.

If we are willing to delve into more theoretical approaches, gravity could also show a signature of modifications of quantum theory as well as through effects coming from gravitational wave backgrounds, inducing different decoherence phenomena. We will have a closer look at them in the next sections.

2.3   DECOHERENCE FROM GRAVITY

Before we get into modifications of quantum mechanics, we will start with the incorporation of relativistic effects into standard quantum experiments, based on the works of Brukner, Zych, Pikovski and Costa [83, 105, 106].

2.3.1   *Proper Time creates Decoherence*

As mentioned above, Newtonian potentials can create phase shifts in quantum states. These phase shifts can be attributed to gradients in the gravitational field, where the relative phase ϕ picked up corresponds to different trajectories in an Interferometer. It is tempting to associate this phase shift with the action $S = mc^2 \int_\gamma d\tau$ along the path, which is determined by its proper time. However, this effect is identical with a particle in an interferometer on flat space-time with an effective Newtonian potential [28, 82, 104] and therefore not a test suited for detecting relativistic effects, e.g. effects induced by time dilation.

In order to test the impact of proper time on a quantum system M. Zych et. al. [105] suggested to consider a state with an internal clock degree of freedom to keep track of the evolution of proper time within an interferometer. To start, consider H_{int} the Hamiltonian describing the internal evolution of a massive state, given by $H_{int} = E_0 |0\rangle\langle 0| + E_1 |1\rangle\langle 1|$. Considering the laboratory frame, we have to transform the time coordinate from laboratory frame to rest frame. So instead of $i\hbar\partial_\tau = H_{int}$ we have $i\hbar\partial_t = \dot{\tau} H_{int}$ with $\dot{\tau} = \sqrt{-g_{\mu\nu}\dot{x}^\mu \dot{x}^\nu}$. The energy of our particle is given by $E = mc^2 - \frac{g_{00}}{\dot{\tau}}$. Our space-time geometry for experiments on earth can be described by the Schwarzschild metric [100]

$$c^2 d\tau = \frac{\left(1 + \frac{\phi(x)}{2c^2}\right)^2}{\left(1 - \frac{\phi(x)}{2c^2}\right)^2} c^2 dt^2 - \left(1 - \frac{\phi(x)}{2c^2}\right)^4 \left(dx^2 + x^2 d\Omega^2\right) \quad (2.43)$$

with $\phi(x) = -GM/x$. For a weak field and low velocities we can approximate our final Hamiltonian $H = H_0 + \dot{\tau} H_{int}$[105] as

$$H \simeq mc^2 + H_{int} + E_k^{GR} + \frac{\phi(x)}{c^2}\left(mc^2 + H_{int} + E_{corr}^{GR}\right) \quad (2.44)$$

where

$$E_k^{GR} = \frac{p^2}{2m}\left(1 + 3\left(\frac{p}{2mc}\right)^2 - \frac{1}{mc^2}H_{int}\right) \quad (2.45)$$

and

$$E_{corr}^{GR} = \frac{1}{2}m\phi(x) - 3\frac{p^2}{2m}. \tag{2.46}$$

In a classic Mach Zehnder setup, the particle state will be of the form $|\Psi\rangle = 1/\sqrt{2}\left(i\,|\Psi_1\rangle + e^{i\varphi}\,|\Psi_2\rangle\right)$ with the states $|\Psi_1\rangle, |\Psi_2\rangle$ describing the state in each arm respectively. Considering an initial state $|x_{in}\rangle\,|\tau_{in}\rangle$ and the above Hamiltonian H we get

$$|\Psi_i\rangle = \exp\left(-\frac{i}{\hbar}\int_\gamma dt\frac{\phi(x)}{c^2}\left(mc^2 + H_{int} + E_{corr}^{GR}\right)\right)|x_{in}\rangle\,|\tau_{in}\rangle \tag{2.47}$$

For small height difference in the interferometer the potential can be approximated to linear terms $\phi(R + \Delta h) = \phi(R) + \frac{GM}{R^2}\Delta h + \mathcal{O}\left(\Delta h^2\right)$. We choose an initial state $|\tau_{in}\rangle = 1/\sqrt{2}\left(|0\rangle + |1\rangle\right)$ to finally get

$$P_\pm(\varphi, m, \Delta E, \Delta V, \Delta T) = \frac{1}{2} \pm \frac{1}{2}\cos\left(\frac{\Delta E\Delta V\Delta T}{2\hbar c^2}\right)$$
$$\cdot \cos\left(\left(mc^2 + \langle H_{int}\rangle_{\tau_{in}} + \bar{E}_{corr}^{GR}\right) + \frac{\Delta V\Delta T}{\hbar c^2} + \varphi\right) \tag{2.48}$$

with $\Delta E = E_1 - E_0$, ΔT the time of flight at different heights and $\Delta V = \frac{GM}{R^2}\Delta h$. This gives the visibility of the interference pattern

$$\mathcal{V} = \left|\cos\left(\frac{\Delta E\Delta V\Delta T}{2\hbar c^2}\right)\right|. \tag{2.49}$$

This change in visibility cannot be observed by just introducing a Newtonian gravitational field. It is a direct consequence of the internal proper time that differs between the two paths due to the difference in gravitational potential. If we use $|\Psi\rangle = 1/\sqrt{2}\left(i\,|x_0\rangle\,|\tau_0\rangle + e^{i\varphi}\,|x_1\rangle\,|\tau_1\rangle\right)$ and calculate the detection probabilities, this becomes more apparent:

$$P_\pm = \frac{1}{2} \pm \frac{1}{2}|\langle\tau_0|\tau_1\rangle|\cos\left(\alpha + \varphi\right) \tag{2.50}$$

The phase α being the phase factor separated from $\langle\tau_0|\tau_1\rangle = |\langle\tau_0|\tau_1\rangle|\,e^{i\alpha}$.

2.3.2   *General decoherence from a proper time difference*

The dephasing in the last section due to proper time also has a more general effect on quantum states subjected to a gravitational gradient. Pikovski et. al. [83] discovered that the proper time difference in internal degrees of freedom lead to a coupling of these degrees of freedom to the center of mass of the quantum state. Consequently, a superposition state with suitable internal states will dephase in the center of mass degree of freedom. Assuming the internal Hamiltonian to be $H_0 = \sum_{i=1}^{N} \hbar\omega_i n_i$ and taking into account the total gravitational mass of the system, which in general relativity amounts to the rest mass plus kinetic contributions $m_{tot} = m_0 + H_0/c^2$, we get an additional interaction term

$$H_{int} = \phi(x)\frac{H_0}{c^2} = \frac{\hbar g x}{c^2}\sum_{i=1}^{N}\omega_i n_i, \tag{2.51}$$

similar as in (2.44). Now, consider our initial state of the center of mass $|\psi_{cm}\rangle = 1/\sqrt{2}\,(|x_1\rangle + |x_2\rangle)$ and our internal degrees of freedom to be in thermal equilibrium

$$\rho_i = \frac{1}{\pi\bar{n}_i}\int d^2\alpha_i e^{-\left(|\alpha_i|^2/\bar{n}_i\right)}|\alpha_i\rangle\langle\alpha_i|. \tag{2.52}$$

The total state initially reads $|\psi_{cm}\rangle\langle\psi_{cm}|\otimes\Pi_i\rho_i$. Because of (2.51) the matrix elements of the state become

$$\rho_{12} = \langle x_1|\rho|x_2\rangle = \frac{1}{2\pi\bar{n}_i}e^{img\Delta x t}\Pi_{i=1}^{N}\int d^2\alpha_i e^{-\left(|\alpha_i|^2/\bar{n}_i\right)}\left|\alpha_i^{(1)}\right\rangle\left\langle\alpha_i^{(2)}\right| \tag{2.53}$$

with $\left|\alpha_i^{1,2}\right\rangle = \alpha_i e^{-i\omega_i t(1+gx_{1,2}/c^2)}$. One can see, that the internal degrees of freedom evolve with different frequencies, leading to a dephasing dependent on the position in the gravitational potential. It is important to note that this dephasing is unique to the property of time dilation and does not occur in Newtonian gravity. The effect on the center of mass can be seen by tracing over the internal degrees of freedom and considering the visibility $\mathcal{V}$ as above.

$$\mathcal{V}(t) = 2\left|\Pi_{i=1}^{N}Tr_i\left(\rho_{12}(t)\right)\right| = \left|\Pi_{i=1}^{N}\left[1+\bar{n}_i e^{-i\omega_i t g\Delta x/c^2}\right]^{-1}\right| \tag{2.54}$$

This can be further approximated by assuming that $\omega_i t g\Delta x/c^2 \ll 1$ and $\bar{n}_i \approx \frac{k_B T}{\hbar\omega_i}$, that is nonrelativistic timescales and high temperatures, respectively. The visibility $\mathcal{V}$ then becomes

$$\mathcal{V} \approx \left(1 + \left(\frac{k_B T g\Delta x t}{\hbar c^2}\right)^2\right)^{-N/2} \approx e^{-(t/\tau_{dec})^2} \tag{2.55}$$

with

$$\tau_{dec} \approx \sqrt{\frac{2}{N}} \frac{\hbar c^2}{k_B T g \Delta x} \tag{2.56}$$

Furthermore, this decoherence can be formulated more generally as a master equation of the form [83]

$$\dot{\rho} = -\frac{1}{\hbar} \left[H_{cm} + \left(m + \frac{N k_B T}{c^2} \right) g x, \rho_{cm}(t) \right]$$
$$- N \left(\frac{k_B T g}{\hbar c^2} \right)^2 \int_0^t ds \left[x, e^{-i H_{cm} s/\hbar} \left[x, \rho_{cm}(t-s) \right] e^{-H_{cm} s/\hbar} \right]. \tag{2.57}$$

If H_{cm} only has a negligible influence (compared to the decoherence time scale) on the off diagonal elements of the density matrix one recovers the familiar decoherence term of double commutators $\mathcal{L}[\rho_{cm}(t)] = -Nt \left(\frac{k_B T g}{\hbar c^2} \right) [x, [x, \rho_{cm}(t)]]$. In this approximation we recover the decoherence time (2.56). It is in this sense a universal decoherence effect for any composite quantum system in a superposition of different proper time paths. It is important to stress that this effect occurs simply by considering basic quantum mechanics and low energy general relativity. No additional assumptions have entered. This is in contrast to other concepts for decoherence, which assume additional effects through the modification of quantum mechanics and therefore new physics beyond the conventional quantum theory.

2.3.3   *Decoherence due to Gravitational Wave Background*

As we have seen above, decoherence can occur from basic assumptions of general relativity incorporated into quantum mechanics. Another phenomenon, gravitational waves, that recently found experimental verification are adding decoherence to quantum systems. Apart from the data gathered by LIGO for black hole mergers [2], there is a plethora of sources for gravitational waves in our galaxy and other galaxies. Their collective overlap of gravitational waves can be summarized into a stochastic background [89]. The exact spectral density of this background is unknown but can, with enough sensitivity of the experiment, show up in gravitational wave detector measurements. A series of papers [57, 65] has analyzed the influence of this gravitational wave background on potential experiments.

First, we need to introduce basics of gravitational waves through linearized gravity [99].

2.3.4   *Linearized Gravity*

We are starting from the Einstein equations

$$G_{ab} = R_{ab} - \frac{1}{2} R g_{ab} = 8\pi T_{ab} \tag{2.58}$$

We are interested in a regime with weak curvature meaning we can approximate the spacetime as flat with only a small deviation. This can be done by rewriting the metric as

$$g_{ab} = \eta_{ab} + h_{ab} \tag{2.59}$$

We now need all the components to build up an expression for the Einstein equation. First, we need the affine connection

$$\Gamma^a_{\ bc} = \frac{1}{2} \eta^{ad} \left(\partial_c h_{db} + \partial_b h_{dc} - \partial_d h_{bc} \right) \tag{2.60}$$

then the Riemann tensor can be calculated from

$$R^a_{\ bcd} = \partial_c \Gamma^a_{\ bd} - \partial_d \Gamma^a_{\ bc} \tag{2.61}$$

From here we can construct the Ricci tensor

$$R_{ab} = R^c_{\ acb} = \frac{1}{2} \left(\partial_c \partial_b h^c_{\ a} + \partial^c \partial_a h_{cb} - \Box h_{ab} - \partial_a \partial_b h^c_{\ c} \right) \tag{2.62}$$

and the curvature tensor

$$R = R^a_{\ a} = \left(\partial_c \partial^a h^c_{\ a} - \Box h^a_{\ a} \right) \tag{2.63}$$

From there we can finally write the Einstein tensor as

$$G_{ab} = R_{ab} - \eta_{ab} R \tag{2.64}$$

However this can be simplified by replacing the h_{ab} with its trace reversed version $\bar{h}_{ab} = h_{ab} - \frac{1}{2}\eta_{ab}h^c{}_c$ which eliminates all terms containing the trace $h^c{}_c$. Choosing a suitable gauge for our system, which in general relativity amounts to an infinitesimal coordinate transformation $x^a = x^a + \xi^a$, e.g. Lorentz gauge $\partial^a \bar{h}_{ab} = 0$ (which can always be achieved through the condition $\Box \xi_b = \partial^a \bar{h}_{ab}$), the Einstein tensor finally reduces to

$$G_{ab} = -\frac{1}{2}\Box \bar{h}_{ab} \tag{2.65}$$

and the linearized Einstein equation becomes

$$\Box \bar{h}_{ab} = -16\pi T_{ab} \tag{2.66}$$

or in vacuum

$$\Box \bar{h}_{ab} = 0 \tag{2.67}$$

The solutions to this equation can be written as superpositions of plane waves

$$\bar{h}_{ab}(\boldsymbol{x},t) = \int \frac{d^4k}{2\pi} \bar{h}_{ab}[\boldsymbol{k}]e^{ik_a x^a} \tag{2.68}$$

with $\bar{h}_{ab}[\boldsymbol{k}] = \sum_{\pm} \left(\epsilon_a^{\pm}\epsilon_b^{\pm}/\sqrt{2}\right) h^{\pm}[\boldsymbol{k}]$. A further simplification can be made by only considering globally vacuum spacetimes, which introduce the traceless transverse gauge. Here, all metric perturbations are taken to be purely spatial ($\bar{h}_{ti} = \bar{h}_{tt} = 0$) and traceless ($\bar{h}^c{}_c = 0$). Because of Lorentz gauge $\partial_a \bar{h}_{ab} = 0$ all spatial components of the metric are transverse components.

We will assume for simplicity, that the stochastic background will be stationary, unpolarized and isotropic. We can rewrite the expansion of plane waves as [68]

$$\bar{h}_{ab}(t) = \sum_{\pm} \int df \int d\Omega\, h^{\pm}[f,\boldsymbol{\Omega}]e^{-2i\pi ft} \left(\epsilon_a^{\pm}\epsilon_b^{\pm}/\sqrt{2}\right) \tag{2.69}$$

with $h^{\pm}[-f,\boldsymbol{\Omega}] = h^{\pm*}[f,\boldsymbol{\Omega}]$. The correlation function of $h^{\pm}[f,\boldsymbol{\Omega}]$ in a stationary, unpolarized, isotropic background simplifies to

$$\langle h^{\pm*}[f,\boldsymbol{\Omega}], h^{\pm}[f',\boldsymbol{\Omega}']\rangle = \delta(f-f')\delta^2(\boldsymbol{\Omega},\boldsymbol{\Omega}')\delta_{\pm}S_h(f) \tag{2.70}$$

From the Fourier amplitudes, we can then relate the introduced spectral density S_h [57] as:

$$\langle \bar{h}_{ab}(t)\bar{h}_{ab}(t')\rangle = \int df S_h[f] e^{-i2\pi f(t'-t)} \tag{2.71}$$

We define the energy density of the gravitational wave as a spatial average over a frequency range

$$\rho_{gw} = \frac{1}{32\pi G} \langle \partial_t \bar{h}_{ab}(t), \partial_t \bar{h}^{ab}(t)\rangle \tag{2.72}$$

For a stochastic background, this amounts to a time average at one point in Fourier space (2.70). Together with (2.69) we get

$$\frac{d\rho_{gw}}{df} = \frac{\pi c^2}{2G} f^2 S_h[f] \tag{2.73}$$

We can associate the energy density per frequency with an average temperature of the gravitational wave giving

$$S_h[f] = \frac{16G}{c^5} k_B T \tag{2.74}$$

This description using a characteristic temperature is valid as long as S_h can be approximated as nearly flat in frequency. This seems to be true for frequencies of $\omega \approx 10^{-6} Hz - 10^{-4} Hz$, which results in $S_h \approx 10^{-34} Hz^{-1}$. The corresponding temperature seems rather large ($T_{gr} \approx 10^{41} K$) which is attributed to the fact that gravity only couples very weakly to massive systems leading to large times to equilibrate. This stochastic background is typically assumed to originate from a plethora of sources, leading to a stochastic noise with quasi gaussian statistics. (papers here)

This noise can change phase relations in an interferometer. We will have a look at one example, a sagnac interferometer.

The phase acquired in a sagnac interferometer is

$$\Phi = \frac{1}{\hbar} \int p_i dx^i = \frac{2m}{\hbar} A\Omega \tag{2.75}$$

with the mass of the particle traveling through the interferometer m, The enclosed area A, and the angle of rotation of the interferometer Ω. The momentum here is $p_\mu = g_{\mu\nu} m v^\nu$ and the enclosed area is $A = v^2 \tau^2 \sin(\alpha)$ with τ the flight time through the interferometer and α the enclosed angle of the two arms. We are now interested in the modification of the phase due to this gravitational background noise. It can only depend on fluctuations in $h_{12}(t)$ which corresponds to the plane of the interferometer while all other components are zero by

definition of the traceless transverse gauge. The fluctuations can then be written as

$$\delta\Phi = \frac{1}{\hbar}\int \bar{h}_{12}v^1v^2 d\tau = \frac{2m}{\hbar}A\delta\Omega \tag{2.76}$$

Since all other components are fixed with the geometry of the interferometer, the noise only manifests in the angular rotation. This phase fluctuation has to be proportional to the average change of the metric component $\delta\Omega \propto \frac{d\tilde{h}}{dt}$ with

$$\tilde{h} = \int h(t-\tau)g(\tau)d\tau \tag{2.77}$$

The function $g(\tau)$ then represents the time of flight through the interferometer, which in this case is simply a triangular function, increasing the average fluctuations over a time τ. Since this gives one particular fluctuation we also need to average now over all phase fluctuations $\delta\Phi$ to arrive at an expression for the contribution of a stochastic gravitational background. This can be done by looking at the average visibility of the interference, given by $\langle\exp(i\delta\Phi)\rangle$. We already know that the fluctuations of $\delta\Phi$ are dependent on the area of the interferometer as well as the rotation angle. We also know that the correlation of the metric fluctuations is described by a noise spectrum S_h. It was shown in [65] that one can express the correlations of $\delta\Phi$ as (see also (2.71))

$$\langle\delta\Phi_t\delta\Phi_s\rangle = \int \frac{df}{2\pi}S_\Phi[f]e^{-i2\pi f(t-s)} \tag{2.78}$$

were the noise spectrum

$$S_\Phi = S_h\tilde{A}(f) \tag{2.79}$$

with $\tilde{A}(f)$ the fourier transform of the area. Since we have a gaussian distributed noise the average of $\langle\exp(i\delta\Phi)\rangle$ corresponds to a gaussian distribution $\exp\left(-\frac{\langle\delta\Phi_t\delta\Phi_s\rangle}{2}\right)$. We can now write

$$\langle\delta\Phi_\tau^2\rangle = \left(\frac{2mv^2}{\hbar}\sin(\alpha)\right)S_h2\tau \tag{2.80}$$

For sagnac interferometers using lasers to generate the beamsplitting effect, resulting in a small angle α, as well as atoms used for the massive particles, we can estimate the effect for an interferometer arm length of $l \approx 1m$. Using caesium atoms with mass $m = 2\cdot 10^{-25}kg$, velocity $v = 1ms^{-1}$, rotation frequency $\Omega = 4\cdot 10^7 Hz$ and an angle $\alpha = 0.035$ (values investigated for a proposed experiment in [65]) we get for the above assumed approximately flat noise spectrum S_h

$$\langle\delta\Phi_\tau^2\rangle = 10^{-21} \tag{2.81}$$

a rather low value. The fringe contrast in such experiments remains unaffected f.a.p.p.

Although a gravitational wave background contributes decoherence to quantum systems, the effect is much smaller than other sources of decoherence in similar setups. An experimental verification of such an effect in tabletop experiments is not feasible in the near future.

2.3.5   *Master equation from stochastic backgrounds*

The above effect of decoherence due to a gravitational wave background can be formulated as a master equation describing decoherence [18]. As seen above, we should expect a coupling between spacetime perturbations, as in fluctuations of the metric tensor, and the energy-momentum tensor. For superposition systems at rest, their rest energy should therefore determine the strength of the coupling. In order to derive a master equation, it is assumed that perturbative quantum field theory can be applied to gravity. A justification for this approach can be argued for, by claiming that for a full developed quantum gravity theory, we should recover similar results in its low energy limit, particularly, with its effective field theory description. Following [18], one arrives at the master equation

$$
\begin{aligned}
\partial_t \rho(t) = & -i\left[H, \rho(t)\right] \\
& - \int_0^t d\tau \int dr dr' \left\{ N(r-r', \tau)\left(2[T_{\mu\nu}(r), [T^{\mu\nu}(r', -\tau), \rho(t)]]\right.\right. \\
& \left. - [T_\mu{}^\mu(r), [T_\nu{}^\nu(r', -\tau), \rho(t)]]\right) \\
& - iD(r-r', \tau)\left(2[T_{\mu\nu}(r), \{T^{\mu\nu}(r', -\tau)\rho(t)\}]\right. \\
& \left.\left. - [T_\mu{}^\mu(r), \{T_\nu{}^\nu(r', -\tau), \rho(t)\}]\right) \right\}
\end{aligned}
$$
(2.82)

with H being the free Hamiltonian of the scalar field and the noise and dissipation terms are

$$
N(r, t) = \left(\frac{\kappa}{4}\right)^2 \int \frac{dk}{(2\pi)^3} \frac{e^{ikr}}{k} \cos(kt)[1 + 2n(k)]
$$
(2.83)

$$
D(r, t) = \left(\frac{\kappa}{4}\right)^2 \int \frac{dk}{(2\pi)^3} \frac{e^{ikr}}{k} \sin(kt)
$$
(2.84)

with $n(k)$ the thermal occupation number at a given temperature. We furthermore restrict ourselves to stationary, macroscopic matter states, described by coherent states

$$
|\alpha(k)\rangle = exp\left[-\frac{1}{2}\int dk|\alpha(k)|^2 + \int dk\alpha(k)\alpha^\dagger(k)\right]|0\rangle
$$
(2.85)

where $\alpha(k) = A_0 R^3 \sqrt{(m^2 + k^2)^{1/2}/2} \exp\left(-ikr_0 - (kR)^2/2\right)$, and thus have a spread of R and a (approximately) static center at r_0. From this, we can analyze the master equation 2.82 using a superposition state of two positions. The resulting initial density matrix is

$$
\rho[\phi, \phi', 0] = \langle\phi|\Psi\rangle\langle\Psi|\phi'\rangle
$$
(2.86)

With

$$\langle \phi | \Psi \rangle = 1/\sqrt{2}(\langle \phi | \alpha(k) \rangle + \langle \phi | \alpha'(k) \rangle). \tag{2.87}$$

For the stationary, nonrelativistic limit we have $T_{00}(\phi) \approx \frac{1}{2}m^2\phi^2$ and arrive at an expression for the noise part of 2.82

$$\partial_t \rho[\phi, \phi', t] =$$
$$\dots - \frac{T}{2\pi} \left(\frac{\kappa}{4}\right)^2 \left(\int dr \left[\frac{1}{2}m^2(\phi(r))^2 - \frac{1}{2}m^2(\phi'(r))^2\right]\right)^2 \rho[\phi, \phi', t] \tag{2.88}$$

This corresponds to decoherence in position but under the condition that the two parts of the superposition state have different energies. Superpositions with the same energy do not decohere in this model. For example, a superposition in position of an atom in the ground state would not see any decoherence from a gravitational background in this case. However, for superpositions of excited and ground state we would get decoherence of the order of $\Gamma \sim 10^{-45}s^{-1}$. If we would look at macroscopic systems (of the order of grams) the decoherence increases to $\Gamma \sim 10^2 s^{-1}$. So this decoherence effect only contributes non-negligibly at macroscopic scales.

This resulting master equation is very similar to a general result obtained in [10]. Here a master equation is calculated from the interaction of a bosonic particle in a weak, stochastic and classical gravitational field. The full master equation is rather lengthy and can be found in [10] on page 6. However, in the case of the nonrelativistic limit and considering the main contribution to be the decoherence in position, they derive a compact master equation

$$\partial_t \rho(t) = -\frac{i}{\hbar}[H, \rho(t)] - \frac{\alpha^2 L c^3}{(2\pi)^3 \hbar^5} \int d^3q \, u^{00}(\mathbf{q}) m^2(\mathbf{q})$$
$$\left[e^{i\mathbf{q}X/\hbar}, \left[e^{-i\mathbf{q}X/\hbar}, \rho(t)\right]\right] + O(h^{\mu i}) + O(\Delta E) \tag{2.89}$$

The function $u^{00}(x)$ is the noise kernel, already assumed to be markovian and invariant under spatial translations. The form of Blencowe can be recovered by assuming $u^{00}(\mathbf{x} - \mathbf{y}) = L^3\delta(\mathbf{x} - \mathbf{y})$ is delta correlated in space. The only difference between these two derivations is the assumption of the bath. In the case of Blencowe, the bath is a quantum bosonic bath, while the derivation in [10] assumes a purely classical bath. However, the resulting structure (and effect) of the decoherence is the same. This makes the distinction of these two models difficult in experiments.

2.4 NONLINEAR EXTENSIONS

In the above chapter we have delved into the question of how gravity can introduce decoherence in quantum systems, either through taking into account time dilation or by assuming that a linear approximation to the Einstein equations can introduce decoherence through fluctuations of the metric. In this section we want to consider deviations from quantum mechanics and how changes of the linear time evolution can lead to different predictions for experiments and the challenges arising from doing so.

The first attempts to find an underlying nonlinear description of quantum mechanics, from which its linear stochastic behavior emerges, was carried out by De Broglie in 1960 [20]. However, no explicit nonlinear equation was proposed. The first attempt to modify the Schrödinger equation was undertaken by Bialynicky-Birula and Mycielski in 1976 [17]. They proposed a logarithmic extension of the form $-b\psi \ln |\psi|^2$. The advantage of such a modification is that it leaves the energy consistent with the Plank identity $E = \hbar\omega$ for stationary states. Their approach also left separate, non-interacting systems separable in time e.g. $\psi(0)\phi(0) \to \psi(t)\phi(t)$ where the time evolution of the two wave functions can be treated separately.

Another proposal for a nonlinear quantum theory was formulated by Steven Weinberg in 1989 [101]. The non-linearity is introduced through changing the property of observables. In quantum mechanics, observables are described by Hermitian matrices, or equivalently, through the bilinear form $\langle\psi|A|\psi\rangle$. We will use the notation $|V\rangle$ as a vector notation describing the vectors V_k and its complex conjugate $\langle V| \to V_k^*$. Weinberg introduces the non-bilinear form $a(|\psi\rangle, \langle\psi|)$. These functions are invariant under multiplication with a complex number, similar to usual quantum mechanics, i.e. $Za(|\psi\rangle, \langle\psi|) = a(Z|\psi\rangle, Z\langle\psi|)$, which is equivalent to $|\psi\rangle \frac{\partial a}{\partial|\psi\rangle} = a$. (This is read as a derivative of the components of $|\psi\rangle$) The functions a form an algebra with obvious addition and multiplication by scalar. The scalar product becomes $a \cdot b = \frac{\partial a}{\partial|\psi\rangle} \frac{\partial b}{\partial\langle\psi|}$. The unit element then is simply $|\psi\rangle\langle\psi|$. The last ingredient are symmetry transformations as in quantum mechanics $\epsilon\delta|\psi\rangle = -i\epsilon\hat{A}|\psi\rangle$, which, with our function a, amount to $\delta|\psi\rangle = -i\epsilon\frac{\partial a}{\partial\langle\psi|}$. Specifically, a transformation in time t generated by a Hamiltonian function $h(|\psi\rangle, \langle\psi|)$ reads

$$\delta|\psi(t+\epsilon)\rangle = |\psi\rangle + \epsilon\delta|\psi\rangle \tag{2.90}$$

and therefore, our time evolution equation becomes

$$\frac{\partial|\psi\rangle}{\partial t} = -i\frac{\partial h}{\partial\langle\psi|} \tag{2.91}$$

To give an example of this nonlinear evolution [46], let us assume a Hamiltonian function

$$h(|\psi\rangle, \langle\psi|) = \frac{\langle\psi|\sigma_z|\psi\rangle^2}{\langle\psi|\psi\rangle} \tag{2.92}$$

and the resulting nonlinear Schrödinger equation

$$\frac{d\,|\psi\rangle}{dt} = -2i\frac{\langle\psi|\sigma_z|\psi\rangle}{\langle\psi|\psi\rangle}\sigma_z\,|\psi\rangle \tag{2.93}$$

As was noted by Nicolas Gisin [46][84] in a follow up paper to Weinbergs nonlinear modifications, the above time evolution has one notable flaw with respect to relativistic properties: it allows superluminal communication. In the specific case here, if one considers the mean value of $\langle\sigma_y\rangle$ and the initial state is a Bloch vector in $(0,0,\pm1)$-direction, then the mean value will always be zero. However, for an initial state in $(1,1,\pm1)$-direction, we get a rotation around the z-axis clockwise or counterclockwise depending on the sign. Thus, after a quarter rotation we will get a positive value for $\langle\sigma_y\rangle$ different from the other initial condition. Due to this, one can distinguish different preparations. This can be used to transfer information faster than light through preparing an entangled state. The measurement on one party, A, will prepare the state for the other party, B, in a distinct initial state. Measuring the state for B then reveals the preparation made by A without the need for communication.

This argument can be made more general by looking at properties of standard quantum mechanics. The time evolution of a wave function is determined by a Hamiltonian such that

$$|\psi(0)\rangle \rightarrow |\psi(t)\rangle = e^{-iHt}\,|\psi\rangle \tag{2.94}$$

On the other hand, in order to describe a measurement, one uses the von Neumann postulate [45] that gives the outcome associated with an observable P with the properties $P^2 = P^\dagger P = P$.

In the context of density matrices this leads to the following expression

$$\rho(t) = P\rho(0)P + (1-P)\rho(0)(1-P) \tag{2.95}$$

where $\rho(0) = \sum_i c_i|\psi_i\rangle\langle\psi_i|$ is a decomposition of the initial state. The time evolved state is independent of the decomposition of the density matrix. How can a nonlinear time evolution now lead to superluminal signaling? Let us define an evolution

$$g : |\psi\rangle\langle\psi| \rightarrow g(|\psi\rangle\langle\psi|) \tag{2.96}$$

on the set of pure states. For a mixture of states the evolution then gives

$$\sum_i c_i \left|\psi_i\right\rangle \left\langle\psi_i\right| \to \sum_i c_i g(\left|\psi_i\right\rangle \left\langle\psi_i\right|).$$ (2.97)

Now let us further assume that

$$\sum_i c_i \left|\psi_i\right\rangle \left\langle\psi_i\right| = \sum_i d_i \left|\phi_i\right\rangle \left\langle\phi_i\right|$$ (2.98)

but

$$\sum_i c_i g(\left|\psi_i\right\rangle \left\langle\psi_i\right|) \neq \sum_i d_i g(\left|\phi_i\right\rangle \left\langle\phi_i\right|),$$ (2.99)

that is different mixtures evolve differently in time. Then according to the Schmidt decomposition of a composite system we can write a general state

$$\left|\Psi\right\rangle = \sum_{ij} A_{ij} \left|i\right\rangle \otimes \left|j\right\rangle = \sum_i \sqrt{c_i} \left|\psi_i\right\rangle \otimes \left|\alpha_i\right\rangle = \sum_j \sqrt{d_j} \left|\phi_j\right\rangle \otimes \left|\beta_j\right\rangle$$ (2.100)

with

$$\left\langle i|A|j\right\rangle = \sum_k \sqrt{c_k} \left\langle i|\psi_k\right\rangle \left\langle\alpha_k|j\right\rangle = \sum_k \sqrt{d_k} \left\langle i|\phi_k\right\rangle \left\langle\beta_k j|\right\rangle$$ (2.101)

If a time evolution would depend on the decomposition of a density matrix, then one party in an entangled state could encode information in his part of the state through preparing a specific decomposition that would then be discernible for the other party instantaneously through measurement. This communication channel contradicts relativistic principles and should therefore be avoided by the theory. One example of this will be introduced in the next chapter. We will see one way to achieve nonlinear extensions of quantum mechanics without adding superluminal signaling in a later section.

2.5 SCHRÖDINGER NEWTON EQUATION

One way of extending quantum mechanics non linearly, and also incorporate classical gravity is to start from the Einstein equation

$$G_{ab} = 8\pi \frac{G}{c^4} T_{ab} \tag{2.102}$$

with $G_{ab} = R_{ab} + g_{ab}R$. If we assume that gravity is quantized, we also need to assume that the Einstein tensor is a quantized operator, i.e. $G_{ab} = \hat{G}_{ab}$. However, if gravity is assumed to not be quantized, we have to find an expression of G_{ab} that does not depend on the operator $\hat{T}_{ab}$ directly [26]. One such option was formulated by Møller [69]and Rosenfeld [86] independently by rewriting the Einstein equation as

$$G_{ab} = 8\pi \frac{G}{c^4} \langle \psi | \hat{T}_{ab} | \psi \rangle \tag{2.103}$$

To calculate an evolution equation in a Newtonian regime we use linearized gravity again

$$g_{ab} = \eta_{ab} + h_{ab} \tag{2.104}$$

where h_{ab} is a small perturbation to the metric. Equation (2.103) then becomes

$$\Box h_{ab} = -\frac{16\pi}{c^4} G \left(\langle \psi | \hat{T}_{ab} | \psi \rangle - \frac{1}{2} \eta_{ab} \langle \psi | \eta^{\rho\sigma} \hat{T}_{\rho\sigma} | \psi \rangle \right) \tag{2.105}$$

In the Newtonian limit the dominant term is $\langle \psi | \hat{T}_{00} | \psi \rangle$ which gives

$$\nabla^2 V = \frac{4\pi G}{c^2} \langle \psi | \hat{T}_{00} | \psi \rangle \tag{2.106}$$

where the potential V becomes $V = -\frac{c^2}{2} h_{00}$. In the linearized theory the interaction between gravity and matter is given by

$$H_{int} = \int d^3 r h_{ab} \hat{T}_{ab} \tag{2.107}$$

Note that the gravitational perturbation h_{ab} is not an operator, signifying that gravity is not assumed to be quantized here. Together with (2.106) we get

$$H_{int} = -G \int \int d^3 r d^3 r' \frac{\langle \psi | \rho(r') | \psi \rangle}{||\boldsymbol{r} - \boldsymbol{r'}||} \rho(\boldsymbol{r}) \tag{2.108}$$

with $\hat{T}_{00} = -\frac{c^2 \rho}{G}$. For a single particle and the given potential we arrive at the Schrödinger Newton equation [30, 48–51, 53, 70, 80].

$$i\hbar \frac{\partial \psi(\mathbf{r}, t)}{\partial t} = -\frac{\hbar}{2m} \nabla^2 \psi(\mathbf{r}, t) - Gm^2 \int \frac{|\psi(\mathbf{r}', t)|^2}{||\mathbf{r} - \mathbf{r}'||} d^3 r' \psi(\mathbf{r}, t) \quad (2.109)$$

Similar equations have been found in different contexts. The Gross-Pitaevski equation describes systems of identical bosons in a Bose Einstein condensate where the nonlinearity observed above stems from interactions within the condensate. However in this case, the N-body dynamics are still linear and the center of mass motion is still described by the free evolution of the linear Schrödinger equation. If one takes the above equation as fundamental, it also introduces the nonlinearity for single particles and thereby changing the linear dynamic of standard quantum mechanics.

A similar form can be derived by introducing the gravitational interaction of particles within an object with the ansatz $\psi(\mathbf{x}, t) = \psi(\mathbf{x}_1, t) \ldots \psi(\mathbf{x}_N, t)$ for N particles. The resulting Schrödinger equation takes the form

$$i\hbar \frac{\partial \psi(\mathbf{x}_i, t)}{\partial t} = -\frac{\hbar}{2m} \nabla^2 \psi(\mathbf{x}_i, t) - \sum_{i \neq j; j=1}^{N} Gm_i m_j \int \frac{|\psi(\mathbf{x}_j', t)|^2}{||\mathbf{x}_i - \mathbf{x}_j'||} d^3 x_j' \psi(\mathbf{x}_i, t)$$

$$(2.110)$$

which explicitly does not contain the self interaction term $i = j$. Calculating the center of mass solution here just leads to the expected free evolution. Contrary, in the SN equation the self interaction term remains even for the center of mass, as well as single particle systems. As Adler pointed out in [4] the interpretation of the self interaction term needs careful consideration. In the case of two different particles, the interaction term is simply their gravitational interaction weighted with the probability of finding the particles at their respective positions. In the case of self interaction the particle at position $\mathbf{x}_i$ would feel the gravitational interaction of itself at $\mathbf{x}_i'$ weighted with the probability of finding the particle at $\mathbf{x}_i'$. This is a contradiction of the Born rule. Knowing the location of the particle, the probability to locate it on a different position should be zero. The interpretation of the wave function in this context becomes tied to the mass density. This also has drastic consequences for superposition states, since the additional nonlinear term introduces self interactions of the wave function. Any branch of the wave function now is a source of a gravitational attraction leading to soliton solutions. If one assumes a gaussian state with sufficient mass, then one can expect a self focusing of the wave function that counteracts the dispersion of the free evolution. As a first approximation to gain a qualitative understanding, as well as a rough guess of the parameters needed to observe such an effect

we will simply compare the acceleration of the dispersion of a wave packet with the gravitational acceleration expected for the associated mass.

Given an initial wave packet

$$\psi(r, t = 0) = \left(\pi\sigma^2\right)^{-\frac{3}{4}} e^{-\frac{r^2}{2\sigma^2}} \tag{2.111}$$

we want to gain an intuition for the order of magnitude at which we will expect the self interaction to dominate. Starting from the free evolution

$$\psi(r, t) = \left(\pi a^2\right)^{-\frac{3}{4}} \left(1 + \frac{i\hbar t}{m\sigma^2}\right)^{-\frac{3}{2}} e^{-\frac{r^2}{2\sigma^2\left(1 + \frac{i\hbar t}{m\sigma^2}\right)}} \tag{2.112}$$

we have the peak at $r_{peak} = \sigma\sqrt{1 + \frac{\hbar^2 t^2}{m^2\sigma^4}}$ and its acceleration $\ddot{r}_{peak} = \frac{\hbar^2}{m^2 r_{peak}^3}$. We can now compare this to the gravitational acceleration $\ddot{r} = \frac{Gm}{r^2}$ at time $t = 0$ which occurs due to the self interaction. The self interaction starts to dominate when the gravitational acceleration is at the same magnitude as the acceleration of the dispersion. From this we can calculate a mass $m = \left(\frac{\hbar^2}{G\sigma}\right)^{\frac{1}{3}}$. This is the critical mass at which the two accelerations exactly balance each other. For an initial width of $\sigma = 100nm$ we get a mass $m = 1.12 \cdot 10^{-17}kg$. As an example, let us consider a silicon sphere with density $\rho = 2329kg \cdot m^{-3}$. The radius of this sphere would be $r = 2.2 \cdot 10^{-7}m$. This would imply that the self interaction of a sphere of that radius and a wave packet spread of similar magnitude as its radius would be an approximately stationary solution. To make this calculation more rigorous, let us consider the following ansatz. According to Harrison [53] only negative total energy of the state can counteract the dispersion. Therefore, it can be used as a lower bound for the mass needed for collapse. First, the total energy as given by (2.109) can be written as

$$E = \frac{\hbar^2}{2m} \int |\psi(x, t)|^2 d^3x - \frac{Gm^2}{2} \int \int \frac{|\psi(x, t)|^2 |\psi(y, t)|^2}{||x - y||} d^3x d^3y \tag{2.113}$$

Calculating the total energy for a spherically symmetric wavefunction

$$E = \frac{2\pi\hbar^2}{m} \int_0^\infty dr \left(\partial_r \psi(r)\right)^2$$
$$- 8\pi Gm^2 \int_0^\infty dr \left(\int dr' \frac{r'^2}{r} \psi^2(r)\psi^2(r') + \int_r^\infty dr' r' \psi^2(r)\psi^2(r')\right) \tag{2.114}$$

and inserting our initial state (2.111)we arrive at

$$E = \frac{\hbar^2}{2m\sigma^4} - \frac{2Gm^2}{\sqrt{\pi}\sigma^3} \sinh^{-1}(1) \tag{2.115}$$

Now for the total energy to be negative initially, the mass has to fulfill

$$m > \left(\frac{\sqrt{\pi}\hbar^2}{4G\sigma \sinh^{-1}(1)}\right)^{\frac{1}{3}} \approx \left(\frac{\hbar^2}{2G\sigma}\right)^{\frac{1}{3}} \tag{2.116}$$

which leads to roughly the same estimate as in our crude example.

So far we have only used rough approximations and lower bounds. In order to get exact quantitative results, numerics are necessary. This was done by the author, along the lines of [26, 47] as an implementation in Mathematica. (Appendix A, mathematica)

The basic idea is to use a Crank-Nicholson scheme in spherically symmetric coordinates. The wave function $\psi(r\Delta\rho, t\Delta\tau)$ is discretized with step sizes $\Delta\rho, \Delta\tau$. The resulting differential equation becomes

$$e^{\frac{i\Delta\tau}{2\hbar}H}\psi(r\Delta\rho, (t+1)\Delta\tau) = e^{-\frac{i\Delta\tau}{2\hbar}H}\psi(r\Delta\rho, t\Delta\tau) \tag{2.117}$$

If we linearize the equation we get

$$\psi(r\Delta\rho, (t+1)\Delta\tau) = (Q^{-1} - \mathbb{1})\psi(r\Delta\rho, t\Delta\tau) \tag{2.118}$$

$$Q = \frac{1}{2}\left(\mathbb{1} + \frac{i\Delta\tau}{2\hbar}H\right) \tag{2.119}$$

If we solve $Q\chi(r\Delta\rho, t\Delta\tau) = \psi(r\Delta\rho, t\Delta\tau)$, we can then write the time evolution as

$$\psi(r\Delta\rho, (t+1)\Delta\tau) = \chi(r\Delta\rho, t\Delta\tau) - \psi(r\Delta\rho, t\Delta\tau) \tag{2.120}$$

The Schrödinger Newton equation cannot be seen as an intrinsic description of the measurement collapse. If the self interaction of the wave function would be responsible for a definite outcome in a measurement process, we would run into contradictions with the outcomes produced by the Born rule of measurement, mentioned above. This can be seen by looking at Pointer states attributed to measurement outcomes of a superposition. Consider the following state

$$\psi(\mathbf{r}) = \frac{1}{\sqrt{2}}\left(\psi_1(\mathbf{r}) + \psi_2(\mathbf{r})\right) \tag{2.121}$$

If we attribute Pointer states to the possible outcomes

$$\psi(\mathbf{r}, \mathbf{R}) = \frac{1}{\sqrt{2}} \left(\psi_1(\mathbf{r})\phi_1(\mathbf{R}) + \psi_2(\mathbf{r})\phi_2(\mathbf{R}) \right) \tag{2.122}$$

we can see that these Pointer states would carry appreciable mass and therefore would evolve according to the Schrödinger Newton equation. The corresponding final state would then be found at $\frac{R_1+R_2}{2}$ which would be the average position. This peculiar effect highlights the problem of taking the wave function as an effective mass distribution acting on itself through the potential V. Furthermore, since the Schrödinger Newton equation is fully deterministic, it cannot contain an explanation for the random outcomes in a measurement. In that sense, the Schrödinger Newton equation cannot be seen as an objective collapse of the wave function. We still need something similar to the Born rule to interpret the measurement results.

As with all deterministic nonlinear modifications that do not modify the measurement assumption, the Schrödinger Newton equation violates non-signaling [12]. This can be best seen by looking at the following gedankenexperiment. Consider a Stern-Gerlach experiment with a spin-position state. If we assume that the spin part of the state is not coupled to the position part of the wave function (the two evolutions of the spatial and spin wave function are separable), then after the Stern-Gerlach apparatus the state reads $\Psi(\mathbf{x}, t, \pm) = \psi_\pm(\mathbf{x}, t) \otimes |z_\pm\rangle$. The effect on the spatial part is governed by the Schrödinger Newton equation, and manifests itself as a self interaction that leads to a self focusing of the wave function. If we compare this to an initial state in spin x direction, we expect a state $\Psi(\mathbf{x}, t, \pm) = \frac{1}{\sqrt{2}} \left(\psi_+(\mathbf{x}, t) \otimes |x_+\rangle + \psi_-(\mathbf{x}, t) \otimes |x_-\rangle \right)$ after the apparatus. If we plug this into the Schrödinger Newton equation, we can see a gravitational interaction between the two directions associated with $|x_+\rangle$ and $|x_-\rangle$.

$$i\hbar \frac{\partial \psi_\pm(\mathbf{x}, t)}{\partial t} = -\frac{\hbar}{2m} \nabla^2 \psi_\pm(\mathbf{x}, t) - V(\psi_\pm, \mathbf{x}, t)\psi_\pm(\mathbf{x}, t) \tag{2.123}$$

$$V(\psi_\pm, \mathbf{x}, t) = \frac{Gm^2}{2} \int \frac{|\psi_+(\mathbf{x}, t)|^2}{||\mathbf{x} - \mathbf{y}||} d^3y + \frac{Gm^2}{2} \int \frac{|\psi_-(\mathbf{x}, t)|^2}{||\mathbf{x} - \mathbf{y}||} d^3y \tag{2.124}$$

Apart from the self focusing of ψ_+ and ψ_- there is also a mutual gravitational attraction between the two partial wave functions. Their distance on the screen in a Stern Gerlach experiment therefore is smaller in this basis compared to the $|z_\pm\rangle-$basis. This enables us to distinguish the two initial preparations. If we consider an entangled state, with two sides of Stern Gerlach measurements, measuring in one basis can now prepare the state for the other party in a distinguishable

way. This enables communication between the two parties independent of distance and hence faster than light.

The Schrödinger Newton equation is thus no exception of a non-linear deterministic quantum theory, in that it allows superluminal signaling.

One particularly interesting way of testing effects of the Schrödinger Newton equation was introduced by Huan Yang et. al. [103]. Instead of only considering the evolution without external potential of the wave function according to the Schrödinger Newton equation, we consider an additional harmonic potential. This assumption and the different timescales of the center of mass degree of freedom and the internal degrees of freedom allows for a separation of the center of mass equation.

$$i\frac{\partial \psi}{\partial t} = \left(-\frac{\nabla^2}{2M} + \frac{1}{2}M\omega_c^2 x^2 + \frac{1}{2}C(x - \langle x \rangle)^2 \right) \psi \tag{2.125}$$

with C a constant factor given by

$$C = -\frac{1}{2}\frac{\partial^2}{\partial x^2} \left[\int d^3y d^3z \frac{\rho_{\text{int}}(y)\rho_{\text{int}}(z)}{|y - z + x|} \right]_{x=0} \tag{2.126}$$

or for a homogeneous mass distribution: $C = GM\rho$. This lets us introduce the Schrödinger Newton frequency $\omega_{SN} = \sqrt{G\rho}$. Note that this frequency is independent of the mass of the test particle. To achieve higher frequencies, one would have to increase the density or drop the assumption of a homogeneous mass distribution. If the mass would be localized around the nucleus of the lattice positions, one would gain an amplification factor of $\Lambda = \left(\frac{d_{lattice}}{r_{nuclei}} \right)^3 \approx 10^3$.

One experimental setup then would be to study the time evolution of a squeezed initial state. We expect an additional phase $\Delta\phi = \omega_c t \left(\frac{\omega_{SN}^2}{\omega_c^2} \right)$ in the rotation of the phasespace ellipse.

In the next section, we will look at a different class of theories in order to circumvent the faster-than-light signaling, but still employ nonlinearities within the Schrödinger equation.

2.6   ADDITIONAL NOISE, COLLAPSE MODELS

We have discussed the effects of nonlinear modifications of quantum mechanics and the problems arising from it. We can see that in order to incorporate nonlinearities, we need to prevent the possibility of superluminal signaling. This can be done by adding an additional stochastic term. Models of these resulting nonlinear stochastic equations are typically known as collapse models.

2.6.1   *Properties of collapse models*

The first ideas of collapse models was published in 1985 [44] and subsequent years [42, 43]. These models were designed to answer the question of an objective transition of microscopic systems to macroscopic systems. Or in other words the transition from the unitary evolution of the state vector in quantum mechanics to the nonlinear collapse in measurements of quantum states. As we discussed before, nonlinear modifications of the Schrödinger equation can not describe this transition of microscopic to macroscopic systems. It also introduces the problem of superluminal signaling, which contradicts special relativity. Collapse models do not share the effect of superluminal signaling. In fact, the balance of nonlinear and stochastic additions precisely prevent superluminal signaling [13]. This property as well as their flexibility in introducing a specific mechanism for collapse make them an interesting toy model for regimes in which gravity related effects might enter. Also, if one entertains the idea that gravity is indeed a classical field, the coupling of a quantum field with a classical one would need a consistent description. Collapse models could be one of the candidates for such an endeavor. It should be mentioned here that collapse models themselves also suffer from some shortcomings, especially in the case of a generalization to relativistic properties. Thus, even if gravity is not quantized, collapse models do not provide a full description of dynamics in the relativistic regime. We will have a look at the issues later in this chapter.

On the other hand, if gravity is indeed a quantum field of some kind, the study of collapse models might still be interesting, albeit only to refine the region in which possible gravity effects might enter experiments. Experimental test based on collapse models can also be seen as tests for standard quantum theory. Ultimately, since the full description of quantum gravity (or something completely new) is still eluding physicists, giving more emphasis on experimental tests of unexplored regimes in order to discover a hint for further progress seems to be the way forward.

We want to start by introducing the mathematical backbone needed for the construction of collapse models, Ito stochastic calculus [39].

2.6.2 *Ito Stochastic Calculus*

In order to understand stochastic processes, we will start out by looking at the continuous version of a random walk, Brownian motion.

Let us start by assuming a Random Walk

$$\zeta_k = \sum_{k=1}^{t} \eta_k \tag{2.127}$$

with η being independent, identically distributed values and $\langle \eta_k \rangle = 0$ as well as $\langle \langle \eta_k^2 \rangle - \langle \eta_k \rangle^2 \rangle = 1$. In order to have a limited process over time we are going to rescale this random walk by replacing the spacing k with k/m such that

$$\zeta_k^m = c_m \cdot \zeta_k \tag{2.128}$$

with scaling constant $c_m > 0$. Now if our interval t is a multiple of $1/m$, the variance changes as

$$\langle \langle \eta_{mk}^2 \rangle - \langle \eta_{mk} \rangle^2 \rangle = c_m^2 \cdot \langle \langle \eta_k^2 \rangle - \langle \eta_k \rangle^2 \rangle = c_m^2 \cdot m \cdot t \tag{2.129}$$

In order to have a convergent process independent of spacing m, c_m has to be larger than $1/\sqrt{m}$. This allows us to define a process ζ_t^m such that

$$\zeta_t^m = \frac{1}{\sqrt{m}} \zeta_{mt} \tag{2.130}$$

whenever t is a multiple of $1/m$, and we interpolate between intervals. This new process has $\langle \zeta_t^m \rangle = 0$ and $\langle \langle \zeta_t^{m\,2} \rangle - \langle \zeta_t^m \rangle^2 \rangle = t$ for all t that are multiples of $1/m$. Furthermore, increments of this process over the interval $\{k/m, (k+1)/m\}$ obey

$$\zeta_{k+1}^m - \zeta_k^m = \frac{1}{\sqrt{m}} \left(\zeta_{m(k+1)} - \zeta_{mk} \right) \tag{2.131}$$

If we now consider the limit process of a continuous motion, the resulting process B_t should have independent increments $B_{k+1} - B_k$ for non-overlapping intervals with an expectation value of zero and a variance of $t_{k+1} - t_k$. But since our process is a sum of η_k with $\langle \eta_k \rangle = 0$ as well as $\langle \langle \eta_k^2 \rangle - \langle \eta_k \rangle^2 \rangle = 1$ and a rescaling, our increments of the process converge weakly towards a normal distribution

$$\zeta_{k+1}^m - \zeta_k^m \to N(0, t_{k+1} - t_k) \tag{2.132}$$

We can now formally define the process of Brownian motion as a probability distribution over the set of continuous functions $B : \mathbb{R} \to \mathbb{R}$ satisfying

1. $B(0) = 0$

2. $\forall s : s \in [0, t[\Rightarrow B(t) - B(s)$ is a normal distribution with mean 0 and variance $t - s$

3. Intervals $B_{t_k} - B_{s_k}$ are independent for non-overlapping intervals $\{t_k - s_k\}$

One of the key differences to a deterministic process is the difference in variance we get for Brownian motion. For a deterministic function we have

$$\sum_i \Delta f_i^2 \leq \sum \Delta t^2 \cdot \max f'^2 \leq \max f'^2 \cdot \sum_i \Delta t^2 \leq \max f'^2 \cdot \max \Delta t \cdot T$$

(2.133)

which approaches zero for $\max \Delta t \to 0$ in contrast to Brownian motion where the variance over an interval $\{0, T\}$ approaches T. Furthermore, Brownian motion is nowhere differentiable with probability 1. One has to be careful then to define the differential form dB_t. In particular, whenever we add Brownian noise to a system, for example by describing a stochastic property of a physical system in the form of a differential equation, we need to make sense of dB_t. On every point along a random walk there is no formal limit converging towards an interval dB_t. Let us first consider a function depending on B_t, $f(B_t)$. If we want to write the derivative of f we cannot use the derivative of B_t directly. However we can try to write this as

$$df = f'(B_t) \cdot dB_t$$

(2.134)

This statement should follow from the limit of the difference equation written as a Taylor expansion

$$f(x + \Delta x) - f(x) = \Delta x \cdot f'(x) + \frac{1}{2}(\Delta x)^2 \cdot f''(x) + \dots$$

(2.135)

where we can claim that the second order terms are negligible for $\Delta x \to 0$. But if we replace x by B_t we can see that $(\Delta B)^2$ does not approach zero in the limit but rather $\lim_{B_t \to 0}(\Delta B)^2 = \Delta t$ as defined by the variance of B_t. Because of this, we need to take the second order term into account which leads to

$$df = f'(B_t) \cdot dB_t + \frac{1}{2}f''(B_t) \cdot dt$$

(2.136)

where we used $dB_t^2 = dt$ (again from the variance). The equation (2.136) is known as Ito's Lemma. In order to see the correct way of

integrating over a Brownian motion consider the function $f(x) = \frac{1}{2}x^2$. If we use B_t, a stochastic variable, instead of a deterministic variable x, from Ito's Lemma it immediately follows that

$$df(B_t) = B_t dB_t + \frac{1}{2}dt \tag{2.137}$$

which, in integral form is

$$\int_0^T B_t dB_t = \frac{1}{2}B_T - \frac{T}{2}. \tag{2.138}$$

At this point, we want to look at another way of arriving at this result to gain some extra insight. The integral above can also be written as a sum similarly to the definition of a Riemann sum for continuous functions.

$$\int_0^T B_t dB_t = \lim_{k \to \infty} \sum_{k<n} B(t_k)\left(B(t_{k+1}) - B(t_k)\right) \tag{2.139}$$

We will use the following identity:

$$B(t_k) = \frac{1}{2}\left(B(t_{k+1}) + B(t_k)\right) - \frac{1}{2}\left(B(t_{k+1}) - B(t_k)\right) \tag{2.140}$$

Plugging this into our definition for the integral gives

$$\int_0^T B_t dB_t = \frac{1}{2}\sum_{k<n}\left(B^2(t_{k+1}) - B^2(t_k)\right) - \frac{1}{2}\sum_{k<n}\left(B(t_{k+1}) - B(t_k)\right)^2 \tag{2.141}$$

where the first term is simply $1/2(B_T)^2$ since $B_0 = 0$ and the second term is again the squared increment, giving $1/2 \cdot T$ as expected. It is important to note here that, contrary to the Riemann integral, the choice of interval matters in the initial definition. If we consider instead of $(B(t_{k+1}) - B(t_k))$ the interval $\frac{1}{2}\left(B(t_{k+1}) - B(t_{k-1})\right)$ we arrive at an integral of

$$\int_0^T B_t dB_t = \frac{1}{2}B_T \tag{2.142}$$

which gets a result closer to the Riemann definition for deterministic variables. The different choice of interval is known as Stratonovich calculus. Choosing the interval in the integration however, changes the properties of the result. For instance, only the Ito definition gives a martingale as a result for the integral. A martingale is a stochastic process that is defined through the independence of the conditional

expectation value of the next event from all previous events except the present value.

It is important to note that both definitions are interchangeable.

Some differences have to be pointed out when using Ito stochastic calculus in calculations. Consider the differential in normal calculus

$$df(t, x) = \frac{\partial f}{\partial t} dt + \frac{\partial f}{\partial x} dx \tag{2.143}$$

but now with B_t instead of x. The differential form becomes

$$df(t, B_t) = \left(\frac{\partial f}{\partial t} + \frac{1}{2} \frac{\partial^2 f}{\partial x^2} \right) dt + \frac{\partial f}{\partial x} dB_t \tag{2.144}$$

adding an additional term. Furthermore, if one considers two functions $f(t, B_t)$, $g(t.B_t)$ the differential of the product of two functions $d(f \cdot g)$ amounts to

$$d(f \cdot g) = f \cdot dg + g \cdot df + df \cdot dg \tag{2.145}$$

where the additional term $df \cdot dg$ arises. This term can be attributed again to the property of $(dB_t)^2 = dt$. This rule will come in handy for the next section. In terms of Stratonovich calculus, since the additional term in the integral vanishes, the above (2.145) can be written as

$$d(f \cdot g) = f \circ dg + g \circ df \tag{2.146}$$

which implies that the Stratonovich product is

$$f \circ dg = f \cdot dg + \frac{1}{2} df \cdot dg \tag{2.147}$$

If we now want to describe the transition from a differential equation in Ito form

$$df = a(t, f) \cdot dt + b(t, f) \cdot dB_t \tag{2.148}$$

one finds the corresponding Stratonovich form

$$df = \left(a(t, f) - \frac{b(t, f)}{2} \frac{\partial b(t, f)}{\partial f} \right) dt + b(t, f) \circ dB_t \tag{2.149}$$

With these mathematical tools, we will now derive a nonlinear stochastic time evolution in a quantum mechanics setting.

2.6.3 *A stochastic evolution of the state vector*

Using the above properties of Ito stochastic calculus, we will now look at the time evolution of a state vector when we introduce a stochastic process [9][14, 15, 45]. Such a process will act on the wave function as

$$d \left| \psi \right\rangle = \left(C \cdot dt + \sum_i A_i \cdot dB_i \right) \left| \psi \right\rangle \tag{2.150}$$

where C is an operator and the A_i are a set of operators. We will, for simplicity assume that the operators $A_i = \mathbf{A}$ are Hermitian operators. The B_i are a set of random Wiener processes, with the properties

$$\langle\langle dB_i \rangle\rangle = 0 \quad , \quad \langle\langle dB_i dB_j \rangle\rangle = \gamma \delta_{ij} dt \tag{2.151}$$

and a constant γ. It is important to note, that because of the above rule (2.145), the norm of $\left| \psi \right\rangle$ is not preserved. In order to define a process that has similar properties as the usual Schrödinger description, we have to incorporate the normalization of the state vector corresponding to a realization of our process B_t. We are interested in the state vectors $\left| \phi \right\rangle$, which are built from $\left| \psi \right\rangle$ and their probabilities are given by multiplying with the square norm $|| \left| \psi \right\rangle ||^2$. If we adopt this as our physical states, we can see that adding the norm into the description will give us the nonlinearity found in collapse models. The physical probability given a realization $B(t, t_0)$ then is

$$P_\phi(B(t, t_0)) = P_\psi(B(t, t_0)) || \left| \psi \right\rangle ||^2 \tag{2.152}$$

for a given realization of B_t. Now, because of the linearity of our stochastic evolution (2.150) this property has to hold up at all times. Therefore, we can write the relation between the probabilities given an infinitesimal change $P_\psi = P_\psi(dB_t), P_\phi = P_\phi(dB_t)$ as

$$P_\phi = P_\psi \left(1 + || d \left| \psi \right\rangle ||^2 \right) \tag{2.153}$$

But the assumption that we can do this process at any given time means that the total probability P_ϕ has to be 1, which implies that in order to have this property, the average of the norm $|| d \left| \psi \right\rangle ||^2$ has to be zero. We can now look at the differential change of the norm of $\left| \psi \right\rangle$, using that it should be zero on average with (2.145) and (2.150).

$$|| d \left| \psi \right\rangle ||^2 = (d \left\langle \psi \right|) \cdot \psi + \psi \cdot (d \left| \psi \right\rangle) + (d \left\langle \psi \right|) \cdot (d \left| \psi \right\rangle) \overset{!}{=} 0 \tag{2.154}$$

where we can extract that

$$C + C^\dagger = -\frac{1}{2} \gamma \mathbf{A}^2 \tag{2.155}$$

and write (2.150) as

$$d \left| \psi \right\rangle = \left[\left(C - C^\dagger \right) \cdot dt + \mathbf{A} \cdot dB - \gamma \mathbf{A}^2 \cdot dt \right] \left| \psi \right\rangle . \tag{2.156}$$

We can associate the anti-Hermitian part of the stochastic equation as our Hamiltonian operator $-i/\hbar\, H$.

We can rewrite the norm, now only depending on the stochastic part, as

$$d || \left| \psi \right\rangle ||^2 = 2 \left\langle \psi \right| \mathbf{A} \left| \psi \right\rangle \cdot dB \tag{2.157}$$

which also changes the physical probability distribution to $P_\phi = P_\psi (1 + 2 \left\langle \psi \right| \mathbf{A} \left| \psi \right\rangle \cdot dB)$ for an infinitesimal time step. In order to guarantee that the norm of our normalized state vectors $\left| \phi \right\rangle$ stays constant during their time evolution, we can see from (2.157) that replacing the operators $\mathbf{A}$ with $\mathbf{A} - \left\langle \phi \right| \mathbf{A} \left| \phi \right\rangle$ leads to the desired result, giving

$$d \left| \phi \right\rangle = \left[-\frac{i}{\hbar} H \cdot dt + (\mathbf{A} - \left\langle \phi \right| \mathbf{A} \left| \phi \right\rangle) \cdot dB - \gamma \left(\mathbf{A} - \left\langle \phi \right| \mathbf{A} \left| \phi \right\rangle \right)^2 \cdot dt \right] \left| \phi \right\rangle \tag{2.158}$$

for our physical state vector. We can see from this, that demanding a time evolution that is stochastic in nature, together with the normalization condition to extract the physical states leads to a nonlinear Schrödinger equation with the physical probabilities described by P_ϕ.

Using (2.149), we can also write this result in terms of Stratonovich calculus through the stochastic process $V(t)$ with the properties

$$\left\langle\!\left\langle V_i(t) \right\rangle\!\right\rangle = 0 \quad , \quad \left\langle\!\left\langle V_i(t_1), V_j(t_2) \right\rangle\!\right\rangle = \gamma \delta_{ij} \delta(t_2 - t_1) \tag{2.159}$$

giving

$$\frac{d}{dt} \left| \phi \right\rangle = \left[-\frac{i}{\hbar} H \right.$$
$$+ (\mathbf{A} - \left\langle \phi \right| \mathbf{A} \left| \phi \right\rangle) V(t) - \gamma \left(\mathbf{A} - \left\langle \phi \right| \mathbf{A} \left| \phi \right\rangle \right)^2$$
$$\left. + \gamma \left(\left\langle \phi \right| \mathbf{A}^2 \left| \phi \right\rangle - (\left\langle \phi \right| \mathbf{A} \left| \phi \right\rangle)^2 \right) \right] \left| \phi \right\rangle \tag{2.160}$$

with $B_t = \int_0^t V(\tau) d\tau$.

From (2.158) we can also calculate the density matrix representation by considering the equation for a projector $P_\phi = \left| \phi \right\rangle \left\langle \phi \right|$ which reads

$$
dP_\phi = \Bigg[-\frac{i}{\hbar} \left[P_\phi, H \right] \cdot dt
$$

$$
+ \left\{ \left(\mathbf{A} - \langle \phi | \, \mathbf{A} \, | \phi \rangle \right), P_\phi \right\} \cdot dB - \gamma \left[\mathbf{A}^2, P_\phi \right] \cdot dt + 2\gamma \mathbf{A} P_\phi \mathbf{A} \cdot dt \Bigg]
$$

$$(2.161)$$

and defining the density matrix of the ensemble average for a stochastic process B_t as $\langle\langle P_\phi \rangle\rangle_B$ which averages over the term $\{\ldots\} \cdot dB$ and thus gives

$$
\frac{d}{dt}\rho = -\frac{i}{\hbar} \left[\rho, H \right] - \gamma \left[\mathbf{A}, \left[\mathbf{A}, \rho \right] \right]
$$

$$(2.162)$$

which is independent of the specific decomposition of the density matrix.

2.6.4   *Continuous Spontaneous Localization (CSL)*

We derived the general form of collapse models which are driven by a brownian stochastic process. The next step will be to answer the question what the Hermitian operators **A** (see (2.150)) represent. The collapse of the wave function in these models was initially designed to explain the transition from quantum mechanics for microscopic systems to classical physics for macroscopic systems, meaning that the superpositions of macroscopic objects should be suppressed. Superpositions with probabilities of the form

$$|\psi(x, t = 0)|^2 = \frac{1}{2}\sqrt{\pi\sigma^2}e^{-\frac{(x-x_1)^2}{2\sigma^2}} + \frac{1}{2}\sqrt{\pi\sigma^2}e^{-\frac{(x-x_2)^2}{2\sigma^2}} \tag{2.163}$$

should localize at a position x_1 or x_2 at time scales such that microscopic superpositions are preserved over long periods of time, while macroscopic systems should localize rather quickly. The formulation of the time scale is kept vague on purpose to emphasize that this time scale depends on the chosen properties of our collapse model.

We will first introduce one of the most considered models, CSL (Continuous Spontaneous Localization) [13][14, 15, 32, 33, 42–44]. First, let us consider one particle with a given mass and describe its mass with a mass density operator

$$M(\mathbf{x}) = \frac{m}{m_0}\int d^3y \, g(\mathbf{x} - \mathbf{y})a^\dagger(\mathbf{y})a(\mathbf{y}) \tag{2.164}$$

where we introduce a smearing function

$$g(\mathbf{x}) = \left(\frac{\alpha}{2\pi}\right)^{3/2} e^{-\frac{\alpha}{2}\mathbf{x}^2} \tag{2.165}$$

of the mass of the particle. Notice that in doing so we introduce a free parameter into our model. Because of the normalization of this function we recover the total mass operator by integrating over the whole space $M = \int d^3x \, M(\mathbf{x})$. We can introduce this operator now into equation (2.158) to get

$$d\,|\phi\rangle = \left[-\frac{i}{\hbar}H \cdot dt + \int d^3x \, (M(\mathbf{x}) - \langle M(\mathbf{x})\rangle)\, dB(\mathbf{x})\right.$$
$$\left. -\frac{\gamma}{2}\int d^3x \, (M(\mathbf{x}) - \langle M(\mathbf{x})\rangle)^2\, dt\right]|\phi\rangle \tag{2.166}$$

and, as above, the corresponding master equation

$$\frac{d}{dt}\rho = -\frac{i}{\hbar}[\rho, H] - \gamma \int d^3x \, [M(\mathbf{x}), [M(\mathbf{x}), \rho]] \tag{2.167}$$

for the average over the stochastic process B_t. We can also redefine our properties of the stochastic process and absorb $g(\mathbf{x})$ into it yielding

$$\langle\langle dB(\mathbf{x})\rangle\rangle = 0 \quad , \quad \langle\langle dB(\mathbf{x})dB(\mathbf{y})\rangle\rangle = \gamma D(\mathbf{x} - \mathbf{y})\delta(\mathbf{x} - \mathbf{y})dt \quad (2.168)$$

with $D(\mathbf{x}) = \left(\frac{\alpha}{4\pi}\right)^{3/2} e^{-\frac{\alpha}{4}\mathbf{x}^2}$. The parameter $\lambda = \gamma \left(\frac{\alpha}{4\pi}\right)^{3/2}$ is often used instead of the parameter γ and has units of frequency. Also $r_c = \frac{1}{\sqrt{\alpha}}$ with unit of length is often preferred in the literature. As can be seen from this, the CSL model has two free parameters.

We will also introduce the position representation for the density operator which is

$$\frac{d}{dt} \langle\mathbf{x}| \rho |\mathbf{y}\rangle = -\frac{i}{\hbar} \langle\mathbf{x}| [H,\rho] |\mathbf{y}\rangle - \lambda \left(1 - e^{-\frac{(\mathbf{x}-\mathbf{y})^2}{4r_c^2}}\right) \langle\mathbf{x}| \rho |\mathbf{y}\rangle \quad (2.169)$$

This can easily be generalized for multiple particles by summing over individual particle mass operators $M(\mathbf{x})$. The above form shows how CSL is suppressing off diagonal terms in the density matrix with frequency λ and collapse width r_c. We want to emphasize here the difference to standard decoherence models. The suppression of off-diagonal elements here is similar to the representation in the master equation (2.40). The effect of collapse however, is not an ensemble effect, given by the interaction with an environment, but an intrinsic property of the model on the state vector level. The collapse of the wave function as a measurement property (the von-Neumann rule) is absorbed into the evolution. The resulting state vector equation is nonlinear.

2.6.5 *Collapse from gravity*

The connection of stochastic properties of the quantum state evolution
and gravity was already made as early as 1966 by Karolyhazy [60,
61], who noted that in order to have a transition between a quantum
mechanical time evolution and the classical properties of general
relativity one has to consider uncertainty relations in position and
time for trajectories in Minkowski space (e.g. world lines). We want to
introduce the basic argument here, following [37].

First, we will consider the world line segment $s = cT$, which is
considered in a reference frame such that $|\mathbf{v}| = 0$ over the whole
interval. The overall spread of a wave function initially is considered
to be Δx_0. Now the uncertainty of position and velocity of the object
has to obey

$$\Delta x \Delta v \geq \frac{\hbar}{2M} \tag{2.170}$$

From there we can write the corresponding minimum spread in
position after time T as

$$\Delta x = \Delta v T \approx \frac{\hbar}{2M\Delta x_0 c}cT \tag{2.171}$$

We also note that the spread Δx should not be smaller than the
corresponding gravitational Schwarzschild radius GM/c^2. Using this
property and assuming the minimum spread $\Delta x = \Delta x_0$ after time T
at the end points of our world line segment as well as the fact that
these spreads also represent the minimum spread of the segment itself,
$\Delta s = \Delta x$, we can calculate an expression for the uncertainty $(\Delta x)^2$.

$$(\Delta x)^2 = (\Delta s)^2 \approx \frac{\hbar}{2Mc}cT = \frac{\hbar G}{2\Delta s c^3}s \tag{2.172}$$

$$(\Delta s)^2 \approx \left(\frac{\hbar G}{c^3}\right)^{2/3} s^{2/3} \tag{2.173}$$

Or, equivalently, if we use $s = cT$ we can write

$$(\Delta T)^2 \approx \left(\frac{\hbar G}{c^5}\right)^{2/3} T^{2/3} \tag{2.174}$$

giving the uncertainty for an interval T. We are also interested in
the uncertainty for the synchronization of two world lines separated
by a distance r, both at the same velocity $|\mathbf{v}| = 0$. This corresponds to

accumulating an uncertainty over a time interval $2T = \frac{2r}{c}$. Using this, we arrive at

$$(\Delta T)^2_{syn} \approx \left(\frac{\hbar G}{c^5}\right)^{2/3} \left(\frac{r}{c}\right)^{2/3} \tag{2.175}$$

Now, these uncertainties should correspond to the spread of suitable operators of time. We will therefore define the mean value of a time operator $\hat{t}(\mathbf{x}, t)$ as

$$\langle \hat{t}(\mathbf{x}, t) \rangle = t \tag{2.176}$$

and for convenience $\hat{t}(\mathbf{x}, t) = t - \hat{\tau}(\mathbf{x}, t)$ with $\langle \hat{\tau} \rangle = 0$. Accordingly, our time interval becomes $T = \langle \hat{t}(\mathbf{x}, t') - \hat{t}(\mathbf{x}, t) \rangle = t' - t$, and our uncertainty

$$(\Delta T)^2 = \langle (\hat{t}(\mathbf{x}, t') - \hat{t}(\mathbf{x}, t) - T)^2 \rangle =$$

$$\langle ((\hat{\tau}(\mathbf{x}, t') - \hat{\tau}(\mathbf{x}, t))^2 \rangle \approx \left(\frac{\hbar G}{c^5}\right)^{2/3} T^{2/3}. \tag{2.177}$$

We can do the same for two world points at the same time t but different positions $\mathbf{x}', \mathbf{x}$ with $r = |\mathbf{x}' - \mathbf{x}|$ to get a similar expression

$$(\Delta T)^2_{syn} = \langle ((\hat{\tau}(\mathbf{x}', t) - \hat{\tau}(\mathbf{x}, t))^2 \rangle \approx \left(\frac{\hbar G}{c^5}\right)^{2/3} \left(\frac{r}{c}\right)^{2/3}. \tag{2.178}$$

It is important to note that the association of an operator with time as done here, has distinct consequences on the evolution of wave functions in the Schrödinger equation. This can be seen by considering the global phase associated with the mass of an object, which in the standard Schrödinger evolution does not contribute to any physical observable

$$e^{i\Phi(t)} = e^{-\frac{ic^2}{\hbar} \sum_k M_k t} \tag{2.179}$$

However, we see that in our identification of an operator with our parameter of time, we now have to write

$$e^{i\Phi(t)} e^{i\hat{\Phi}(\mathbf{x}, t)} = e^{-\frac{ic^2}{\hbar} \sum_k M_k (t + \hat{\tau}(\mathbf{x}, t))} \tag{2.180}$$

introducing a phase contribution depending on position. We can write the uncertainty in phase

$$\Delta_\Phi(\mathbf{x}', \mathbf{x}, t) = \langle (\hat{\Phi}(\mathbf{x}', t) - \hat{\Phi}(\mathbf{x}, t))^2 \rangle =$$

$$= \frac{c^4}{\hbar^2} \sum_{k,l} M_k M_l \langle (\hat{\tau}(\mathbf{x}'_k, t) - \hat{\tau}(\mathbf{x}_k, t))(\hat{\tau}(\mathbf{x}'_l, t) - \hat{\tau}(\mathbf{x}_l, t)) \rangle \tag{2.181}$$

and finally using (2.178)

$$\Delta_\Phi(\mathbf{x}', \mathbf{x}, t) = \left(\frac{\hbar G}{c^5}\right)^{2/3} \frac{c^2}{\hbar^2} \sum_{k,l} M_k M_l \left(|x'_k - x_l|^{2/3}\right.$$
$$\left. -\frac{1}{2}|x'_k - x'_l|^{2/3} - \frac{1}{2}|x_k - x_l|^{2/3}\right) \quad (2.182)$$

where we have effectively no time dependence anymore. The relative phase uncertainty introduced here is only dependent on the distance $r = |\mathbf{x}' - \mathbf{x}|$ and can be interpreted as follows: As long as $\Delta_\Phi \ll \pi \approx 1$ the wave functions depending on position are very much coherent to each other, the time evolution coincides with the standard Schrödinger evolution. However, if $\Delta_\Phi \gg \pi \approx 1$ we have no coherent evolution of the wave function anymore, and expect a mostly classical evolution. This can be made more precise by introducing coherent cells, defined by the transition point $\Delta_\Phi \approx 1$ where the quantum to classical transition is expected. We can write the uncertainty in phase for a single particle as

$$\Delta_\Phi(a = |\mathbf{x}' - \mathbf{x}|) = \left(\frac{\hbar G}{c^5}\right)^{2/3} \frac{1}{L_{compton}} a^{1/3} \quad (2.183)$$

with $L_{compton} = \frac{\hbar}{Mc}$. For $\Delta_\Phi \approx 1$ we get a critical length a_c:

$$a_c = L^3 \left(\frac{\hbar G}{c^5}\right)^{-4/3} \quad (2.184)$$

For systems built up by multiple indistinguishable particles we have to consider two regimes, $a \ll R$ for R being the characteristic radius of the composite system, and $a \gg R$. If a displacement of center of mass is then a displacement of each individual constituent by a, we can just consider the center of mass displacement and sum over the number of involved particles N. In the case of $N \gg 1$, we can then replace the sum with an integral

$$\Delta_\Phi(\mathbf{x}', \mathbf{x}) = \left(\frac{\hbar G}{c^5}\right)^{2/3} \frac{M_0^2 c^2}{\hbar^2} \frac{N^2}{V^2} \int d^3r\, d^3r' \left(|\mathbf{r}' - \mathbf{r} - a|^{2/3} - |\mathbf{r}' - \mathbf{r}|^{2/3}\right) \quad (2.185)$$

which for $a \gg R$ amounts to an integral over $a^{2/3}$ since $a \gg |\mathbf{r}' - \mathbf{r}|$ and therefore

$$\Delta_\Phi(\mathbf{x}', \mathbf{x}) \approx \left(\frac{\hbar G}{c^5}\right)^{2/3} \frac{a^{1/3}}{L} \quad (2.186)$$

with $L = \frac{\hbar}{M_0 Nc} = \frac{\hbar}{Mc}$ the Compton wavelength corresponding to the total mass. For the case $a \ll R$ we expand $|\mathbf{r}' - \mathbf{r} - a|^{2/3}$ as a taylor series to see that the leading term is proportional to a^2. We arrive at

$$\Delta_\Phi(\mathbf{x}', \mathbf{x}) = \left(\frac{\hbar G}{c^5}\right)^{4/3} \frac{1}{R^{2/3}} \frac{a}{L} \tag{2.187}$$

for the relative phase. Again we can calculate the critical length a_c for these cases by putting $\Delta_\Phi \approx 1$. The resulting expressions for a_c mark the boundary for the quantum to classical transition. In the case of $a_c \gg R$ the center of mass wave function can have an uncertainty of up to a_c, much larger than R without experiencing decoherence. On the other hand, if $a_c \ll R$ if the wave function has an uncertainty of the order of R or larger the decoherence becomes dominant, effectively creating a classical time evolution.

2.6.6 *Penrose Model*

One possible cause for a change of the usual unitary behavior of quantum mechanics could be due to a gravitational effect. Diosi and Penrose [33, 79] introduced a model, which links the collapse of the wavefunction to the inability to superpose different space times. Since for every state with a sufficient mass, a superposition state would take the form

$$\lambda |\psi\rangle |G_\psi\rangle + \mu |\phi\rangle |G_\phi\rangle \tag{2.188}$$

where $|G_\psi\rangle$ and $|G_\phi\rangle$ denote the state of the stationary gravitational field with all its internal degrees of freedom. Since there is a superposition of different states of the gravitational field, Penrose argues that we have a superposition of two spacetime geometries. In that context, the meaning of a stationary state is not well defined anymore, since different space times lead to different time evolution operators. The difference between these two spacetimes can, according to Penrose, be quantified by the difference of the two gravitational potentials integrated over 3-space for a constant t.

$$\Delta E = \int (\nabla \Phi - \nabla \Phi')^2 d^3 x =$$
$$- 4\pi G \iint \frac{(\rho(\mathbf{x}) - \rho(\mathbf{x'}))(\rho(\mathbf{y}) - \rho(\mathbf{y'}))}{|\mathbf{x} - \mathbf{y}|} d^3 x d^3 y \tag{2.189}$$

A similar conclusion was drawn by Diosi, who incorporated this idea within the framework of collapse models [33]. From this quantity, a typical collapse time for a given mass can be calculated, which is just $t = \frac{\hbar}{\Delta E}$.

2.6.7 *Diosi-Penrose Model*

As seen above, motivations for a modification of quantum mechanics can be found by incorporating properties of gravity into the theory. Another approach along the lines of Karolyhazy was introduced by Diosi [31]. Similar to above, we start with an uncertainty relation, the uncertainty relation for the Newtonian gravitational field.

Different to the above assumption we take the minimum spread in (2.171) as given by the size of a clock traveling along the world line $\Delta x_0 \approx R$. The resulting expression changes to

$$(\Delta s)^2 \approx \frac{\hbar G}{c^3} \frac{s}{R} \tag{2.190}$$

If we now consider the uncertainty of the metric tensor g_{ab} of a weak gravitational field, we have only one component different from the

Minkovski metric: $g_{00} = 1 - 2\phi/c^2$. In a flat background the average of the potential $\phi = 0$ and the term in g_{00} only represents the fluctuations of the metric. Over an interval T the contribution of fluctuations is simply the space and time average of the fluctuations of the metric

$$\langle\langle\Delta g_{00}\rangle\rangle_{R,t} \approx \langle\langle\phi\rangle\rangle_{R,t}/c^2 \cdot s \approx \Delta s \tag{2.191}$$

Combining (2.190) and (2.191) finally gives us the minimum uncertainty

$$\langle\langle\phi\rangle\rangle_{R,t} = \sqrt{\frac{\hbar G}{RT}}$$

This uncertainty gives way for an interpretation of the potential $\phi(\mathbf{x},t)$ as a stochastic variable. In doing so, one can propose the properties

$$\langle\phi(\mathbf{x},t)\rangle = 0 \tag{2.192}$$

and

$$\langle(\nabla\phi(\mathbf{x},t)^2)\rangle - \langle\nabla\phi(\mathbf{x},t)\rangle^2 \approx \frac{\hbar G}{R^3\pi T} \tag{2.193}$$

which for the additional assumption of a white noise stochastic variable gives the correlation function

$$\langle\phi(\mathbf{x},t)\phi(\mathbf{x}',t')\rangle = \hbar G|\mathbf{x}-\mathbf{x}'|^{-1}\delta(t-t') \tag{2.194}$$

for the gravitational potential. The corresponding Schrödinger equation is then given by

$$\frac{d\psi}{dt} = -\frac{i}{\hbar}\left(H_0 + \int d^3x\,\phi(\mathbf{x},t)M(\mathbf{x})\right)\psi \tag{2.195}$$

with the mass operator $M(\mathbf{x})$. Now since the potential ϕ is a stochastic variable, it is natural, as in the CSL model, to look at the master equation for the density operator ρ, where $\rho = \langle\psi\psi^\dagger\rangle$ is the average over the stochastic process. From there we can use our correlation (2.194) to calculate the master equation

$$\frac{d}{dt}\rho = -\frac{i}{\hbar}[H_0,\rho] - \frac{G}{2\hbar}\int d^3x d^3x'\frac{1}{|\mathbf{x}-\mathbf{x}'|}[M(\mathbf{x}),[M(\mathbf{x}),\rho]] \tag{2.196}$$

As above we will look at the position representation of this equation which turns out to be

$$\left\langle X|\frac{d}{dt}\rho|Y\right\rangle = -\frac{i}{\hbar}\langle X|[H_0,\rho]|Y\rangle - \frac{1}{\tau(X,Y)}\langle X|\rho|Y\rangle \tag{2.197}$$

where the factor $1/\tau(X, Y)$ is given by

$$\frac{1}{\tau(X, Y)} = \frac{G}{2\hbar} \int d^3x d^3x' \frac{(M_X(\mathbf{x}) - M_Y(\mathbf{x})(M_X(\mathbf{x}') - M_Y(\mathbf{x}')}{|\mathbf{x} - \mathbf{x}'|} \qquad (2.198)$$

and $M_X(\mathbf{x})$ is the mass density corresponding to a configuration given by a state $|X\rangle$. One possible representation would be to look at spherical objects with mass M and radius R, and use center of mass coordinates. Our mass density function can then be written as a homogeneous mass distribution over the whole sphere

$$M_X(\mathbf{x}) = \frac{m}{V}\theta(R - |\mathbf{x} - X|) \qquad (2.199)$$

which, when plugged into our definition for the dampening factor (2.198) yields

$$\frac{1}{\tau(X, Y)} = \hbar \frac{1}{(U(|X - Y|) - U(0))} \qquad (2.200)$$

where $U(\mathbf{r})$ is the gravitational pair potential [79]

$$U(\mathbf{r}) = -Gm^2 \int_{z,z' \leq R} \frac{d^3z d^3z'}{|z - z' + \mathbf{r}|} \qquad (2.201)$$

and can be approximated in the regime of $\mathbf{r} \ll R$ and $\mathbf{r} \gg R$ with

$$\begin{cases} U(\mathbf{r}) \approx -\frac{Gm^2}{R}\left(\frac{6}{5} - \frac{1}{2}\frac{r^2}{R^2}\right) & |\mathbf{r}| \ll R \\ U(\mathbf{r}) \approx -\frac{Gm^2}{|\mathbf{r}|} & |\mathbf{r}| \gg R \end{cases} \qquad (2.202)$$

To put this model into context with the above introduced stochastic models and their formalism, we will also introduce here an alternative formulation leading to the same evolution of the density operator ρ. As above, we introduce a white noise field B_t with

$$\langle\langle dB(\mathbf{x})\rangle\rangle = 0 \quad , \quad \langle\langle dB(\mathbf{x})dB(\mathbf{y})\rangle\rangle = \frac{G}{\hbar}\frac{1}{|\mathbf{x} - \mathbf{y}|}dt \qquad (2.203)$$

where the correlation function is similar to (2.194) and we can write the stochastic equation

$$d|\psi\rangle = \left[-\frac{i}{\hbar}Hdt - \frac{G}{2\hbar}\int d^3x d^3y \frac{1}{|\mathbf{x} - \mathbf{y}|} \right.$$
$$(M(\mathbf{x}) - \langle\psi| M(\mathbf{x}) |\psi\rangle)(M(\mathbf{y}) - \langle\psi| M(\mathbf{y}) |\psi\rangle)dt$$
$$\left. + \int d^3x (M(\mathbf{x}) - \langle\psi| M(\mathbf{x}) |\psi\rangle)dB(\mathbf{x}) \right]|\psi\rangle \qquad (2.204)$$

which yields the same master equation (2.196) for the averaged density operator ρ.

This type of collapse models seems to be parameter free, giving a complete description of the state vector collapse embedded in the standard quantum evolution. However, this is not true. The model still requires an implicit parameter, a length scale describing the confinement of the mass distribution. As we will discuss in the next part, this model does not conserve energy. In fact, the energy increase in this model is unacceptably high. This can be seen by calculating

$$\langle H \rangle = Tr\left(H\rho(t)\right)$$

using (2.196). The resulting energy increase is [42]

$$\frac{d\langle H \rangle}{dt} \approx \frac{G\hbar m}{R^3}$$

which gives $d_t\langle H \rangle \approx 10^{-26} J/s$ for a single nucleon. In case of a macroscopic object with $n \approx 10^{23}$ particles the energy increases proportionally, giving $d_t\langle H \rangle \approx 10^{-3} J/s$. This enormous energy increase was not detected in any experiments.

2.6.8 *Energy non-conservation*

As we have seen above, the additional mechanism of collapse leads to an energy increase on average [42]. This can be pictured by the idea that every interaction with the noise field can be interpreted as a "kick" to the system that changes its momentum on average. The decoherence term is similar to the one in (2.40) but the dissipation term in collapse models is missing. This term is crucial in standard decoherence to dissipate energy to the environment, leading to a state of equilibrium. Since there is no explicit environment in collapse models, the energy is trapped in the system. This leads to a non-conservation and increase of energy.

In order to find an expression for this increase, we will return to equation (2.169), following from our master equation

$$\frac{d}{dt}\rho = -\frac{i}{\hbar}\left[\rho, H\right] - \gamma \int d^3x \left[M(\mathbf{x}), \left[M(\mathbf{x}), \rho\right]\right] \tag{2.205}$$

for the CSL model. We will restrict ourselves to one dimension for simplicity here, giving the equation in position representation

$$\frac{d}{dt}\langle x| \rho |y\rangle = -\frac{i}{2\hbar m}\left(\frac{\partial^2}{\partial x^2} - \frac{\partial^2}{\partial y^2}\right)\langle x| \rho |y\rangle - \lambda\left(1 - e^{-\frac{(x-y)^2}{4r_c^2}}\right)\langle x| \rho |y\rangle \tag{2.206}$$

for the time evolution of the density matrix. The formal solution of this equation is given by [43]

$$\langle x| \rho |y\rangle = \frac{1}{2\pi\hbar}\int_{-\infty}^{\infty} dk \int_{-\infty}^{\infty} dz\, e^{-\frac{i}{\hbar}kz} F(k, x-y, t)\langle x+z| \rho_s |y+z\rangle \tag{2.207}$$

with

$$F(k, x, t) = \exp\left(-\lambda t\left(1 - \frac{1}{t}\int_0^t d\tau\, e^{\frac{(x-k\tau/m)^2}{2r_c^2}}\right)\right) \tag{2.208}$$

a characteristic function with properties $F(0,0,t) = 1$, $\partial_k F(0,0,t) = 0$, $\partial_q F(0,0,t) = 0$, $\partial_k^2 F(0,0,t) = -\frac{\lambda}{6m^2 r_c^2}t^3$, $\partial_q^2 F(0,0,t) = -\frac{\lambda}{2r_c^2}t$ and $\partial_q(\partial_k F(0,0,t)) = \frac{\lambda}{4r_c^2}t^2$. ρ_s signifies the solution of the standard Schrödinger equation without the additional collapse term. For $\lambda = 0$ we recover the solution $\langle x| \rho |y\rangle = \langle x| \rho_s |y\rangle$. From this, calculating the expectation values of $\hat{x}$ and $\hat{p}$ can be done rather easily through calculating the trace $Tr(\hat{x}\rho)$, which leads to the expressions

$$\langle \hat{x}\rangle = \langle \hat{x}\rangle_s \tag{2.209}$$

$$\langle \hat{x}^2 \rangle = \langle \hat{x}^2 \rangle_s + \frac{\lambda}{6m^2 r_c^2} t^3 \qquad (2.210)$$

$$\langle \hat{p} \rangle = \langle \hat{p} \rangle_s \qquad (2.211)$$

$$\langle \hat{p}^2 \rangle = \langle \hat{p}^2 \rangle_s + \frac{\lambda}{2r_c^2} t \qquad (2.212)$$

for the expectation values and squared expectation values respectively. This implies that the variances have deviations from the standard Schrödinger evolution. The variance of the momentum operator also implies that

$$\langle E \rangle = \frac{\langle \hat{p}^2 \rangle}{2m} = \langle E \rangle_s + \frac{\lambda}{4m r_c^2} t \qquad (2.213)$$

which increases linearly in time. The given result here is for a single particle. However, it can be shown that the same result holds for multiple particles and scaling with the mass of the system.

To give an alternative way of reaching this result, we will calculate the transition of a system with energy $E_i = \hbar \omega_i$ initially to an energy $E_f = \hbar \omega_f$ after the collapse interaction has taken place. A similar calculation was done in [7] using the idea, that the collapse effect can be written as a perturbation on the Hamiltonian that describes the time evolution of the system (see also [6]). This can be done due to a curious ambiguity in the representation of the density matrix. If the additional noise term is chosen to be either imaginary or real valued on the state vector level the density matrix representation remains the same. However, on the level of the state vector, choosing an imaginary noise does not result in a collapse representation. Nevertheless, the change of the energy rate of the system remains the same in both descriptions, giving us a tool to calculate the change in energy through perturbation of the Hamiltonian.

In order to see this, let us consider the following generalization of (2.158) of the state vector evolution

$$\begin{aligned} d \left| \phi \right\rangle = \Big[&-\frac{i}{\hbar} H \cdot dt + (\chi \mathbf{A} - \chi_{Re} \left\langle \phi \right| \mathbf{A} \left| \phi \right\rangle) \cdot dB \\ &- \gamma \left(|\chi|^2 \mathbf{A}^2 - 2\chi\chi_{Re} \mathbf{A} \left\langle \phi \right| \mathbf{A} \left| \phi \right\rangle + \chi_{Re} \left(\left\langle \phi \right| \mathbf{A} \left| \phi \right\rangle \right)^2 \right) \cdot dt \Big] \left| \phi \right\rangle \end{aligned}$$

$$(2.214)$$

with an additional phase factor of $\chi = \chi_{Re} + i\chi_{Im}$. Now continuing with calculating the stochastic average of an operator P_ϕ to get the master equation we get

$$\frac{d}{dt}\rho = -\frac{i}{\hbar}[\rho, H] - \gamma|\chi|^2[\mathbf{A}, [\mathbf{A}, \rho]] \tag{2.215}$$

which only depends on the absolute value of χ. This means that we can choose $\chi = i$ and simplify our state vector evolution equation without changing its physical predictions. Specifically, the evolution equation of the state vector becomes linear, meaning the terms containing the averages $\langle\phi|\mathbf{A}|\phi\rangle$ drop out. This also lets us rewrite the Hamiltonian by incorporating the stochastic part which reads

$$d|\phi\rangle = \left[-i\left(\frac{1}{\hbar}H - \mathbf{A}\frac{dB}{dt}\right) \cdot dt - \gamma\mathbf{A}^2 \cdot dt\right]|\phi\rangle \tag{2.216}$$

and resulting in the Hamiltonian $H + H_p = H - \mathbf{A}\frac{dB}{dt}$. We can use this to rewrite the Hamiltonian for the effective CSL model with $\chi = i$, giving us [6]

$$H_p = -\int d^3x M(\mathbf{x})\frac{dB(\mathbf{x})}{dt} \tag{2.217}$$

where we used $M(\mathbf{x})$ from (2.165) and our usual noise defined by (2.151) and the stochastic average of $\frac{dB(\mathbf{x})}{dt}\frac{dB(\mathbf{x})}{dt'}$ given by

$$\left\langle\left\langle\frac{dB(\mathbf{x})}{dt}\frac{dB(\mathbf{y})}{dt'}\right\rangle\right\rangle = \frac{\gamma}{2\pi}\int_{-\infty}^{\infty}e^{-\omega(t-t')}\delta^3(\mathbf{x}-\mathbf{y}) \tag{2.218}$$

which reduces to (2.151) through integration over t'. From this we can write down the transition amplitude associated with our perturbation

$$z_{fi}(t) = -\frac{i}{\hbar}\int_0^t H_p e^{i\omega_{fi}t'}dt' \tag{2.219}$$

which we can now use to calculate the expectation value with respect to the noise of our energy $\langle\langle E(t)\rangle\rangle = \langle\langle\sum_f \hbar\omega_{fi}|z_{fi}(t)|^2\rangle\rangle$. Since we are only interested in the energy increase for white noise, our calculation simplifies compared to [7] in that our collapse parameter λ is independent of ω. This simplifies the noise term $\frac{dB}{dt}$ and we arrive at the energy gain rate

$$t^{-1}\langle\langle E(t)\rangle\rangle = \frac{r_c^3}{\pi^{3/2}m_n^2}\int d^3y \sum_f e^{-r_c^2y^2}\lambda\hbar\omega_{fi}\left|\left(\sum_l m_l e^{i\mathbf{y}\cdot\mathbf{x}_l}\right)_{fi}\right|^2 \tag{2.220}$$

for large   timescales t. In order to evaluate the matrix element $\sum_l m_l e^{i\mathbf{y} \cdot \mathbf{x}_l}$ we consider the simplest case of only one family of atoms in a lattice, such that the masses of every lattice point are identical. We also notice that due to the exponent $e^{-r_c^2 y^2}$ in (2.220) every displacement smaller than r_c will be suppressed. If we now transfer into coordinates that represent the unperturbed position and displacements, e.g. $\mathbf{x}_l = \mathbf{r}_l + \mathbf{u}_l$ we can see that displacements will be suppressed and we can replace the part $e^{i\mathbf{y} \cdot \mathbf{u}_l}$ through its taylor expansion $e^{i\mathbf{y} \cdot \mathbf{u}_l} \approx 1 + i\mathbf{y} \cdot \mathbf{u}_l$. The displacement $\mathbf{u}_l$ represents the phonons in our lattice and we can write it in terms of creation and annihilation operators. Again, following the notation of [7] and assuming that we initially are in the zero phonon state, we get

$$\mathbf{u}_l = \frac{\Omega}{8\pi^3}(\hbar M)^{1/2} \sum_j \int \frac{d^3 k}{(2\omega_j(\mathbf{k}))^{1/2}} \mathbf{e}^{*(j)}(\mathbf{k}) e^{i\mathbf{k} \cdot \mathbf{r}_l} a_j^\dagger(\mathbf{k}) \qquad (2.221)$$

neglecting $a_j(\mathbf{k})$. Ω represents the unit cell volume. Evaluating all the integrals and using $\sum_l e^{i(\mathbf{q}-\mathbf{k}) \cdot \mathbf{r}_l} = \frac{8\pi^3}{\Omega} \delta^3(\mathbf{q} - \mathbf{k})$ we finally arrive at

$$\langle\langle E(t) \rangle\rangle = \frac{3}{4} \frac{\hbar^2 \lambda M}{m_N^2 r_c^2} t \qquad (2.222)$$

for the energy gain rate. This linear increase in energy over time is a distinct feature of collapse models with white noise and introduces a way of testing these models by searching for this heating effect in isolated quantum systems. We will come back to experiments searching for this effect in the later chapters.

2.6.9   *Modifications to accommodate energy conservation*

As we have seen in the last part, collapse models do not conserve energy. However, this "flaw" in the model can be overcome by considering more complex approaches. Let us introduce two variants of how this can be done. The first we are going to talk about will be the introduction of non-white noise instead of the usual white noise assumption.

One important property of white noise is, that it is Markovian, since its correlation function is zero for any nonzero time interval. So, modifying the underlying noise will result in a non-Markovian model [78]. Now, how can a non-white noise influence the expectation value of the energy gain? Let us consider the above calculation for white noise (2.151) and its correlations. We introduce a dependence of γ on frequency so we can write the stochastic average of $\frac{dW(\mathbf{x})}{dt}\frac{dW(\mathbf{x})}{dt'}$ as [7]

$$\left\langle\left\langle \frac{dW(\mathbf{x})}{dt}\frac{dW(\mathbf{y})}{dt'} \right\rangle\right\rangle = \frac{1}{2\pi}\int_{-\infty}^{\infty} \gamma(\omega)e^{-\omega(t-t')}\delta^3(\mathbf{x}-\mathbf{y}) \quad (2.223)$$

and thus introduce a colored correlation. As we mentioned above, this hinges on the property to replace the underlying dynamics of collapse models with a description of an effective linear stochastic equation that recovers the same properties of the master equation as the collapse stochastic equation does. That this is in fact the case was shown in [4], where this property holds for a first order approximation in γ. The effective linear stochastic evolution equation reads

$$d\left|\phi\right\rangle = \left[-\frac{i}{\hbar}H + \chi\mathbf{A}dW(\mathbf{x}) - 2\sqrt{\gamma}\chi_{Re}\mathbf{A}\int_0^t ds D_{ij}(t,s)\frac{\delta}{\delta\frac{dW(\mathbf{x})}{ds}} \right]\left|\phi\right\rangle$$
$$(2.224)$$

where the last part in the integral is the functional derivative with respect to the noise field $\frac{dW(\mathbf{x})}{dt}$. The last part in this effective equation is related to the fact that we need to have a normalized expectation value with respect to the noise dW. This implies that the last part in (2.224) comes about through the Furutsu-Novikov formula, to give the general form of an expectation value of a functional times the noise $\frac{dW}{dt}$. With this equation, one can show [4] that to first order in γ this leads to a master equation of the form

$$\frac{d}{dt}\rho = -\frac{i}{\hbar}[H,\rho] + |\chi|^2\gamma\int_0^t ds D_{ij}(t,s)\left[\mathbf{A}(t)\rho\mathbf{A}(t-s)\right.$$
$$\left. +\mathbf{A}(t-s)\rho\mathbf{A}(t) - \mathbf{A}(t)\mathbf{A}(t-s)\rho - \rho\mathbf{A}(t-s)\mathbf{A}(t)\right]] \quad (2.225)$$

which is non-Markovian and again, does only depend on the absolute value of χ allowing us to use $\chi = i$ to recover a linear effective

stochastic equation for the density matrix. Also, if we assume no correlations in time for our noise, D_{ij} reduces to the white noise correlations, giving us the expected structure, since $\mathbf{A}(t - s) = \mathbf{A}(t)$. We can thus carry out the same calculation as in the above chapter [7] to arrive at the energy gain rate

$$\langle\langle E(t) \rangle\rangle = \frac{3}{4} \frac{\hbar^2 \lambda_{nw} M}{m_N^2 r_c^2} t \tag{2.226}$$

and

$$\lambda_{nw} = \frac{2}{3\pi^{3/2}} \int d^3 q \, e^{-r_c^2 \mathbf{q}^2} \frac{\mathbf{q}^2}{r_c} \lambda(\omega_L(\mathbf{q})) \tag{2.227}$$

where $\lambda(\omega_L(\mathbf{q}))$ comes from the factor $\mathbf{q} \cdot \mathbf{e}^{*(j)}$ which singles out a longitudinal phonon with frequency $\omega_L(\mathbf{q})$. Now if the noise introduced has a cutoff below the frequency $\omega_L(\mathbf{q})$, where we have $|\mathbf{q}| \approx \frac{1}{r_c}$ we will get a strongly reduced energy gain rate. This becomes relevant in the context of experiments in which systems with high effective phonon frequencies are used to test collapse models. Specifically tests using x-ray radiation of free electrons in a medium have very high characteristic frequencies and we will have a closer look at those in a later chapter.

The second approach is to introduce dissipation into the model. The typical collapse operator does not take into account any form of dissipation. In order to introduce this feature into the collapse model [91], we have to revisit the collapse operator. It was suggested in [90] to replace the collapse parameter in the standard master equation of the CSL model (2.166) with

$$\mathbb{L}(\mathbf{y}) = \sum_j \frac{m_j}{(1 + k_j)^3} \int \frac{dx}{(\sqrt{2\pi} r_c)^3} e^{-\frac{|\mathbf{x}-\mathbf{y}|^2}{2r_c^2(1+k_j)^2}} a_j^\dagger(\mathbf{x}) a_j \left(\frac{1 - k_j}{1 + k_j} \mathbf{x} + \frac{2k_j}{1 + k_j} \mathbf{y} \right) \tag{2.228}$$

which is not a self adjoint operator anymore. The factor $k_j = \frac{\hbar}{2m_j v r_c}$ with a velocity v is introduced to represent the dissipation property. As can be seen, if $v \to \infty$ we recover the standard CSL operator. It is helpful to also introduce the momentum representation of this operator

$$\mathbb{L}(\mathbf{y}) = \sum_j \frac{m_j}{(2\pi\hbar)^3} \int d\mathbf{P} d\mathbf{Q} \, a_j^\dagger(\mathbf{P} + \mathbf{Q}) e^{-\frac{i}{\hbar} \mathbf{Q} \cdot \mathbf{y}} e^{-\frac{r_c^2}{\hbar^2} \left(|(1+k_j)^2 \mathbf{Q} + 2k_j \mathbf{P}|^2 \right)} a_j(\mathbf{P}) \tag{2.229}$$

which simplifies for one particle to

$$\mathbb{L}(\mathbf{Q}, \mathbf{P}) = \frac{m}{(2\pi\hbar)^3} \int d\mathbf{Q} e^{-\frac{i}{\hbar}\mathbf{Q}\cdot\mathbf{x}} e^{-\frac{r_c^2}{\hbar^2}\left(|(1+k)^2\mathbf{Q}+2k\mathbf{P}|^2\right)} \tag{2.230}$$

such that we can write the master equation for one particle as

$$\frac{d}{dt}\rho = -\frac{i}{\hbar}[H,\rho] + \frac{\gamma}{m_0^2}\mathbb{L}(\mathbf{Q},\mathbf{P})\rho\mathbb{L}^\dagger(\mathbf{Q},\mathbf{P}) - \frac{1}{2}\left\{\mathbb{L}(\mathbf{Q},\mathbf{P})\mathbb{L}^\dagger(\mathbf{Q},\mathbf{P}),\rho\right\} \tag{2.231}$$

which is of the Lindblad form. From this equation we can directly compute the mean energy term by calculating $H(t) = Tr\left(\frac{P^2}{2m}\rho\right)$. Since H commutes with any function of the momentum $\mathbf{P}$ and $e^{-\frac{i}{\hbar}\mathbf{Q}\cdot\mathbf{x}}P^2 e^{\frac{i}{\hbar}\mathbf{Q}\cdot\mathbf{x}} = (\mathbf{P}+\mathbf{Q})^2$ we get the expression

$$\frac{d}{dt}H(t) = \frac{\gamma m}{2(2\pi\hbar)^3 m_0^2} \int dQ\, Tr\left[e^{-\frac{r_c^2}{\hbar^2}\left(|(1+k)^2\mathbf{Q}+2k\mathbf{P}|^2\right)}\left(|\mathbf{Q}|^2 + 2\mathbf{P}\cdot\mathbf{Q}\right)\rho\right] \tag{2.232}$$

and from there integrating over Q gives

$$\frac{d}{dt}H(t) = \frac{3\hbar^2\lambda m}{4(1+k)^5 r_c^2 m_0^2} - \frac{4k\lambda m^2}{(1+k)^5 m_0^2}H(t) \tag{2.233}$$

for the mean energy. Solving this differential equation then gives us

$$H(t) = e^{-\frac{4k\lambda m^2}{(1+k)^5 m_0^2}}\left(H(0) - \frac{3\hbar^2}{16kmr_c^2}\right) + \frac{3\hbar^2}{16kmr_c^2} \tag{2.234}$$

where we now avoid the divergence of the mean energy and instead see an asymptotic behavior for $t \to \infty$. This asymptotic term can be associated with a temperature, since we can write $\frac{3}{2}k_B T = \frac{3\hbar^2}{16kmr_c^2}$ and using $k = \frac{\hbar}{2mvr_c}$ to get

$$T = \frac{\hbar v}{4k_B r_c} \tag{2.235}$$

which is only infinite in the limit $v \to \infty$ or $k \to 0$ which recovers our standard white noise CSL model. This is similar to (2.40) where the dissipation term governs the equilibration with an environment.

2.6.10 *Parameter dependence*

We have seen that all variations of collapse models have one or more parameters that are undefined by the theory itself. These parameters can in principle be chosen at will and are only bounded by experiments and theoretical arguments restricting them. We will have a closer look at these restrictions and how they influence the search for experiments to test collapse models.

We will start off with the CSL model parameters λ and r_c. These parameters represent a rate and length respectively. For the collapse length r_c we choose a value that represents the transition between the quantum and classical world, where superpositions are suppressed at a reasonably large scale while allowing quantum behavior at a microscopic scale. It is easy to picture that a collapse length of the order of a nucleus would collapse any massive quantum system in an interval of that size. Interferometric experiments would therefore lose any property of interference rather quickly [41–43]. The only way to compensate would be to choose a very small collapse rate, rendering collapse models rather useless, as minuscule collapse rates would also not have an effect on larger scales. On the other hand, choosing your collapse length to be macroscopic would lead to possible macroscopic superpositions not collapsing, since if we choose for example r_c to be of the size of one meter, we would not collapse superpositions of that size in a reasonable time scale.

To give this a more quantitative basis, let us go back to (2.169) where our rate of collapse, in terms of reduction of off diagonal terms in the position representation, was given by

$$\Gamma_{CSL} = \lambda \left(1 - e^{-\frac{x^2}{4r_c^2}} \right) \tag{2.236}$$

which is proportional to λ for length scales of $x \gtrsim r_c$. For a number of particles n within a radius of r_c and clusters of particles N that are larger than r_c the rate is approximately [4]

$$\Gamma_{CSL} \cong \lambda n^2 N \frac{m_p^2}{m_N^2} \tag{2.237}$$

which is a good approximation for some estimates of the collapse strength if compared to experimental setups. Specifically, following the argument of Adler [3], the idea of collapse models is to reduce the wave function onto appropriate eigenvalues in the position basis, based on the concept of macroscopic behavior. To indeed recover an effective classical description for macroscopic systems, the transition region from quantum to classical physics has to explain every available phenomenon falling into this region. Adler pointed out, that specifically the process of latent image formation in analog photography

should constitute a process with collapse properties. The basic idea is, that the process of photon interaction with the photosensitive emulsion happens independently from the development of the photograph. So either the quantum nature of the photon track within the emulsion is preserved until the process of development, or the collapse of the photon track to one trajectory is completed independently. In the latter case, the amount of involved atoms and the time scale of the process create a bound on collapse parameters. We want to stress here, that the resulting image relies on an explicit measurement of the photon state, invoking the same fundamental questions of the problem of outcomes in a measurement. However, the whole imaging process does not contradict other interpretations of quantum mechanics and is fully consistent with standard decoherence. As such, bounds on collapse models are derived through the explicit assumption that an "objective" collapse process is needed here as described to be consistent *within* the collapse model framework.

The image formation process in its essence are silver salts which through interaction with photons create silver and bromine ions moving through a gelatine emulsion. The silver ions accumulate at the surface of clusters of the silver salts which form the "pixels" of the picture. One of those clusters needs around ≈ 30 silver atoms to be developable. Also in order to get a definite track of a photon one assumes ≈ 20 of the "pixels" to have formed. The formation time of one "pixel", that is ≈ 30 silver atoms to move to the surface is of the order of $3 \cdot 10^{1\pm2} s^{-1}$. We assume that since our photo should be captured within that time window, the collapse process to an effective classical state also has to be complete. We can estimate the collapse rate λ with our approximation (2.237). Since we have 30 silver and bromine atoms moving with nucleon numbers 108 and 80 respectively, we have $n \approx 5 \cdot 10^3$ and $N \approx 20$. This gives

$$\lambda \approx 5 \cdot 10^{-8\pm2} s^{-1} \tag{2.238}$$

assuming $r_c \approx 10^{-7} m$, which corresponds roughly to the size of one "pixel". Historically, the assumptions for λ and r_c were much more conservative and chosen to be large enough to have an appreciable effect on macroscopic masses ($\approx 1g$) while still remaining negligible for microscopic systems. The value for the reduction rate was therefore chosen to be $\lambda \approx 10^{-16} s^{-1}$, since this would be enough to get a reduction rate for macroscopic systems of $\approx 1g$ (2.237) to be $\Gamma_{CSL} \approx 10^7 s^{-1}$, without affecting microscopic quantum systems. The Adler calculation constitutes a lower bound on the collapse rate since lower values for λ would lead to longer times for the transition from quantum to classical than what seems compatible with latent image formation.

We can also define upper bounds for the parameter based on the heating through collapse noise. Since such a heating has not been

measured so far, it must be negligible in relevant systems. An example for such an upper bound can be found by calculating the heating of protons in the universe [3]. Assuming that the heating rate is given by (2.222), and $M = 1$, only taking into account the proton mass, for our given value (2.238) the temperature increase over the lifetime of the universe is $T \approx 7 \cdot 10^3 K$. Now this energy should be radiated in the form of photons and contribute to the cosmic microwave background. The total energy increase should not exceed a fraction of the CMB, which gives an upper bound for $\lambda \lesssim 10^{-4} s^{-1}$. Even following more sophisticated methods of bounding λ from above do not seem to give stronger bounds. Details can be found in [3].

2.6.11 *Limits and issues with collapse models*

Collapse models were initially introduced as a possible solution to the problem of outcomes of measurements. Simply put, if a state is in a superposition, how does a measurement single out a definite outcome? This question is different from the question of a preferred basis. The appearance of a preferred basis is explained by the mechanism of decoherence and related to the interaction with an environment. However, decoherence leads to entanglement with the environment and does not break the unitarity of the evolution of the composite system. This selection of a definite outcome is at the core of the interpretations of quantum mechanics. Collapse models integrate this selection into the evolution of the quantum state through nonlinearities. As we have seen above, this necessitates another change, the introduction of an additional noise to prevent superluminal signaling. The instantaneous state change of quantum mechanics (the spooky action at a distance) in quantum mechanics does not allow the propagation of information precisely because of the unitarity of the evolution. The additional noise then comes with its own problem, namely breaking the conservation of energy. We have seen possible extensions of the model here to compensate by either introducing a colored noise our through additional dissipation. But again this also creates other problems. Namely, a colored noise inherently selects a reference frame since the cutoff cannot be Lorentz invariant. This implies that there is a preferred frame for the noise field. The same holds true for the dissipative extension, which again is dependent on the reference frame of the system.

The concept of an objective collapse fits well into the idea of a classical macroscopic world. However, if all fundamental forces are described by quantum theories, the notion of objective collapse becomes harder to justify, since it would fundamentally forbid quantum effects at characteristic length and mass scales, making them unnecessary to describe gravitational interactions of suitably massive objects. However, at these scales relativistic effects become prevalent. Collapse models so far cannot be consistently applied to such systems. On

the other hand, for mesoscopic systems, it isn't clear yet where collapse model effects would become dominant. In principle, experiments measuring genuine gravitational interactions of superposition states might not be impossible even if collapse models would indeed turn out to be relevant. Thus, they might not address the properties of the gravitational field after all.

The generalization of collapse models to relativistic physics is not straight forward as well. One issue here was pointed out in [59]. The collapse, being a random process, localized in space cannot influence all branches of a superposition instantaneously, since space-like separated branches would experience the collapse in different time orderings depending on the reference frame. The correct renormalization is dependent on the correct time ordering of the collapse events. This contradiction could in principle be resolved by introducing collapses that are strictly time-like connected to each other. But this also faces issues since a macroscopic object in superposition could then experience a collapse event at one position that does not lead to instantaneous collapse for the whole object. Successive collapse events would only occur time-like separated from each other, which would preserve superpositions until collapse can occur for the whole macroscopic extension. This contradicts the initial goal of collapse models of macroscopic collapse of superpositions in this relativistic setting. A solution for compatible extensions of collapse models to a relativistic setting has not been found to date. It might even be impossible to do [58].

2.7   CHAMELEON FIELDS

So far we concentrated our efforts on quantum mechanics and possible changes to the underlying dynamics. In this last section we also want to venture into a different direction, namely the question of dark energy and possible additions to the standard model.

The expansion of our universe was experimentally verified by multiple experiments [64, 66, 87, 92]. The easiest way to explain this phenomenon is to introduce a background energy field, often called "dark energy". This field in its simplest form is non interacting with any standard model particle. However, the magnitude of the field has to be very small (at the order of $10^{-120}M_{Pl}^4$) to explain the measured expansion rate. More complex models to describe this phenomenon involve scalar fields which would introduce another (fifth) force that should be detectable in experiments. However, tabletop experiments and measurements at the solar system level have come back empty handed. This would limit any additional force to energy scales far beyond the planck scale which in turn poses a problem to incorporate into standard quantum field theory. One way to circumvent this issue is to make this force dependent on its environment. One such candi-

date are Chameleon theories [19, 62, 63]. The initial idea is to have a scalar field ϕ with a density dependent mass of the chameleon particle. This would "screen" the effective force at laboratory experiments as well as solar system measurements, while still contributing meaningfully at larger scales. The typical starting point of such theories is a Lagrangian of the form

$$\mathcal{L} = \sqrt{-g} \left(\frac{M_{Pl}^2 R}{2} + \frac{(\partial \phi)^2}{2} + V(\phi) \right) + \mathcal{L}_m(\psi, \tilde{g}_{\mu\nu}) \qquad (2.239)$$

with R the Ricci scalar, M_{Pl} the Planck mass and $\mathcal{L}_m$ a matter Lagrangian coupling the matter field ψ to a metric $\tilde{g}_{\mu\nu}$ which is related to the Einstein-frame metric $g_{\mu\nu}$ through

$$\tilde{g}_{\mu\nu} = e^{2\beta\phi/M_{Pl}} g_{\mu\nu} \qquad (2.240)$$

with β a coupling constant. The exponential term is quite often denoted as $A^2(\phi)$ in the literature. In the case of non-relativistic matter, one can rewrite the matter density as $\tilde{g}_{\mu\nu} T^{\mu\nu} \approx -\tilde{\rho}$. In the Einstein-frame this is related to the density ρ as

$$\rho = \tilde{\rho} e^{3\beta\phi/M_{Pl}} \qquad (2.241)$$

which is independent of ϕ in the Einstein-frame. The equation of motion then becomes

$$\nabla^2 \phi = \frac{\partial V}{\partial \phi} + \frac{\beta}{M_{Pl}} \rho e^{\beta\phi/M_{Pl}} \qquad (2.242)$$

The effective potential seen by the chameleon field is

$$V_{\text{eff}} = V(\phi) + \rho e^{\beta\phi/M_{Pl}} \qquad (2.243)$$

We haven't specified the potential $V(\phi)$ yet. In order to explain the expansion of the universe we assume $V(\phi) > 0$. On the other hand we want to suppress the force at higher densities, which leads to $V'(\phi) < 0$ as well as $V''(\phi) > 0$, two important properties for the screening mechanism to work. The first derivative has to be negative to allow a solution in which we assume a constant density over all space. In this case the derivatives of the field vanish and we end up with

$$-\frac{\partial V}{\partial \phi} = \frac{\beta}{M_{Pl}} \rho e^{\beta\phi/M_{Pl}} \qquad (2.244)$$

where the right hand side is strictly positive (β has to be positive due to quantum stability [94]). The second derivative is associated with

the mass of the chameleon particle and thus positive. The typically assumed form of $V(\phi)$ therefore is an exponential function in ϕ:

$$V(\phi) = \Lambda^4 \left(1 + \frac{\Lambda^n}{\phi^n}\right) \tag{2.245}$$

with the constants Λ and n, satisfying these properties. If we set the constant Λ to $\Lambda_{DE} \approx 2.4 meV$, then the constant term describes the dark energy contribution to the expansion of the universe. The parameter n can be chosen such that the derivative properties stay untouched. Another simplifying assumption is to taylor expand the exponential term in ϕ giving

$$\nabla^2 \phi = \frac{\partial V}{\partial \phi} + \frac{\beta}{M_{Pl}} \rho \tag{2.246}$$

which shows the two competing terms in the laplace equation. With this form of the potential we can calculate the bulk field ϕ_{bg}

$$\phi_{bg} \rightarrow \frac{\partial V_{\text{eff}}}{\partial \phi} = -n\Lambda^{4+n} \frac{1}{\phi^{n+1}} + \frac{\beta}{M_{Pl}} \rho = 0 \tag{2.247}$$

$$\phi_{bg} = \left(\frac{n\Lambda^{4+n} M_{Pl}}{\beta \rho}\right)^{\frac{1}{n+1}} \tag{2.248}$$

We can also define the mass of the chameleon particle as well as its compton wavelength λ_c given by

$$m^{-1}(\rho) = 1/\sqrt{V''_{eff}(\phi_{bg})} = \lambda_c(\rho) = \sqrt{\frac{1}{n(n+1)\Lambda^{4+n}} \phi_{bg}^{n+2}} \tag{2.249}$$

The effective potential

$$V_{\text{eff}} = \Lambda^4 \left(1 + \frac{\Lambda^n}{\phi^n}\right) + \frac{\beta}{M_{Pl}} \rho \phi \tag{2.250}$$

can be modeled as two components.

There are two regimes of interest. The linear regime, in which the derivative of $V(\phi)$ is small. The effective equation becomes similar to the Poisson equation for the gravitational field. An example for which these conditions are met would be a small, high-density source embedded in a low density background. For larger radii of our high-density source, the derivative term increases its absolute value and, since it is negative, cancels out the density contribution more and more. The source term becomes smaller. This nonlinear effect is known as "screening", drowning out the effective force. For sufficiently large densities, the chameleon force is suppressed. This demonstrates all
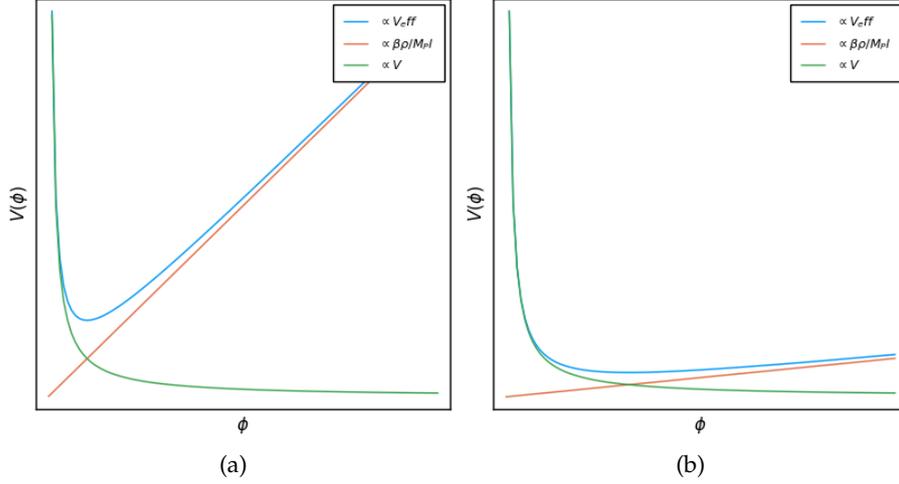
Figure 2.1: Effective potential landscape. (a) Potential with high density and $n > 0$ (linear regime). (b) Potential with low density and $n > 0$ (nonlinear regime).

the desired properties we initially wanted from the chameleon field, hiding its contribution in tabletop experiments for sufficiently large densities.

This transition from the linear- to the nonlinear regime happens only inside high density objects. This exponential suppression is also known as "thin shell effect" [63] since only the outer layers of a mass with high density contribute to the chameleon force.

This effect can be approximately calculated by assuming a radial symmetric setup, a sphere in a background density. This was demonstrated in [21]. We will give a brief recap of this calculation, since we will use these results later in this work.

2.7.1 *Thin shell effect*

To start we transform the evolution equation to spherical coordinates

$$\frac{1}{r^2} \cdot \frac{\partial}{\partial r} \left(r^2 \frac{\partial \phi}{\partial r} \right) = \frac{\partial V}{\partial \phi} + \frac{\beta}{M_{Pl}} \rho \tag{2.251}$$

with $\rho = \rho_S \Theta(r_s - r) + \rho_{min} \Theta(r - r_s)$. Θ denotes the Heaviside function.

In order to derive an approximate solution it is instructive to think of three different regimes of the above equation. First, far away from the sphere we expect the field to approach ϕ_{bg} (2.248). Since we assume that ρ_{min} is small, we expect the potential term to dominate. We

can expand the potential $V_{\text{eff}}(\phi)$ around ϕ_{bg} and keep the harmonic component, which after taking the derivative gives

$$\frac{1}{r^2} \cdot \frac{\partial}{\partial r}\left(r^2 \frac{\partial \phi}{\partial r}\right) = \left.\frac{dV_{\text{eff}}^2}{d\phi^2}\right|_{\phi=\phi_{bg}} (\phi - \phi_{bg}) \tag{2.252}$$

with $\left.\dfrac{dV_{\text{eff}}^2}{d\phi^2}\right|_{\phi=\phi_{bg}} = m_{bg}^2$

For the case of the inside of the sphere we have two regimes. We expect the field to approach ϕ_s, the minimum of the field for density ρ_s. If the sphere is small, the field may remain larger than ϕ_s and we can approximate the effective potential with $V_{\text{eff}} = \frac{\beta}{M_{Pl}}\rho\phi$, giving us solutions similar to the gravitational potential.

In the last case the field drops to ϕ_s within the sphere for $r_s > 0$. In this regime, which is located within a radius r_c from the center of the sphere, we can again approximate with a harmonic potential, giving

$$\frac{1}{r^2} \cdot \frac{\partial}{\partial r}\left(r^2 \frac{\partial \phi}{\partial r}\right) = \left.\frac{dV_{\text{eff}}^2}{d\phi^2}\right|_{\phi=\phi_s} (\phi - \phi_s) \tag{2.253}$$

with $\left.\dfrac{dV_{\text{eff}}^2}{d\phi^2}\right|_{\phi=\phi_s} = m_s^2.$

In order to give a complete (approximate) solution we join the solutions together by matching ϕ and its first derivative at r_c and r_s. This fixes all constants of the solutions and gives [21]

$$\phi = \begin{cases} \phi_s & r < r_c \\ \phi_s + \frac{1}{8\pi r_s}\frac{\beta}{M_{Pl}}m_s\frac{r^2 - 3r_c^2 r + 2r_c^3}{rr_s^2} & r_c < r < r_s \\ \phi_{bg} - \frac{1}{4\pi r_s}\frac{\beta}{M_{Pl}}m_s\left(1 - \frac{r_c^3}{r_s^3}\right)\frac{r_s}{r}e^{-m_{bg}r} & r > r_s \end{cases} \tag{2.254}$$

and

$$r_c = r_s\sqrt{1 - \frac{8\pi}{3}\frac{M_{Pl}}{\beta m_s}r_s\phi_{bg}} \tag{2.255}$$

from which we can also extract a criterion for the appearance of the "thin shell" governed by r_c. The last factor in (2.255) has to be smaller than one for a real solution giving the inequality

$$\phi_{bg} \leq \frac{3\beta m_s}{8\pi r_s M_{Pl}} \tag{2.256}$$

We can also rewrite the solution for the field outside the sphere depending on the the appearance of r_c since in the case $r > r_s$ it

adds an additional factor. In [21] this factor $\left(1 - \frac{r_c^3}{r_s^3}\right) \equiv \lambda_s$ is used to determine the thin shell contribution to the potential outside the sphere. Knowing the field outside the sphere we can calculate the chameleon acceleration with

$$\vec{a} = -\frac{\beta}{M_{Pl}} \vec{\nabla} \phi = \left(1 - \frac{r_c^3}{r_s^3}\right) \frac{\beta m_s}{4\pi r^2 M_{Pl}} \tag{2.257}$$

where we used $m_{min} r \ll 1$. Comparing this with the gravitational acceleration gives

$$\frac{a_\phi}{a_N} = \left(1 - \frac{r_c^3}{r_s^3}\right) \frac{\beta m_s}{4\pi r^2 M_{Pl}} \frac{r^2}{G m_s} = 2 \left(1 - \frac{r_c^3}{r_s^3}\right) \beta^2 \tag{2.258}$$

containing the factor β. From now on the coupling parameter β will be written as $\frac{M_{Pl}}{M}$ to better reflect its relation to the Planck mass.

As was shown in [21] as well, an approximate solution for the force between two spheres can be calculated, resulting in

$$F_r = \frac{G m_1 m_2}{r^2} \left[1 + \left(1 - \frac{r_{c,1}^3}{r_1^3}\right) \left(1 - \frac{r_{c,2}^3}{r_2^3}\right) \left(\frac{M_{Pl}}{M}\right)^2 \right] \tag{2.259}$$

with two spheres with radii r_1, r_2, mass m_1, m_2 and distance r. This result can be used to calculate an approximate expectation of the chameleon force depending on the size and density of massive spheres. As we will see in chapter 4 this force might be sufficiently strong to be measured experimentally by the method used in [102].

EXPERIMENTAL APPROACHES

In this chapter we will look into experiments trying to test the different theoretical ideas we have discussed in the last chapter. We will start with the pursuit of experiments testing general relativistic proper time changes in quantum systems using photons. We will then look into proposals to test the Schrödinger Newton equation in harmonic oscillator systems. Lastly, we will analyze experiments aimed at testing collapse model effects in various ways. From interferometry, additional x-ray radiation of free electrons in bulk materials, to heating of cantilever systems associated with the collapse noise.

3.1 TESTING GRAVITATIONAL TIME DILATION IN QUANTUM SYSTEMS

Testing a loss of visibility due to time dilation in an interferometry experiment with clock degrees of freedom can be done in two ways. One option is to consider massive particles traveling through the interferometer which carry a "clock" degree of freedom, for example spin. Some preliminary calculations based on the visibility (2.49) can be done for several masses that could be considered as experimental test bed. Taking atoms as test mass where the clock degree of freedom is realized through oscillating hyperfine states, we can calculate the visibility through the expected oscillation frequency $\omega = \frac{\Delta E}{\hbar}$ and compare it to the time of flight as well as the height difference of the two paths. For frequencies of $\omega \approx 10^{15} Hz$ and assumed flight times of $\Delta T \approx 1s$ one would need a height difference of $\Delta h \approx 10m$ in order to get a measurable reduction in visibility. So far, experiments achieving such flight times let alone interferometer sizes on the order of meters is not feasible. To give a few comparisons, the COW experiment [77] had a height difference of $\Delta h \approx 2cm$ with a flight time of $\Delta T \approx 10^{-4}s$. For molecular interferometers [40] $\Delta h \approx 10cm$ with flight times of $\Delta T \approx 10^{-3}s$.

Another way of testing this proposal could be done by not using massive particles, but photons. We can describe a similar phenomenon of reduction of visibility by comparing single photon flight times in an interferometer [106]. We start with an approximately flat metric of the form

$$ds^2 = \left(1 - \frac{2GM}{rc^2}\right) dt^2 - \frac{1}{c^2} r^2 d\theta^2 \tag{3.1}$$

with an infinitesimal angle $d\theta$ which is constant for a far away observer. Since we are interested in a light like trajectory, we can easily extract the time coordinate along a horizontal trajectory

$$t_r = \frac{t}{c\sqrt{1 - \frac{2GM}{rc^2}}} \tag{3.2}$$

which is dependent on the distance from the gravitational source. This ensures that the photons flight time can be seen as a clock for its own reference frame. If one considers an observer at the upper path, this time difference between the two trajectories can be approximated as

$$\Delta\tau \approx \frac{lgh}{c^3} \tag{3.3}$$

with l the horizontal path length, h the vertical distance of the paths and g the gravitational acceleration. If we now consider a superposition state of a single photon traveling along the interferometer arms we get

$$|1\rangle_{u,d} = \int d\nu f(\nu) \left(e^{i\frac{\nu}{c}(x - ct_r)} \pm e^{i\frac{\nu}{c}(x - c(t_r + \Delta\tau))} \right) a_\nu^\dagger |0\rangle \tag{3.4}$$

with the photon frequency ν and the corresponding mode shape $f(\nu)$. The associated detection probability on a detector is

$$P = \frac{1}{2}\left(1 \pm \int d\nu |f(\nu)|^2 \cos(\nu\Delta\tau) \right). \tag{3.5}$$

This probability has two limiting cases, recovering two physical effects. In the case that the frequency shift due to time dilation accumulated is small compared to the inverse of the frequency $\tau \lesssim 1/f$ of the photon mode, we recover the classical phase shift associated with Newtonian gravity. However in the case of a large time dilation $\tau \gtrsim 1/f$, the fast oscillating cosine term averages to zero over the mode width. This means that there is no meaningful overlap of the two mode shapes when recombining and hence loss of visibility. To reach such a regime we need an effective area of the interferometer $A \approx t\frac{c^3}{g}$. At first glance, this is rather large, since minimum times corresponding to light pulses in the femto second regime still would require an area of $A \approx 10^9 m$. However, a smaller width of the photon wavepacket can be achieved in principle [71]. Also, fiber optics allow travel distances of polarization encoded qubits of $x \approx 100km$ without losing their coherence. [56]

Another approach to test a change in the visibility due to time dilation was suggested by [22] using single electrons in penning traps.

These systems can be described through their orbital degree of freedom as well as their spin degrees of freedom. The general Hamiltonian neglecting contributions from the Dirac equation reads

$$H = \frac{\mathbf{p}^2}{2m}\left(1 - \frac{\mathbf{p}^2}{4m^2c^2}\right) + \boldsymbol{\mu} \cdot \mathbf{B}\left(1 - \frac{\mathbf{p}^2}{2mc^2}\right) \tag{3.6}$$

The corresponding spectrum of the trapped electron is given by $\hbar\omega_c\,(n+1/2)$ as well as $\hbar\omega_c m_s$ with quantum numbers $n = 0, 1, \dots$ and $m_s = \pm 1/2$. We can see that because of relativistic corrections the frequency associated with the spin degree of freedom is modified

$$\omega_c + \delta_c = \omega_c \left(1 - \frac{\hbar\omega_c}{mc^2}\left(n + \frac{1}{2}\right)\right) \tag{3.7}$$

or in other words depending on the orbit of the electron its internal spin clock runs at a different rate. We can therefore use superpositions of orbital quantum states to probe the relativistic time dilation. Note that this time dilation is an effect of special relativity, no gravitational effects enter here. The Dirac equation used here does not contain any gravitational interactions.

At a magnetic field of $5T$, we get a frequency shift of $\delta_c = 2\pi \cdot 150 Hz$. Taking into account the average trapping time in a penning trap defined by the inverse of the free radiation

$$\gamma_0 \approx \frac{1}{4\pi\epsilon_0}\frac{4e^2\omega_c^2}{3mc^3} \approx 2\pi \cdot 2Hz \tag{3.8}$$

we can see that such an experiment seems feasible, especially considering the typical coherence time of spin degrees of freedom $T_{spin} \geq 1year$ and coherence time for orbital superpositions to be of the order of $T_{orb} = 1/|\gamma_0 l|$.

These types of setups also allow to analyse possible entanglement of either two photons, using the reduction of visibility, or two electrons, using their cyclotron states. probing the effect of time dilation in a Bell test ruling out any local realistic description of the generated correlations. In the case of photons we can achieve this by having a Franson-type interferometer. This type of interferometer uses two correlate photon wave packets which are sent into two arms respectively. The arms of the interferometer are themselves Mach-Zehnder interferometers. One side is embedded in a curved space-time (a gravitational field) leading to two different arm length due to time dilation. This setup allows for Bell tests of the entangled state of the two photon wavepackets. If a Bell inequality can be violated, these photon states in curved space-time cannot be described by a local-realistic theory.

Similarly, this can be done for the above described electron setup. Starting off with superposition states in the spin degree of freedom,

acting as clock states $|\psi\rangle_{1,2} = 1/\sqrt{2} \left(|\uparrow\rangle_{1,2} + |\downarrow\rangle_{1,2} \right)$ for two electrons. The different cyclotron states are realized with two atoms in penning traps connected with a waveguide. The resulting state reads

$$|\Psi\rangle = 1/\sqrt{2} \left(|\psi,0\rangle_1 \otimes |\psi,1\rangle_2 + |\psi,1\rangle_1 \otimes |\psi,0\rangle_2 \right)$$

with the states $|0\rangle, |1\rangle$ the different cyclotron paths. If a violation of a Bell inequality can be detected with such a setup, the elapsed time for a local state itself would not be local. One interesting detail here is, that one could in principle do a similar experiment with one electron and one positron looking into time reversal symmetries of the involved particles.

3.2   TESTING THE SCHRÖDINGER NEWTON EQUATION

The Schrödinger Newton equation predicts a changed time evolution of the wave function due to self interaction. We can define a potential for a composite system by

$$\nabla^2 U = 4\pi \sum_k \int d^{3n}\mathbf{x} |\psi|^2 m_k \delta(\mathbf{x} - \mathbf{x}_k) \,. \tag{3.9}$$

We are now interested in a description of the center of mass for a harmonic oscillator system. If we assume to be in the regime of massive composite particles such that we can attribute the center of mass motion to be

$$x_{cm} = \sqrt{\frac{\hbar}{2m\omega_{cm}}} \tag{3.10}$$

and internal motions with zero point fluctuation of individual lattice atoms x_{zpf} and thermal contributions x_{th}. If we consider low equilibrium temperatures with environments $T_{env} \leq 100mK$, to be in the regime

$$x_{zpf} \gg x_{th} \gg x_{cm} \tag{3.11}$$

we can taylor expand the contribution of the Schrödinger Newton potential [103] in the multiparticle Schrödinger Newton equation

$$i\hbar\partial_t\psi = \sum_k \left(-\frac{\hbar^2\nabla_k^2}{2m_k} + \frac{m_k U}{2} \right)\psi + V(\mathbf{x})\psi \tag{3.12}$$

with the potential term given by

$$\sum_k \frac{m_k U}{2} = -\sum_{k,j} \frac{Gm^2}{2} \iiint \delta(\mathbf{y} - \mathbf{y}_j')|\psi_{int}(\mathbf{y}')|^2 d^{3n-3}y'$$
$$\frac{1}{|\mathbf{x} - \mathbf{z} + \mathbf{y}_k - \mathbf{y}|} d^3y \psi_{cm}^2(\mathbf{z}) d^3z \tag{3.13}$$

where the integral

$$-\frac{Gm}{2} \int \delta(\mathbf{y} - \mathbf{y}'_j)|\psi_{int}(\mathbf{y}')|^2 d^{3n-3}\mathbf{y}' \frac{1}{|\mathbf{x} - \mathbf{z} + \mathbf{y}_k - \mathbf{y}|} d^3\mathbf{y} =$$
$$= -\frac{Gm}{2} \int \frac{\rho_{int}(\mathbf{y}_k)}{|\mathbf{x} - \mathbf{z} + \mathbf{y}_k - \mathbf{y}|} d^3\mathbf{y} = V_{grav}(\mathbf{z}) \tag{3.14}$$

describes the gravitational potential of a lattice in a center of mass frame. Expanding this integral around **x** and **z** gives

$$\sum_k \frac{m_k U}{2} = \sum_k V_{grav}(\mathbf{y}_k) + (x_{cm} - \langle x_{cm} \rangle) \sum_k \partial_{\mathbf{z}} V_{grav}(\mathbf{y}_k)$$
$$+ \frac{1}{2}(x_{cm} + 2x_{cm}\langle x_{cm}\rangle - \langle x_{cm}^2 \rangle)\sum_k \partial_{\mathbf{z}}^2 V_{grav}(\mathbf{y}_k) \quad (3.15)$$

The first term only depends on internal degrees of freedom that do not contribute to the center of mass motion. The second term describes interactions of the center of mass with internal degrees of freedom. Since the time scales of fluctuations of motion for these degrees of freedom are on vastly different time scales we can neglect these contributions. The only relevant term then is the second order term

$$\mathscr{C} = -\frac{G}{2}\partial_{\mathbf{z}}^2 \left(\int \frac{\rho_{int}(\mathbf{y})\rho_{int}(\mathbf{y}')}{|\mathbf{z} + \mathbf{y} - \mathbf{y}'|} d^3y d^3y' \right)_{\mathbf{z}=0} \quad (3.16)$$

and the simplified Schrödinger Newton equation for a center of mass harmonic oscillator becomes [38, 50, 103]

$$i\hbar\partial_t \psi = \left(-\frac{\hbar^2\nabla^2}{2m} + \frac{m\omega_{cm}^2 x^2}{2} + \frac{1}{2}\mathscr{C}(x - \langle x \rangle)^2 \right)\psi \quad (3.17)$$

We can associate the parameter $\mathscr{C}$ with a characteristic frequency $\omega_{SN} = \sqrt{\mathscr{C}/m}$ effectively modifying the resonances of the simplified Schrödinger newton equation. Depending on the choice of the mass distribution we can consider different frequencies. For example, if we consider a homogeneous mass distribution, the SN factor becomes $\mathscr{C} = Gm\rho$ giving an associated frequency of $\omega_{SN,hom} = \sqrt{G\rho}$. However, if we take the mass to be confined around the nucleus of atoms in their lattice positions with fluctuations x_{zpf}, we arrive at the different expression

$$\omega_{SN}^{confined} = \sqrt{\frac{Gm_0}{12\sqrt{\pi}x_{zpf}^3}} \quad (3.18)$$

with a mass m_0 per lattice point. This is larger by a factor of ~ 100. Typical frequencies are in the range of $\omega_{SN}^{confined} \approx 10^{-2}Hz$ for materials like silicon.

The modification of the Schrödinger equation can then also be expressed through effective Heisenberg equations

$$\dot{x} = \frac{p}{m}, \quad \dot{p} = -m\omega_{cm}^2 x - m\omega_{SN}^2(x - \langle x \rangle) \quad (3.19)$$

from which it becomes evident that first moments are unchanged, while second moments evolve with a modified frequency $\omega = \sqrt{\omega_{cm} + \omega_{SN}}$. This leads to a different evolution for a squeezed state, where the rotation with frequency ω_{cm} in phase space now is accompanied by a rotation with different frequency $\sqrt{\omega_{cm} + \omega_{SN}}$ of the ellipse representing its uncertainty. However, since the ratio of ω_{cm} to ω_{SN} is typically rather small, resolving such an effect is challenging. One proposal to test changes in the resonance frequency is given in [51]. The idea here is to concentrate on the shift in energy levels caused by the shift in resonance frequency due to the self interaction. In the above case, because of the assumption that the wave function is narrower than the extent of the particles location, we only get a constant shift for all levels. This approximation breaks down for wave functions of the order of the localization of the nucleons making up the macroscopic object. The energy splitting can be calculated to be

$$\Delta E = \frac{G\hbar m}{4\sigma^3 \omega_0} f_n(\alpha)$$

with σ the localization of a nucleus and $f_n(\alpha)$ a frequency dependent function, which is rather complex and can be found in [51]. In the case of narrow wavefunctions however $f_n(\alpha)$ does not contain a dependency on n. The parameter α appearing in f_n is the ratio of the width of the ground state of the total mass and the localization of the nucleus and is dimensionless

$$\alpha = 2\sigma\sqrt{M\omega_0/\hbar} \tag{3.20}$$

For values of $\alpha \approx 1$ a dependence on n appears in f_n giving a frequency shift

$$\Delta\omega_{nm} = \frac{1}{4}\frac{Gm}{\omega_0\sigma^3}\left(f_n(\alpha) - f_m(\alpha)\right) \tag{3.21}$$

In order to give an estimate of the expected effect in an experiment we can determine the mass M from (3.20) by demanding $\alpha \approx 5$ to achieve a non-degenerate energy shift. The parameter σ is taken to be the Debye-Waller factor at a temperature of $T \approx 100mK$ giving $\sigma \approx 2.77 \cdot 10^{-12}m$. The resulting mass is $M \approx 10^{15}u$ which corresponds to an osmium sphere of radius $r \approx 2.6\mu m$. For a harmonic trap frequency of $\omega_0 \approx 100Hz$, we get a splitting $\Delta f \approx 0.1mHz$. A concrete proposal was investigated in [51] using an osmium superconducting disk inside a linear Paul ion trap in a dilution refrigerator. The effect would be probed in the longitudinal direction of the setup. It is important to note that this effect is not dependent on having the massive system in the ground state. The effect of frequency shift is also present in thermal states, reducing experimental demands.

3.3   TESTING PENROSE MODEL

The here investigated experiment, performed at the University of California, Santa Barbara [76], achieved to cool a mechanical mode to its ground state with conventional cryogenic refrigeration. The ground state is reached for temperatures below $0.1K$. The readout is done via a superconducting qubit (a Josephson junction in parallel with a capacitor and an inductor) which is coupled to the oscillator. The oscillator itself is built out of a thin film of aluminium nitrite, sandwiched by aluminium metal electrodes. The thickness of the resonator is $3.3 \cdot 10^{-7}m$ with an area of $5.58 \cdot 10^{-10}m^2$. By applying voltage, the resonator expands or contracts with a resonance frequency of $6\,GHz$. In this experiment it was possible to swap excitations between the superconducting qubit and the mechanical resonator, which allowed to perform a Ramsey type experiment. Thus the mechanical oscillator could be prepared in a superposition state $|g\rangle + |e\rangle$ of the ground state and the first excited state. The measured dephasing time of this state was $t = 20ns$. Due to the macroscopic nature of this superposition state, it seems justifiable to ask, whether deviations from the typical quantum mechanical behavior can be seen. This would emerge in a possible reduction of the coherence time of this state.

In order to give quantitative results for the coherence time, we have to calculate the self energy of the considered oscillator. Since the actual shape of the mass distribution is not specified in the theory of Penrose and Diosi, we consider spheres to construct the lattice. If each of the mass spheres has a mass of m_1 and a radius of r, the systems total mass is m and the superposition states have a spatial separation of Δx, we can approximate the above self energy by the expression:

$$\Delta E = -Gmm_1 \left(\frac{6}{5r} - \frac{1}{\Delta x} \right) \tag{3.22}$$

with $\Delta x \geq 2r$ and

$$\Delta E = \frac{Gmm_1}{r^3} \Delta x^2 \tag{3.23}$$

with $\Delta x < 2r$.

One way to estimate the displacement of the unit cell is to consider the influence of the qubit after coupling. An additional energy of one phonon is added. This additional energy is the electrostatic energy $E_{\text{charge}} = \frac{Q^2}{2C}$. This energy leads to a displacement according to the piezoelectric effect: $\Delta x = d_{33} \frac{Q}{C}$.

This displacement is only between two layers of atoms. Due to the structure of the material and the fact that the vibrational modes can be understood as elongation only in one direction, the successive

distance between arbitrary layers from the center of the material is just Δx multiplied with the number of layers in between.

The number of atoms of each layer for the dimensions of the Aluminium Nitrite crystal is $N_p = 6.66 \cdot 10^9$. And the number of layers is $N_l = 663$. This allows us to calculate the total self energy for Aluminium and Nitrogen.

$$\Delta E_{Al|N} = 4N_p G m_{Al|N}^2 \left(\frac{6N_l}{5r} - \sum_{k=1}^{N_l} \left(\frac{1}{k\Delta x} \right) \right) \tag{3.24}$$

This leaves us with a function $\Delta E(r)$ which is the sum of the two different types of matter ($\Delta E = \Delta E_{Al} + \Delta E_N$). We implicitly assumed here, that the condition $\Delta x \geq 2r$ holds. If this would not be so, one has to consider 3.23.

From [76] we can now take the coherence time of their Ramsey fringe experiment in order to have the lifetime of a superposition of ground state and excited state of the mechanical oscillator ($t \approx 20ns$). We can thus find an upper bound for the radius of our mass distribution $r \leq 1.09 \cdot 10^{-22}m$. This is smaller than the radius of a nucleus by several orders of magnitude. If the radius would be of the order of a nucleus, the expected coherence time due to gravitational effects would be $t \approx 0.19s$, a time frame in which standard decoherence effects clearly dominate.

3.4 TESTING COLLAPSE MODELS

3.4.1 *Testing collapse with interferometers*

Collapse models predict a fast decoherence for superposition states, as long as the superposed mass is large enough. We will start our analysis of possible experiments with matter interferometers [34]. We are interested in decoherence effects originating from collapse models that deviate from the predictions of standard quantum mechanics and environmental decoherence. In order to incorporate the influence of collapse into the calculation for the evolution of the wave function we will turn to the formal solution for the collapse dynamic [73, 93] (2.208). The free evolution of the density matrix then reads

$$\rho(\mathbf{x}, \mathbf{x}', t) =$$
$$\frac{1}{(2\pi\hbar)^3} \int dk \int d\omega e^{-\frac{i}{\hbar}\mathbf{k}\cdot\omega} F(\mathbf{k}, \mathbf{x} - \mathbf{x}', t) \rho^{QM}(\mathbf{x} - \omega, \mathbf{x}' - \omega, t) \tag{3.25}$$

To describe the time evolution in an interferometer, we divide the time evolution in sections corresponding of the different stages of

the setup. Starting with an initial wave function and corresponding density matrix $\rho(\mathbf{y}_0, \mathbf{y}'_0, 0) = \delta(\mathbf{x}_1 - \mathbf{y}_1)\delta(\mathbf{x}_1 - \mathbf{y}'_1)$. We evaluate the free evolution of the density matrix until the first grating which gives solutions of the form

$$\rho(x_1, x'_1) = e^{\frac{ik}{2L_1}(x_1^2 - x_1'^2)} e^{-\frac{ik}{2L_1}(x_1^2 - x_1'^2)x_0} F\left(\frac{\hbar k}{L_1}(x_2 - x'_2), 0, 0; x_2 - x'_2, 0, 0; t_1\right)$$
(3.26)

Which is just the free evolution multiplied with the additional function F and a distance to the first grating L_1. We then apply a transmission function for the grating $t(x_1)$. We can now add as many grating as we choose by repeating the above steps. The final step is to characterize the probability to detect the interference pattern at a position on the screen. For a single grating it takes the form

$$p(x) = \int_{-\infty}^{\infty} dx_1 \int_{-\infty}^{\infty} dx'_1 D(x_1 - x'_1) t(x_1) t^*(x'_1)$$
$$e^{-i\frac{mv}{\hbar}(x_1 - x'_1)(x_1/L_1 + x/L_2)} e^{i\frac{mv}{2\hbar}(1/L_2 + 1/L_1)(x_1^2 - x_1'^2)} \quad (3.27)$$

where the function D is given by the modification F of the free evolution

$$D(x_1 - x'_1) =$$
$$F\left(\frac{\hbar k}{L_2}(x_1 - x'_1), 0, 0; 0, 0, 0; t_2\right) F\left(\frac{\hbar k}{L_1}(x_1 - x'_1), 0, 0; x_1 - x'_1, 0, 0; t_1\right)$$
(3.28)

Care has to be taken to make sure that this simplified calculation holds up in real experiments. First, the size of the molecule used in the interferometer is small compared to the length of the interferometer $L_{1,2}$ to treat the interaction with the grating as instantaneous, enabling the use of a transmission function. Also in order to ignore influences in other directions, we require that the grating slits are much larger in height compared to the molecule wavefunction extension in the perpendicular direction to the plane we focus on. Another important point is the actual source wave function, which was taken here as point like. However, the initial wave function can also prepared in different initial configurations.

The transmission functions can be written as fourier transformations if we assume that gratings are periodic and treated as effectively infinite in the x-direction.

$$|t|^2 = \sum_{l=-\infty}^{\infty} A_l e^{2i\pi l \frac{x_1}{d}}$$
(3.29)

with a periodicity d. For further details on the calculation we refer the reader to [93]. For a near field interferometer like in [74] we can then describe the interference pattern through an expression depending on the transmission functions and the correction terms coming from collapse models

$$S(x_{shift}) = \sum_n A_n^* C_n^* B_n D\left(\frac{2\pi n}{d}\frac{l}{k}\right)e^{-2i\pi n\frac{x_{shift}}{d}} \tag{3.30}$$

were the transmission coefficients A, B, C now describe three different gratings with the last grating movable in x-direction. The parameter x_{shift} describes the relative position of the third grating. The key factor to measure the change in interference now is again the function D introducing the collapse effect. Using (2.208) we can write the factor D as

$$D\left(\frac{2\pi n}{d}\frac{l}{k}\right) = \exp\left[-\lambda\frac{m^2}{m_0^2}(t_1 + t_2)\left(1 - \frac{\sqrt{\pi}}{2}\frac{\mathrm{erf}(\frac{\pi nl}{dkr_c})}{\frac{\pi nl}{dkr_c}}\right)\right] \tag{3.31}$$

from which we can calculate the ratio of visibilities with and without the collapse effect.

$$\frac{\mathcal{V}_{CSL}}{\mathcal{V}} = \exp\left[-2\lambda\frac{m_0 d}{2}N\frac{m^3}{m_0^3}\left(1 - \frac{\sqrt{\pi}r_c}{Nd}\mathrm{erf}\left(\frac{Nd}{2r_c}\right)\right)\right] \tag{3.32}$$

This closed expression can be used to analyze the collapse effect in experiments like [74] where a sufficient reduction is assumed to diminish the visibility by a factor of $\frac{\mathcal{V}_{CSL}}{\mathcal{V}} = \frac{1}{2}$. In this case, the gratings are implemented through standing waves of a laser with wavelength $\lambda_L = 157nm$. the grating period then is $d = \lambda_L/2$. We want to make sure that the effective separation in our interference pattern is larger than the assumed collapse length, so we choose the second Talbot order $N = 2$ doubling the separation. This enables us to test for $r_c \approx 10^{-7}m$. For these values and a cluster mass of $m = 1.6 \cdot 10^{-21}kg$, which corresponds to $\sim 10^6 atoms$, we can set a bound for $\lambda \gtrsim 5 \cdot 10^{-6}s^{-1}$.

3.4.2 *Testing collapse with x-ray emissions from free electrons*

Another way of testing the parameter range of collapse models is given by the idea that collapse should also influence the free radiation of particles. Their effective Hamiltonian has to be modified according to the stochastic potential. We will show a quick motivation of this phenomenon using the formula for dipole radiation of a free charge. [3]

$$P = \frac{1}{6\pi\epsilon_0 c^3}e^2 a^2 \tag{3.33}$$
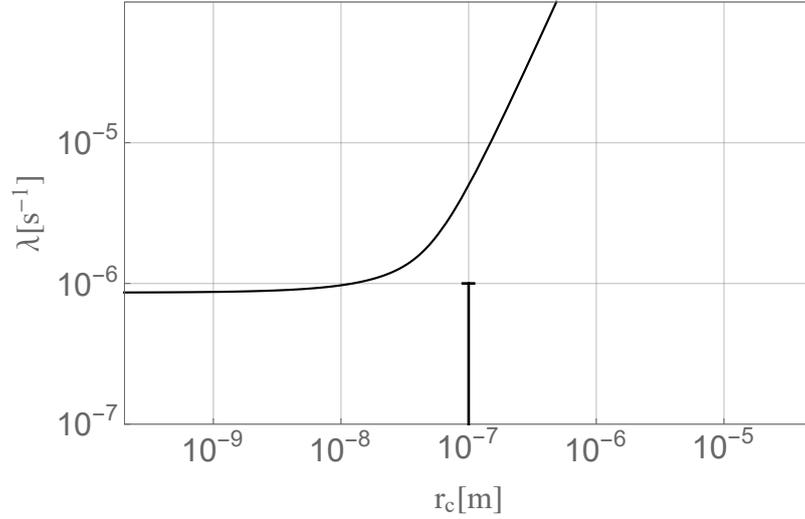
Figure 3.1: The evaluated parameter region for a molecule interferometer with $\sim 10^6 amu$. The bound for collapse models at $r_c \approx 10^{-7}m$ is $\lambda \gtrsim 5 \cdot 10^{-6}s^{-1}$ giving a weaker bound than the Adler bound (straight line).

with a being the acceleration of the free charge. In order to apply our effective collapse model calculation, we associate the acceleration a with the average over the stochastic process of a, which means we need to calculate $\langle\langle \ddot{x} \rangle\rangle$. The motivation behind this is, that the free electron will undergo localization processes of its wavefunction along its trajectory changing its momentum at random. These localizations follow the stochastic process defined in (2.217) plus the kinetic energy term. The related equations of motion read

$$\dot{x} = \frac{p}{m} \tag{3.34}$$

$$\ddot{x} = \frac{\hbar}{m_0} \int d^3x \frac{dB_t}{dt} \partial_x M(x) \tag{3.35}$$

The stochastic average of (3.35) then gives an additional factor γ and

$$\langle\langle \ddot{x} \rangle\rangle = \frac{\hbar\gamma}{m_0 dt} \int d^3x \left(\partial_x M(x)\right)^2 = \frac{3\hbar^2\lambda}{2m_0^2 r_c^2 dt}$$

Or equivalently, using $\frac{1}{dt} = \delta(0) = \frac{1}{\pi} \int_0^\infty dk$ and the dipole radiation formula, we get

$$P = \frac{e^2}{4\pi^2\epsilon_0 c^3} \frac{\hbar^2\lambda}{m_0^2 r_c^2} \int_0^\infty dk \tag{3.36}$$

Since the CSL model used here is non-relativistic, the result only applies for non-relativistic regimes, namely for $k \ll m$. Equivalently, this can be written in terms of the energy gain

$$\frac{d\Gamma(E)}{dE} = \frac{e^2}{4\pi^2 \epsilon_0 c^3} \frac{\hbar^2 \lambda}{m_0^2 r_c^2} \frac{1}{E} \tag{3.37}$$

This energy gain can be measured by detecting the emission rate of photons over time, where we consider valence electrons contributing to the radiation profile. The above formula should be applicable as long as there is no relativistic effects at play. Such an experiment was carried out [29] using a germanium block of about $m \approx 80kg$. Measuring the radiation in an energy range of $\Delta E = 4.5 - 48.5 keV$ and fitting the measured curve with a function

$$\frac{d\Gamma(E)}{dE} = \frac{\alpha}{E} \tag{3.38}$$

gives a value of $\alpha = 115 \pm 17$ and a $\chi^2 = 0.9$. This puts an upper limit on the emission of $\alpha = 143$ with a confidence level of $\sim 95\%$. Evaluating the expression for the emission gives

$$\lambda \gtrsim 1.8 \cdot 10^{-11} s^{-1} \tag{3.39}$$

for a value of $r_c = 10^{-7}m$.

The resulting bounds would rule out the parameter regime of Adler. However, we already discussed the energy non-conservation of collapse models. If one wants to uphold energy conservation, a frequency cutoff has to be established. Depending on where this cutoff is chosen, the effect of collapse models on free electrons are strongly diminished. The bound calculated here is only limiting the parameter space if no frequency cutoff is considered. In order to rule out such extensions we have to go to experiments utilizing lower frequencies.
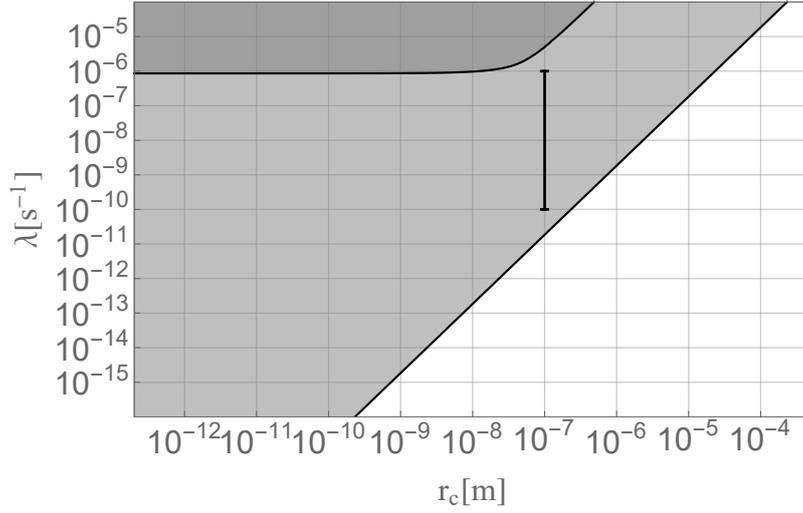
Figure 3.2: The excluded parameter regime for the radiation rate of free electrons in germanium. The bound for collapse models at $r_c \approx 10^{-7}m$ is $\lambda \gtrsim 7 \cdot 10^{-11}s^{-1}$. The bound from interferometer experiments in dark grey as comparison.

3.5 MASSIVE CANTILEVER EXPERIMENTS

Collapse models have another property, as already discussed in the theory section, that the induced collapse due to the stochasticity of the model leads to a heating effect in the observed system. We will look at a few of the proposed systems to test this heating and have a closer look at the feasibility and applicability. First, let us consider a massive cantilever as our test system. In order to describe the heating, we will use our established idea that we only need to consider the master equation to calculate the temperature increase (2.205).

$$\frac{d}{dt}\rho = -\frac{i}{\hbar}[\rho, H] - \gamma \int d^3x \, [M(\mathbf{x}), [M(\mathbf{x}), \rho]] \tag{3.40}$$

We will furthermore define the mass operator $M(\mathbf{x})$ to be

$$M(\mathbf{x}) = \sum \frac{m_i}{m_0} g(|\mathbf{x} - \mathbf{x}_i|, r_c) \tag{3.41}$$

where the function $g(y, r_c)$ is taken to be a gaussian distribution

$$g(y, r_c) = \frac{1}{\sqrt{2\pi r_c^2}} e^{-\frac{y^2}{2r_c^2}} \tag{3.42}$$

with r_c as its variance. The coordinates $\mathbf{x}_i$ are the relative coordinates of lattice points in our object with $\mathbf{x}$ being the center of mass coordinate. In order to simplify calculations of relative coordinates in massive

objects we will introduce the fourier transform of the mass operator, which is

$$M(\mathbf{x}) = \frac{r_c^3}{(2\pi)^{3/2}} \int d^3k \, e^{-\frac{r_c^2 k^2}{2}} e^{i\mathbf{k}\cdot\mathbf{x}} \sum_i \frac{m_i}{m_0} e^{i\mathbf{k}\cdot\mathbf{x}_i} \tag{3.43}$$

and contains the fourier transform of the mass density

$$\widetilde{\rho}(\mathbf{k}) = \sum_i m_i e^{i\mathbf{k}\cdot\mathbf{x}_i} = \int d^3x \, \rho(\mathbf{x}) e^{i\mathbf{k}\cdot\mathbf{x}} \tag{3.44}$$

for the mass being distributed with delta peaks around the position of the lattice points.

$$\rho(\mathbf{x}) = \sum m_i \delta(\mathbf{x} - \mathbf{x}_i) \tag{3.45}$$

We can now introduce the Lindblad term of the above master equation as

$$\mathscr{L}_{CSL}[\rho(t)] = \frac{\lambda r_c^3}{\pi^{3/2} m_0^2} \int d^3k \, e^{-r_c^2 k^2} |\widetilde{\rho}(\mathbf{k})|^2 \left[e^{i\mathbf{k}\cdot\mathbf{x}}, \left[e^{-i\mathbf{k}\cdot\mathbf{x}}, \rho(t) \right] \right] \tag{3.46}$$

for the center of mass motion of the massive object. We can furthermore expand the exponential terms $e^{\pm i\mathbf{k}\cdot\mathbf{x}}$ in first order as long as the oscillations of the center of mass are much smaller in amplitude than r_c. We therefore arrive at an effective master equation term of the form

$$\mathscr{L}_{CSL}[\rho(t)] = -\frac{D_{CSL}}{\hbar^2} [\mathbf{x}, [\mathbf{x}, \rho(t)]] \tag{3.47}$$

The diffusion rate in this equation is then given by

$$D_{CSL} = \lambda \frac{\hbar^2}{r_c^2} \alpha \tag{3.48}$$

with α being a geometry factor dependent on the mass density distribution. If we restrict the motion of oscillation in one direction, e.g. the x-direction, it takes the form

$$\alpha = \frac{r_c^5}{\pi^{3/2} m_0^2} \int d^3k \, e^{-r_c^2 k^2} k_x^2 |\widetilde{\rho}(\mathbf{k})|^2 \tag{3.49}$$

We already know from (2.224) that we can exploit an ambiguity of the definition of collapse models to arrive at the same effective equation for the density matrix. This ambiguity, which turns the underlying state vector equation into a linear equation, allows us to

calculate the energy increase through an effective hamiltonian. We can reformulate the problem of a cantilever under the influence of collapse models using an effective hamiltonian with an additional noise source. The additional term takes the form

$$H_{CSL} = -\hbar \frac{dB_t}{dt} \sqrt{\frac{\lambda\alpha}{r_c^2}} \hat{\mathbf{x}}$$

(3.50)

with $\frac{dB_t}{dt}$ our usual white noise, compare to (2.217). In order to have the full hamiltonian of an oscillator with an environment in the form of a phononic bath we get

$$H = \frac{\hat{\mathbf{p}}^2}{2m} + \frac{m\omega_0\hat{\mathbf{x}}^2}{2} - \hbar\frac{dB_t}{dt}\sqrt{\frac{\lambda\alpha}{r_c^2}}\hat{\mathbf{x}} - \gamma_m\hat{\mathbf{p}} + \hat{\chi}(t)$$

(3.51)

where the correlation of $\hat{\chi}(t)$ is given by

$$\left\langle\left\langle \chi(t)\chi(t') \right\rangle\right\rangle_\omega = 2m\gamma_m k_B T \delta(t - t')$$

(3.52)

in the high temperature limit $k_B T \gg \hbar\omega$ (compare (2.40)).

We can now write the equations of motion for the position and momentum operators

$$\partial_t\hat{\mathbf{x}} = \frac{\hat{\mathbf{p}}}{m}$$

(3.53)

$$\partial_t\hat{\mathbf{p}} = -m\omega_0^2\hat{\mathbf{x}} + \hbar\frac{dB_t}{dt}\sqrt{\frac{\lambda\alpha}{r_c^2}} - \gamma_m\hat{\mathbf{p}} + \hat{\chi}(t)$$

(3.54)

In the semiclassical approximation, on can focus only on the fluctuation from a steady state solution. The equations of motion corresponding to the fluctuations $\delta\mathbf{x}, \delta\mathbf{p}$ can then be written as fourier transforms which gives explicit expressions for $\delta\tilde{\mathbf{x}}(\omega)$ and $\delta\tilde{\mathbf{p}}(\omega)$.

$$\delta\tilde{\mathbf{p}}(\omega) = -i\omega\frac{\left(\hbar\frac{dB_t}{dt}\sqrt{\frac{\lambda\alpha}{r_c^2}} + \hat{\chi}(t)\right)}{\omega^2 - \omega_0^2 + i\omega\gamma}$$

(3.55)

$$\delta\tilde{\mathbf{x}}(\omega) = \frac{1}{m}\frac{\left(\hbar\frac{dB_t}{dt}\sqrt{\frac{\lambda\alpha}{r_c^2}} + \hat{\chi}(t)\right)}{\omega^2 - \omega_0^2 + i\omega\gamma}$$

(3.56)

With these explicit expressions the noise power spectrum can be easily calculated from the relation

$$\left\langle \delta\tilde{\mathbf{x}}(\omega)\delta\tilde{\mathbf{x}}(\Omega) \right\rangle = S_{\mathbf{x}}(\omega)\delta(\omega + \Omega)$$

(3.57)

and its explicit form

$$S_{\mathbf{x}}(\omega) = \frac{1}{2\pi} \int d\Omega e^{-i(\omega + \Omega)t} \langle \delta\tilde{\mathbf{x}}(\omega)\delta\tilde{\mathbf{x}}(\Omega)\rangle \tag{3.58}$$

Using the correlations for the thermal noise and CSL noise terms (3.52)(2.151) we arrive at the noise power spectrum for the position [97]

$$S_{\mathbf{x}}(\omega) = \frac{\hbar}{2m\omega_0} \frac{2m\gamma_m k_B T (\hbar\omega_0)^{-1} + \frac{\lambda\alpha}{r_c^2}\hbar(m\omega_0)^{-1}}{(\omega - \omega_0)^2 + \gamma_m^2/4} \tag{3.59}$$

The relation of the spectral density of momentum is given by $S_{\mathbf{p}}(\omega) = m^2\omega^2 S_{\mathbf{x}}(\omega)$. We can calculate the energy increase due to collapse models to be

$$\langle\langle H \rangle\rangle = k_B T + \frac{\hbar\lambda\alpha}{2r_c^2 m\gamma_m} \tag{3.60}$$

which equivalently can be written as a temperature increase compared to the expected temperature due to thermal noise

$$\Delta T_C = \frac{\hbar Q \lambda\alpha}{2k_B r_c^2 m\omega_0} \tag{3.61}$$

where we introduced the quality factor $Q = \frac{\omega_0}{\gamma_m}$. We can see from this result that using harmonic oscillator systems can in principle be used to test the stochastic aspect of collapse models if it is possible to determine the equilibrium temperature of the oscillator and compare it with its environment temperature. From (3.61) we can see that the damping γ_m should be kept as small as possible in order to enhance the effect of the collapse model. The mass dependence is not immediately obvious in this relation and depends on the factor α which in turn depends on the geometry of the system. To get a better understanding of α let us consider some simple geometry, a cube, as was done in [72]. For calculating α we need to define $\tilde{\rho}(\mathbf{k})$ which is the fourier transform of $\rho(\mathbf{x})$. For a cube of volume $V = a^3$ the density distribution is comprised of step functions in the x,y and z direction which fourier transforms to functions of the form $\mathrm{sinc}(x) = \sin(x)/x$. This gives the fourier transformed density distribution

$$\tilde{\rho}(\mathbf{k}) = \frac{m}{V}\Pi_{i=1}^3 \mathrm{sinc}\left(\frac{ak_i}{2}\right) \tag{3.62}$$

which we directly put into (3.49) to obtain

$$\alpha(a) = \left(\frac{\rho}{m_0}\right)^2 32 r_c^6 \left(e^{-\frac{a^2}{4r_c^2}} - 1 + \frac{\sqrt{\pi}a}{2r_c}\mathrm{Erf}\left(\frac{a}{2r_c}\right)\right)^2 \left(1 - e^{-\frac{a^2}{4r_c^2}}\right)$$
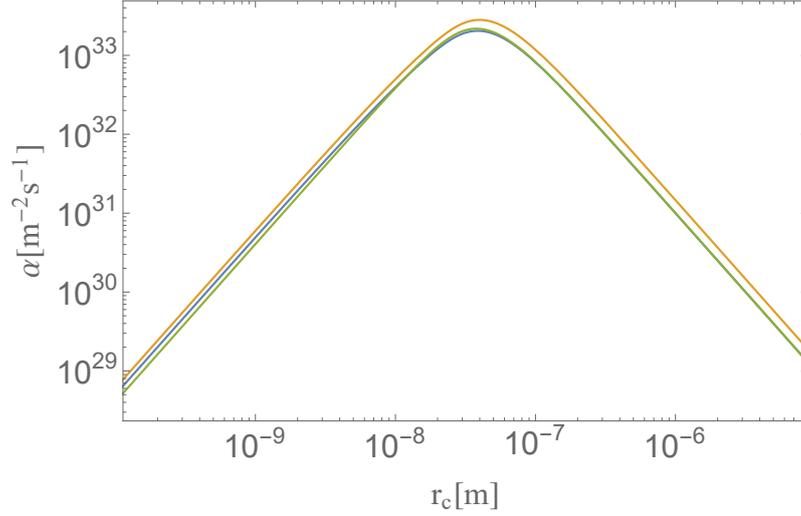
Figure 3.3: Different geometries of test masses with the same density ($\rho = 7430 kg m^{-3}$) and mass ($m = 7.43 \cdot 10^{-18} kg$). Cube (blue), disc with same diameter to height ratio 1:1 (yellow) and sphere (green).

$$ \tag{3.63} $$

or in the limit $a \gg r_c$

$$ \alpha(a) \approx \frac{8\pi\rho^2 r_c^4}{m_0^2} a^2 \tag{3.64} $$

This scales with a^2 and therefore $\alpha \propto m^{2/3}$ for a fixed density. In comparison, in the limit of $a \ll r_c$ the geometry factor α scales as

$$ \alpha(a) \approx \frac{m^2}{2m_0^2} \tag{3.65} $$

Interestingly, this implies that it is not optimal to just increase the mass of the system, since the overall increase of temperature due to CSL heating scales with $\Delta T_C \propto m^{-1/3}$ in this limit. Indeed, it is optimal to design the test mass on the same scale as the parameter r_c to test. As can be seen in [72] even for different geometries, like spheres, cylinders or thin membranes, the overall temperature increase is at best constant with increased mass.

3.6   EXPERIMENTS TESTING HEATING DUE TO COLLAPSE MODELS

3.6.1   *Bulk heating of cantilevers*

Proposals for testing the heating in oscillator systems have been put forward by multiple groups [11, 72]. One of the first papers [96, 97]
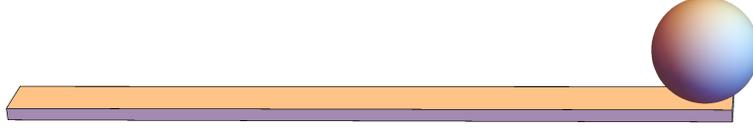
Figure 3.4: Cantilever with attached microsphere. The cantilever has dimensions $(l_x, l_y, l_z) = (100\mu m, 5\mu m, 0.1\mu m)$ and the sphere has diameter $d = 4.5\mu m$. The sphere is made of a neodymium-iron-boron alloy with density $\rho = 7430kg/m^3$. The cantilever is made of silicon with density $\rho = 2330kg/m^3$.

proposes a simple cantilever system, made of a bending cantilever with a microsphere attached to the end.

The microsphere is made of a neodymium-iron-boron alloy with density $\rho = 7430kg/m^3$ and diameter $d = 4.5\mu m$. The cantilever is made of silicon with a density of $\rho = 2330kg/m^3$ and dimensions of $(l_x, l_y, l_z) = (100\mu m, 5\mu m, 0.1\mu m)$ fig:3.4. In the case of a sphere the geometry factor becomes

$$\alpha(d) = \left(\frac{m}{m_0}\right)^2 \left(e^{-\frac{d^2}{4r_c^2}} - 1 + \frac{d^2}{8r_c^2}\left(e^{-\frac{d^2}{4r_c^2}} + 1\right)\right)\frac{384r_c^6}{d^2} \qquad (3.66)$$

which again in the limit $a \gg r_c$ becomes

$$\alpha \approx \frac{4\pi^2\rho^2r_c^4}{3m_0^2}d^2 \qquad (3.67)$$

Since the cantilever density is much smaller than the microsphere density, one can neglect the effect of the cantilever for values of $r_c > 10^{-7}m$ [97]. The resonance frequency of the oscillator is $\omega_0/2\pi = 3084Hz$ with a quality factor of $Q = 3.8 \cdot 10^4$. To detect the effect of heating in this scheme, the center of mass motion of the neodymium microsphere is detected via a SQUID sensor and a superconducting pickup loop. The cantilever is in thermal contact with the surrounding chamber. The chamber is a dilution refrigerator whose temperature range for the experiment is between $T_E = 10mK$ and $T_E = 1K$. The temperature is measured with a resistive thermometer. The power spectrum of the SQUID signal is then used to determine the average energy of the center of mass mode of the microsphere. In order to determine an effect of the collapse onto the heating of the sphere, the relation of the environment temperature to the extracted temperature from the center of mass mode is investigated. According to (3.60) the influence of the CSL model is temperature independent. That implies that in a plot of the two temperature values we should not expect a change in slope but rather a shift of the intersection with the zero value.

The reported value for the CSL heating then is

$$\Delta T_C \leq 2.4 mK \tag{3.68}$$

which corresponds to $\lambda \approx 2 \cdot 10^{-8} s^{-1}$ for $r_c = 10^{-7} m$.

From (3.61) we can see that in order to improve the result, the main steps of such cantilever experiments is to improve the quality factor, while on the other hand keeping the resonance frequency low. We already discussed that increasing the mass of the particle does not increase the effect, if the particle is larger than r_c. This can also be seen in the above graph for the microsphere, where the maximum for λ is reached at $r_c \approx d$.

An updated version of the experiment was proposed in [98] with much higher quality factors. Due to this, they observe a magnetic spring effect coming from their SQUID. This dynamically modifies the quality factor and leads to a modified spectral density of the displacement

$$S_q(\omega) = \left(\frac{\hbar^2 \lambda \alpha}{m^2 r_c^2} + \frac{4\gamma k_B T}{m} \right) \frac{1}{\left(\omega^2 - \omega_0^2 \right)^2 + \frac{\omega^2 \omega_0^2}{Q_a^2}} \tag{3.69}$$

which again shows a temperature independent force contribution arising from the CSL model. The setup is very similar to the above experiment with a cantilever with dimensions $(l_x, l_y, l_z) = (450\mu m, 57\mu m, 2.5\mu m)$ and a microsphere with diameter $d = 31\mu m$ and a density of $\rho = 7430 kg/m^3$. The resonance frequency is $\omega_0/2\pi = 5.136 \cdot 10^4 Hz$. The quality factor has to be inferred from the mechanical quality factor Q_a and is $Q = 6 \cdot 10^5$ at $1K$ and scales with $1/T$ below a temperature of $T \approx 500 mK$ with a maximum of $Q \approx 10^7$ for a temperature of $T \approx 20 mK$. In order to take into account the varying quality factor, the relevant data from the spectral density plots is extracted by plotting T/Q as the x-axis. Again, as can be seen from (3.69) the CSL part neither scales with temperature nor quality factor, such that the offset from zero is indicative for an effect.

Contrary to the first experiment [97], there seems to be an offset present in the data, that can not be contributed to thermomechanical noise. This type of noise would manifest as a saturation of the temperature for the oscillator readout.

So far, these experiments are the only ones for meaningful bounds at low frequencies. But even with high Q factors, the above experiments cannot rule out the parameter regime given by Adler (2.238) and the possible effect seen in the improved experiment was not reproduced in other setups.
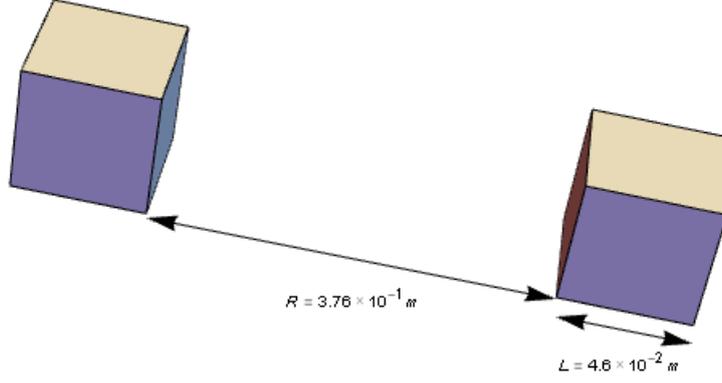
$$R = 3.76 \times 10^{-1} \, m$$

$$L = 4.6 \times 10^{-2} \, m$$

Figure 3.5: The two cubic masses of LISA Pathfinder with distance $R = 3.76 \cdot 10^{-1} m$ and side length $L = 4.6 \cdot 10^{-2} m$.

3.6.2   *Bounds from noise in massive systems*

Another scenario to find possible improvements of the collapse parameters in regimes where $r_c > 10^{-7} m$ can be found in large low noise systems at millikelvin temperatures. Two experiments come to mind, LISA [8] and LIGO [1].

Let us start with bounds from LISA [25, 54]. The configuration of the experiment involves two cubic masses at a distance R fig:3.5.

The cubes have a side length of $L = 4.6 \cdot 10^{-2} m$ and are a distance $R = 3.76 \cdot 10^{-1} m$ apart. They are made of a gold and platin alloy with a mass of $m = 1.928 kg$. In order to describe the decoherence, we write the Lindblad term of the system as (3.47)

$$\mathscr{L}[\rho] = -\frac{1}{2} \sum_{\alpha,\beta} \sum_{i,j} \eta_{ij}^{\alpha,\beta} [\mathbf{x}_{\alpha,i}, [\mathbf{x}_{\beta,j}, \rho]] \tag{3.70}$$

where the **x** coordinates describe the center of mass of the cube and the index α, β goes from 1 to 2 for the two mass distributions respectively. The relevant collapse term incorporates the two mass distributions in analogy to (3.49) with the difference that we have two mass distributions centered a distance R apart.

As before, in order to understand the influence of collapse on the behavior of the dynamics of the system, we rewrite the collapse effect through an effective potential (3.50). We can again write the dynamics of the system through the usual Langevin equations for the individual mass distributions

$$\partial_t \hat{\mathbf{x}}_{\mathbf{ff}} = \frac{\hat{\mathbf{p}}_\alpha}{m} \tag{3.71}$$

$$\partial_t \hat{\mathbf{p}}_\alpha = -m\omega_0^2 \hat{\mathbf{x}}_\alpha + \hbar \frac{dB_t}{dt} \sqrt{\frac{\lambda\alpha}{r_c^2}} - \gamma_m \hat{\mathbf{p}}_\alpha + \chi(t) \tag{3.72}$$

where the noise $\chi(t)$ is uncorrelated. The fourier transform of the collapse force noise though is dependent on the geometry of the system leading to

$$\tilde{F}_\alpha(\omega) = \frac{i\hbar\sqrt{\lambda}r_c^{3/2}}{(4\pi^3)^{3/4}m_0} \int d\mathbf{x}\, \frac{dB_t}{dt} \int d^3k \tilde{\rho}_\alpha(\mathbf{k}) e^{-\frac{r_c^2 k^2}{2} - i\mathbf{k}\mathbf{x}}\mathbf{k} \tag{3.73}$$

with $\frac{dB_t}{dt}$ again a white noise and $\tilde{\rho}_\alpha(\mathbf{k})$ the fourier transform of one of the mass distributions. We therefore get for the correlations of $\tilde{F}_\alpha(\omega)$

$$\langle \tilde{F}_\alpha(\omega)\tilde{F}_\beta(\Omega)\rangle = \frac{2\hbar^2\lambda r_c^3\delta(\omega+\Omega)}{\sqrt{\pi}m_0^2} \int d^3k\, \tilde{\rho}_\alpha(\mathbf{k})\tilde{\rho}_\beta^*(\mathbf{k}) e^{-r_c^2 k^2}k_x^2$$

$$= S_{FF}(\omega)\delta(\omega+\Omega) \tag{3.74}$$

However in the LISA experiment the monitored motion of the system is the relative position of the two masses, such that instead of $\tilde{F}_\alpha(\omega)$ we have to use $\tilde{F}_{rel}(\omega) = \frac{1}{2}\left(\tilde{F}_1(\omega) - \tilde{F}_2(\omega)\right)$. Also, since $\tilde{\rho}_1(\mathbf{k}) = \tilde{\rho}_2(\mathbf{k})$ we get for the force noise spectral density

$$S_{FF}(\omega) = \frac{\hbar^2\lambda r_c^3}{2\pi^{3/2}m_0^2} \int d^3k\, e^{-r_c^2 k^2}|\tilde{\rho}(\mathbf{k})|^2 \left(1 - e^{iRk_x}\right)k_x^2 \tag{3.75}$$

Since LISA's mass distribution is cuboid, we get a similar result as in (3.63) except for a correction term which arises from the term e^{iRk_x} in (3.75).

$$S_{FF}(\omega) =$$
$$\frac{16m^2\hbar^2\lambda}{L^2m_0^2}\left(\frac{r_c}{L}\right)^4 \left(\frac{1}{2}e^{-\frac{(R+L)^2}{4r_c^2}}\left(e^{\frac{RL}{r_c^2}} - 2e^{\frac{L(2R+L)}{4r_c^2}} + 1\right) - e^{-\frac{L^2}{4r_c^2}} + 1\right)$$
$$\left(-\frac{\left(\sqrt{\pi}L\right)\operatorname{Erf}\left(\frac{L}{2r_c}\right)}{2r_c} - e^{-\frac{L^2}{4r_c^2}} + 1\right)^2 \tag{3.76}$$

In the LISA experiment the two cuboid masses are essentially in free fall encapsulated in a spacecraft which is following the motion. In the experiment itself an acceleration noise spectrum is measured which can be directly related to a force noise spectrum. If we now assume that the measured noise in LISA is produced by a collapse
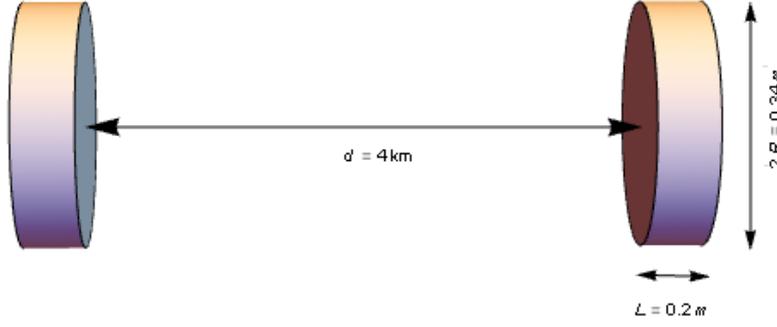
Figure 3.6: The two approximately cylindrical mirror masses of LIGO with distance $d = 4 \cdot 10^3 m$, length $L = 2 \cdot 10^{-1} m$ and a diameter of $2R = 3.4 \cdot 10^{-1} m$.

effect only, we can calculate from (3.76) the relevant parameters λ and r_c. The acceleration noise in the experiment is

$$S_{gg}(\omega) = 2.7 \cdot 10^{-29} m^2 s^{-4} / Hz \tag{3.77}$$

and relates directly to the force noise spectrum $S_{gg}(\omega) = \frac{4}{m^2} S_{FF}(\omega)$.

Another good candidate for a bound on the collapse parameters in the high mass regime is the LIGO [25] interferometer. Here two arms of the interferometer house two massive mirrors each with a mass of $m = 40 kg$. They are approximately the shape of a cylinder with radius $R = 1.7 \cdot 10^{-1} m$ and a length of $L = 2 \cdot 10^{-1} m$. The distance between two mirrors is $d = 4 \cdot 10^3 m$. The measurement here focuses on the relative length change of both arms $\Delta d = |\Delta d_1 - \Delta d_2|$. The induced strain noise of the two arms is related to the relative displacement by $\Delta d = hd$. From this we can see that any displacement noise of the mirrors is directly related to a strain noise measured in the experiment. As seen above, solving the Langevin equations directly gives us an expression for the noise spectral density in position

$$S_{xx}(\omega) = \frac{4}{m^2} \frac{S_{FF}}{(\omega^2 - \omega_0^2)^2 + \omega^2 \gamma^2} \tag{3.78}$$

which for the case of the free mass limit $\omega \gg \omega_0$ reduces to

$$S_{xx}(\omega) = \frac{4}{m^2 \omega^4} S_{FF} = d^2 S_{hh}(\omega) \tag{3.79}$$

relating the strain noise to the corresponding force noise. The inferred strain noise from advanced LIGO is about $S_{hh}(\omega_{opt}) = 10^{-46} Hz^{-1}$ with a corresponding force noise of $S_{FF}(\omega_{opt}) = 9.025 \cdot 10^{-27} N \, Hz^{-1}$ at a frequency of $\omega_{opt} = 180 - 220 Hz$.
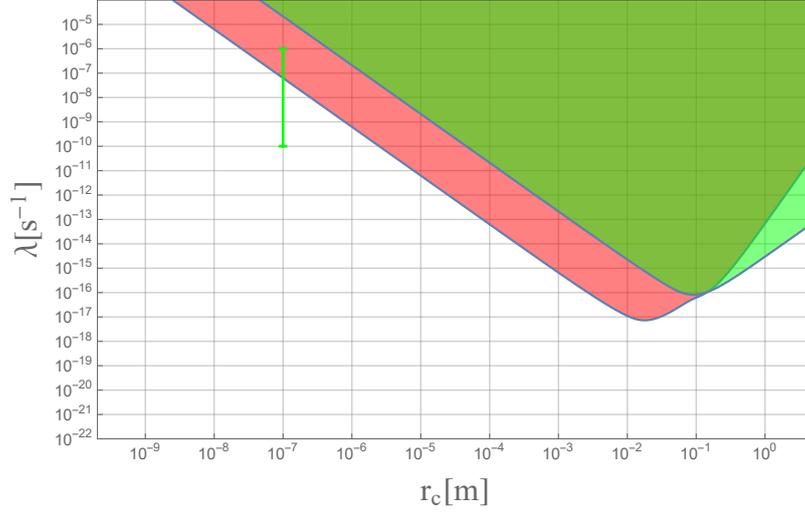
Figure 3.7: Excluded regions for the parameters λ and r_c for LISA (red) and LIGO (green). The smallest value of λ is achieved for r_c close to the size of the mass distribution in the respective experiments. The green line represents the Adler bound.

In order to calculate the effect of the collapse noise, we again use (3.75) this time with the geometry of a cylinder for $\tilde{\rho}(\mathbf{k})$.

$$
S_{FF}(\omega) =
$$
$$
\frac{8\lambda m^2 \hbar^2}{L^2 m_0^2} \left(\frac{r_c}{R}\right)^2 \left(\frac{1}{2} e^{-\frac{(d+L)^2}{4r_c^2}} \left(e^{\frac{dL}{r_c^2}} - 2e^{\frac{L(2d+L)}{4r_c^2}} + 1 \right) - e^{-\frac{L^2}{4r_c^2}} + 1 \right)
$$
$$
\left(1 - e^{-\frac{R^2}{2r_c^2}} \left(I_0\left(\frac{R^2}{2r_c^2}\right) + I_1\left(\frac{R^2}{2r_c^2}\right) \right) \right) \quad (3.80)
$$

The calculated bounds versus the parameter r_c is plotted in fig:3.7

Comparing all the bounds derived so far in fig:3.8 we can see that it is characteristic for center of mass systems to have the lowest possible value for λ for r_c being approximately the size of the tested structure. We will look into possibilities to enhance the effect at length scales different from the characteristic size of the structure in the next sections.
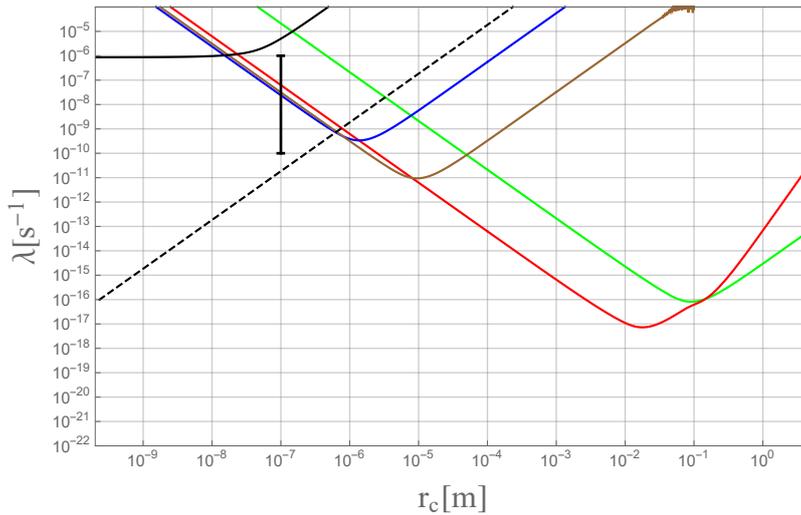
Figure 3.8: Excluded regions for the parameters λ and r_c for LISA (red), LIGO (green), cantilever experiments (brown, blue) and interferometry experiments (black). Also the bound for x-ray emissions of free electrons is included (black, dashed). The Adler bound is marked in black, at $r_c = 10^{-7}$

3.6.3 *Varying the density of the test mass*

A method of enhancing the collapse effect of a given geometry can be seen from the calculations of the effect on LIGO and LISA where multiple masses with some distance between them are considered. One way of manipulating the outcome for the collapse noise can be achieved by considering different densities of the objects. In the case of LIGO and LISA type experiments there wouldn't be much of an effect since the correlations between the different masses decreases rapidly with distances larger than r_c, which leads to quasi independent contributions for individual masses. One might then have the idea to reduce the distance between objects with different densities. Or more compactly, use materials with varying densities in a geometry that allows the same treatment than what was done in the case of LISA or LIGO type experiments. One way to do this was suggested in [24]. The proposed setup is to layer materials with different densities in one direction in order to benefit from correlation terms arising between the different materials.

We have already seen in the last chapter how the langevin equation of a system is related to the collapse effect (3.74)(3.72). If we consider the time evolution of the center of mass from these equations with the total mass $M = \sum m_\alpha$ and the total stochastic force $F = F_\alpha$ we

can again calculate the noise spectral density of the force from the correlation function of the individual noise contributions to get

$$S_{FF}(\omega) = \frac{\hbar^2 \lambda r_c^3}{\pi^{3/2} m_0^2} \int d^3k \sum_{\alpha,\beta} \left(\tilde{\rho}_\alpha(\mathbf{k}) \tilde{\rho}_\beta^*(\mathbf{k}) \right) e^{-r_c^2 k^2} k_x^2 \tag{3.81}$$

for the x direction. As before, additional thermal noise terms are uncorrelated. We are now mostly interested in the contributions of the form $\tilde{\rho}_\alpha(\mathbf{k})\tilde{\rho}_\beta^*(\mathbf{k})$ with $\alpha \neq \beta$. A closer look at the noise spectral density above reveals that correlation terms are negligible for distances $d \gg r_c$ between two mass distributions due to the non-overlap over the collapse length. On the other hand, if one considers $d \ll r_c$ then the exponential factor $e^{-r_c^2 k^2}$ only gives a contribution for $|\mathbf{k}| < \frac{1}{d}$ and suppresses values above, giving a minimal contribution. From these heuristic arguments, one can see that a maximum can be achieved by choosing a layer size in the regime of r_c that one wants to test. If we choose densities that consist of layers in one direction and a total shape of a cuboid we can write the fourier transform of the density as

$$\tilde{\rho}(\mathbf{k}) = \frac{4 \sin\left(\frac{k_x L}{2}\right) \sin\left(\frac{k_y L}{2}\right)}{k_x k_y} \tilde{\rho}_z(\mathbf{k}) \tag{3.82}$$

and the layered contribution

$$\tilde{\rho}_z(\mathbf{k}) = \frac{\rho_a \sin(ak_z(N_l + 1)) + \rho_b \sin(ak_z N_l)}{k_z e^{-ik_z\left(a + \frac{D}{2}\right)} \cos\left(\frac{ak_z}{2}\right)} \tag{3.83}$$

with $D = a(2N_l + 1)$ which contains the total number of layers. Again, we can use our calculation for the geometry of a cuboid for the contribution in the x, y directions to obtain

$$\eta_x \eta_y = \frac{16 \lambda r_c^5}{\pi^{1/2} m_0^2} \left(1 - e^{-\frac{L^2}{4r_c^2}} - \frac{\pi^{1/2} L}{2r_c} \mathrm{Erf}\left(\frac{L}{2r_c}\right) \right)^2 \tag{3.84}$$

and the general expression

$$\eta_z = \int dk_z \, e^{-r_c^2 k^2} k_z^2 |\tilde{\rho}_z(\mathbf{k})|^2 \tag{3.85}$$

for the z direction. This can only be solved analytically for a single layer of constant density. In order to get solutions for layered materials, we need to numerically analyze the above expression. The numerical analysis shows [24] that with choosing the layer thickness, one can select a second local maximum in (3.85) at a chosen r_c. Indeed, if using the parameters of [98] and two materials with densities $\rho_a = 16 \cdot 10^3 kg m^{-3}$ and $\rho_b = 2.2 \cdot 10^3 kg m^{-3}$ as well as a total height of $L = 18 \mu m$ and $N_l = 61$ one can improve the bound for λ at $r_c = 10^{-7} m$ to $\lambda \approx 7 \cdot 10^{-10} s^{-1}$.

3.6.4 *Influence of colored noise on the parameter bounds*

We have now a good idea how different experimental setups influence our ability to test different parameter regimes. So far we only considered the collapse noise to have a white spectrum. However, as seen before, assuming a different kind of noise correlation can be beneficial to address the fact that CSL is not energy conserving. To introduce a different noise correlation [4, 5, 23] we have to start at the definition of the noise in (3.50) where we used $\frac{dB_t}{dt}$ with white noise correlations. This needs to be replaced by a more general form

$$\langle w(\mathbf{x},t), w(\mathbf{y},s)\rangle = \delta^3(\mathbf{x}-\mathbf{y})f(t-s) \tag{3.86}$$

The correlations $f(t-s)$ denote a frequency dependence of the noise. The CSL noise function (3.73) takes the more general form

$$\tilde{F}_\alpha(\omega) = \frac{i\hbar\sqrt{\lambda}r_c^{3/2}}{(4\pi^3)^{3/4}m_0}\int d\mathbf{x}\,\tilde{w}(\mathbf{x},\omega)\int d^3k\tilde{\rho}_\alpha(\mathbf{k})e^{-\frac{r_c^2k^2}{2}-i\mathbf{k}\mathbf{x}}\mathbf{k} \tag{3.87}$$

with the fourier transform of the colored noise $\tilde{w}(\mathbf{x},\omega)$. Analogous to the calculation above, we can derive the force noise spectrum to be

$$S_{FF}(\omega) = \frac{\hbar^2\lambda r_c^3}{(4\pi)^{3/2}m_0^2}\tilde{f}(\omega)\int d^3k\,e^{-r_c^2k^2}k_x^2|\tilde{\rho}_\alpha(\mathbf{k})|^2 \tag{3.88}$$

with the fourier transform of the colored noise correlations $\tilde{f}(\omega)$. This convenient expression is identical to the white noise case, except for the correlation function. If we assume that $f(t-s)$ is exponentially decaying for a cutoff at a correlation time τ we can write

$$f(t-s) = \frac{1}{\tau}e^{-\frac{|t-s|}{\tau}} \tag{3.89}$$

where for $\tau \to 0$ we recover the white noise correlations. The fourier transform of this function is

$$\tilde{f}(\omega) = \frac{\omega_\tau^2}{\omega_\tau^2+\omega^2} \tag{3.90}$$

with $\omega_\tau = \frac{1}{\tau}$.

The correct choice (if any) of frequency ω_τ is unknown so far and can only be inferred from possible experiments that detect a collapse effect in a certain frequency regime. However, if there is a noise field responsible for collapse, it can be assumed to have a cosmological origin. If that is the case, then looking at cutoff frequencies related to cosmological phenomena might give a clue on where the cutoff
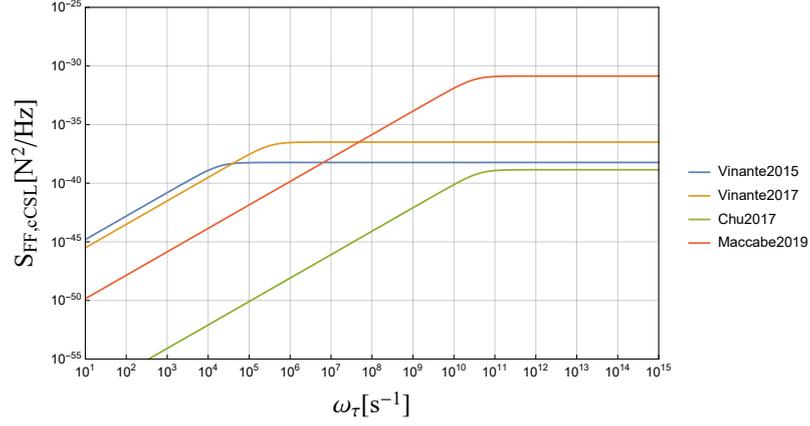
Figure 3.9: Comparison of induced force noise due to cCSL collapse and its dependence on the cutoff frequency ω_τ. Cantilever experiments [97, 98] (Blue, Orange) do not get affected until cutoff frequencies of $\omega_\tau \leq 10^5 Hz$. If one takes into account high frequency experiments (analysis of [27] in green, analysis of waveguide experiments [67] in red), the cutoff becomes relevant for these experiments at $\omega_\tau \leq 10^{11} Hz$ which corresponds to a cutoff characteristic for cosmological phenomena.

could happen. If we assume, for example, that the cosmic background radiation constitutes a reasonable cutoff, we would get a cutoff value of the order of $\omega_\tau \approx 10^{12} s^{-1}$. This would already rule out bounds from X-ray experiments, since the relevant frequencies there are of the order of $\omega_X \approx 10^{19} s^{-1}$, but would allow cantilever experiments to still test a possible collapse heating effect. Potentially, the cutoff could also be at higher frequencies, associated with other cosmological phenomena, like WHIM (warm-hot intergalactic medium). But as mentioned before, only experimental data could give a conclusive answer to this question. A comparison of different collapse experiments and their dependence on the cutoff frequencies can be found in fig:3.9.

3.6.5 *Dissipative collapse models*

As we introduced in the previous chapters, another way of refor-
mulating collapse models with energy conservation, is to introduce
dissipation into the model [75, 90]. We already showed the emerging
Lindblad equation (2.231) and the corresponding Lindblad operator
(2.230)

$$
\mathbb{L}(\mathbf{Q}, \mathbf{P}) = \frac{m}{(2\pi\hbar)^3} \int d\mathbf{Q} e^{-\frac{i}{\hbar}\mathbf{Q}\cdot\mathbf{x}} e^{-\frac{r_c^2}{\hbar^2}\left(|(1+k)^2\mathbf{Q}+2k\mathbf{P}|^2\right)}
\tag{3.91}
$$

In order to describe experiments under the influence of this dissipa-
tive collapse, we need to find an effective linear stochastic description
of the time evolution in order to incorporate it into langevin equations
of the system. Similar to the white noise case, we will compare the
expression to the linear stochastic equation that reproduces the Lind-
blad form of the master equation of the dissipative model. A general
form of such a linear stochastic equation is

$$
d\ket{\phi} = \left\{ -\frac{i}{\hbar} H dt + dC + \frac{1}{2}\left\langle dC^\dagger dC \right\rangle \right\} \ket{\phi}
\tag{3.92}
$$

with an operator C defined as

$$
C = \left(\frac{\lambda r_c^3}{(4\pi)^{3/2} m_0^2} \right)^{1/2} \int d^3x \left(\mathbb{L}(\mathbf{x}) B_t + \mathbb{L}^\dagger(\mathbf{x}) B_t \right)
\tag{3.93}
$$

with B_t our usual white noise. Following the calculation from [75],
we can find an effective master equation for the center of mass, which
reads

$$
\partial_t \rho = -\frac{i}{\hbar}[H, \rho] - \eta[\hat{x}, [\hat{x}, \rho]] - \frac{\gamma_{CSL}^2}{16\eta\hbar^2}[\hat{p}, [\hat{p}, \rho]] - \frac{i\gamma_{CSL}}{2\hbar}[\hat{x}, \{\hat{p}, \rho\}]
\tag{3.94}
$$

with

$$
\eta = \frac{\lambda r_c^3}{2(4\pi)^{3/2}\hbar^5 m_0^2} \int dQ\, |\tilde{\mu}(\mathbf{Q})|^2 e^{-\frac{r_c^2(1+k)^2}{\hbar^2}\mathbf{Q}^2} Q_x^2
\tag{3.95}
$$

and

$$
\gamma_{CSL} = \eta \frac{8r_c^2(1+k)}{N}
\tag{3.96}
$$

where N is the number of particles of the mass. The structure above reveals decoherence both in position and momentum as well as an additional dissipation term. We can also write the state vector equation

$$
d \ket{\phi} = \left\{ -\frac{i}{\hbar} \left(H + \frac{\gamma_{CSL}}{4} \{\hat{x}, \hat{p}\} \right) dt + \left(\hat{x} + i\frac{\gamma_{CSL}}{4\eta\hbar} \hat{p} \right) dB_t^\dagger \right.
$$
$$
\left. - \left(\hat{x} - i\frac{\gamma_{CSL}}{4\eta\hbar} \hat{p} \right) dB_t - \eta \left(\hat{x}^2 + \left(\frac{\gamma_{CSL}}{4\eta\hbar} \right)^2 \hat{p}^2 \right) dt \right\} \ket{\phi} \quad (3.97)
$$

and extract the langevin equation for the operators in the Heisenberg picture. If we use our standard model for a harmonic oscillator (3.51) we can write down the explicit equations

$$
\partial_t \hat{\mathbf{x}} = \frac{\hat{\mathbf{P}}}{m} - \frac{\gamma_{CSL}}{4\eta} \left(\left(\frac{dB_t}{dt} \right)^\dagger + \frac{dB_t}{dt} \right) \quad (3.98)
$$

$$
\partial_t \hat{\mathbf{p}}_\alpha = -m\omega_0^2 \hat{\mathbf{x}}_\alpha - i\hbar \left(\left(\frac{dB_t}{dt} \right)^\dagger - \frac{dB_t}{dt} \right) - (\gamma_m + \gamma_{CSL})\hat{\mathbf{p}}_\alpha + \chi(t) \quad (3.99)
$$

contributing decoherence in position and momentum as well as damping. We again calculate the noise spectral density from these equations to get

$$
S_x(\omega) = \frac{1}{m^2} \frac{2m\gamma_m k_B T + 2\hbar^2 \eta (1 + \frac{\gamma_{CSL}}{4\eta\hbar} m^2(\gamma^2 + \omega^2))}{(\omega_0^2 - \omega^2)^2 + \gamma^2\omega^2} \quad (3.100)
$$

and we can extract the temperature gain of

$$
\Delta T_{CSL} = \frac{\hbar^2 \eta (1 + \frac{\gamma_{CSL}}{4\eta\hbar} m^2(\gamma^2 + \omega_0^2))}{k_B m \gamma} - \frac{\gamma_{CSL}}{\gamma} T \quad (3.101)
$$

One thing to note here is that the above expression, contrary to the standard CSL model can be negative if the environment temperature exceeds the temperature of the dissipative CSL model and one can have a cooling effect. Depending on the characteristic temperature of the dissipative CSL model, we will see a cutoff of the effect. This originates from the diffusion constant η (3.95) which for $(1+k) \approx 1$ reproduces the standard CSL calculations. However, if

$$
T_{CSL} r_c^2 \ll \frac{\hbar^2}{8m_0 k_B} \quad (3.102)
$$

we will expect to see deviations from the standard calculation. If we assume that again the origin of this additional noise is found in cosmological phenomena, we would expect T_{CSL} to be at the order of $T_{CSL} \approx 1K$. So changes to the experimental outcomes would only be expected at $r_c \ll 10^{-9}m$. If one considers the full expression in (3.100) a secondary term also has to be considered, since also the damping is modified. Taking the term from the modified temperature (3.101) in the numerator $\kappa = \hbar^2 \eta (1 + \frac{\gamma_{CSL}}{4\eta\hbar} m^2)$ we can put in the definitions of k and γ_{CSL} to arrive at

$$\kappa = \eta \left(\hbar^2 + \left(\frac{\hbar^2}{8k_B T_{CSL} r_c m_0^{1/2}} \right)^4 \right) \tag{3.103}$$

which becomes only relevant for very low temperatures $T_{CSL} \ll 1K$ or very high frequencies $\omega_0 \geq 10^{14} s^{-1}$ at $T_{CSL} \approx 1K$ (due to the additional term depending on ω (3.101)).

HEATING AND SUPPRESSION OF PHONONS

4.1 GAIN THROUGH HIGH Q AND SNR

In all the above discussed experiments there is one key feature used to improve bounds. The relation (3.61) shows that the effect can be improved by increasing the Q-factor of the system while reducing the resonance frequency of the system. This inevitably leads to either more massive oscillators or one has to use the scaling of layers of different density to probe collapse models at small values for r_c efficiently. However, this does not need to be true if one considers instead of the temperature increase, the mean phonon occupation number. Specifically, we are interested not only in the increase of mean phonon occupation number due to collapse models but also in the signal to noise ratio between the collapse effect and other noise effects, like thermal noise. In the cases, where we are well within the regime of the equipartition theorem $\hbar\omega_0 \ll k_B T$ the ratio of change of phonon number due to CSL and change of phonon number due to thermal effects is

$$SNR = \frac{\lambda\eta(r_c)}{\gamma n_B} = Q\frac{\hbar\lambda\eta(r_c)}{k_B T} \tag{4.1}$$

where we used the phonon number change $\langle m^\dagger m \rangle - n_B = Q\lambda\eta/\gamma$ and that the average phonon number is $n_B \approx k_B T/\hbar\omega_0$. As can be seen from this, increasing the Q-factor enhances the effect as well as a lower temperature. However, since the phonon occupation number follows a plank distribution in general $n_B = (e^{\hbar\omega_0/k_B T} - 1)^{-1}$ the SNR changes in the regime where $\hbar\omega_0 \gtrsim k_B T$ to an exponential dependence $n_B \approx e^{-\hbar\omega_0/k_B T}$ giving

$$SNR = \frac{\lambda\eta(r_c)}{\gamma n_B} = Q\frac{\lambda\eta(r_c)}{\omega_0 e^{-\hbar\omega_0/k_B T}} \tag{4.2}$$

where we keep an improvement due to higher Q-factors but also get an exponential increase with frequency. This can also be seen as a reason for the strict bound arising from X-ray emissions where the effective signal for collapse is largely enhanced. This effect is only suppressed in modifications of CSL like adding colored noise or dissipation. However, as discussed above, this cutoff is typically assumed to have a cosmological origin, which puts this cutoff at about $\omega_{cutoff} \gtrsim 10^{11} Hz$. For sufficient cooling of the setup it is thus possible to reach the regime of enhanced SNR for frequencies below the cutoff.

For example, integrated cantilever experiments operate at frequencies of about $\omega/2\pi \approx 5 \cdot 10^9 Hz$, at cryogenic temperatures of $T \approx 20mK$ which is in the regime of $\hbar\omega_0 \gtrsim k_B T$.

Another aspect, beneficial for high frequency experiments is a potentially higher Q-factor, since the main contributor to damping for high frequency oscillators at cryogenic temperature is clamping losses. At the characteristic size of gigahertz structures, a new technique to reduce damping, phononic shields, can be applied. These devices become small enough at these frequencies to be directly integrated onto the structure and can be made of the same material. The design goal of phononic shields is to create an effective band gap at the resonance frequency of the oscillator. This prohibits excitation to propagate out of the resonator, effectively isolating it from the support structure and environment. One might consider to go even smaller, though at smaller sizes, which could reach resonance frequencies of $\omega \approx 10^{10} Hz$, the structure size becomes too small for the manufacturing methods available.

4.2 BREATHING MODE CALCULATION

The above experiments discussed in Chapter 2 all use center of mass motion of their test masses to infer a change in temperature behavior of the harmonic motion. However, the heating originating from the stochastic influence of the collapse model should also be visible in the behavior of non-center of mass modes and their phonon number. Such a change of occupation number on average can also be used as a test bed for collapse models.

In order to describe such an effect, we have to revisit the calculation of the geometry factor η and its relation to density fluctuations. Similar to the approach to consider different densities in one structure to enhance the collapse effect for different length scales, we can also see a relative motion of atoms in a lattice as density fluctuations of the test object. Let us see, how we can incorporate this effect into the existing model.

We start out at the general form

$$\frac{d}{dt}\rho = -\frac{i}{\hbar}\left[\rho, H\right] - \gamma \int d^3x \left[M(\mathbf{x}), \left[M(\mathbf{x}), \rho\right]\right] \tag{4.3}$$

introduced earlier for the master equation with mass operator

$$M(\mathbf{r}) = \frac{1}{\sqrt{2\pi r_c^2}} \sum_i \frac{m_i}{m_0} e^{-(\mathbf{x}-\mathbf{x_i})^2/2r_c^2} \tag{4.4}$$

To understand the additional term in context of mode displacement, we need to introduce the canonical evolution of the system under investigation. In a harmonic oscillator system the position of one atom in the lattice x_i can be decomposed into its equilibrium position $x_{i,0}$ and a displacement term δx_i. This displacement term can be written in terms of a normal mode decomposition with modes j, giving

$$\delta \hat{\mathbf{x}}_i = \sum_j x_{\mathrm{zpf},j}\, \hat{q}_j\, \mathbf{d}_j(\mathbf{x}_{i,0}) \tag{4.5}$$

with $x_{\mathrm{zpf},j} = (\hbar/2m_{\mathrm{eff},j}\Omega_j)^{1/2}$ the zero point fluctuation, the mode operator $\hat{q}_j$ of the j-th mode and a unitless displacement field $\mathbf{d}_j(\mathbf{x}_{i,0})$ which is normalized to one. This definition allows us to write the effective free Hamiltonian of the operators $\hat{q}_j$, $\hat{p}_j$ as

$$H_{eff} = \frac{1}{2} \sum_j \hbar\Omega_j \left(\hat{q}_j^2 + \hat{p}_j^2\right) \tag{4.6}$$

with mode frequencies Ω_j. If we assume a thermal bath interacting with our phonon modes, and use a viscous damping model we can write the master equation for a single mode j as

$$\frac{d\rho}{dt} = -\frac{i\Omega_j}{2}\left[\hat{q}_j^2 + \hat{p}_j^2, \rho\right] - \frac{i\gamma_j}{2}\left[\hat{q}_j, \{\hat{p}_j, \rho\}\right] - \frac{\gamma_j\left(2n_{\mathrm{B},j} + 1\right)}{2}\left[\hat{q}_j, \left[\hat{q}_j, \rho\right]\right]$$
(4.7)

with γ_j describing the damping of the system due to the thermal bath and n_B is the mean phonon occupation number. This approach is well justified for measurements of single mode mechanical power measurements.

We now want to look for a mode description of our collapse influence on the master equation. We rewrite (4.4) as its fourier transform

$$M(\mathbf{x}) = \frac{r_c^3}{(2\pi)^{3/2}m_0}\int d^3k\, e^{-\frac{r_c^2 k^2}{2}}e^{i\mathbf{k}\cdot\mathbf{x}}\sum_i m_i e^{-i\mathbf{k}\cdot\mathbf{x}_i}$$
(4.8)

and get for our Lindblad term

$$\mathscr{L}_{CSL} = -\frac{(4\pi)^{3/2}\lambda r_c^3}{2m_0^2}\sum_{i,j}m_i m_j \int \frac{d^3k}{(2\pi)^3}e^{-r_c^2 k^2}\left[e^{i\mathbf{k}\cdot\mathbf{x}_i}, \left[e^{-i\mathbf{k}\cdot\mathbf{x}_j}, \rho\right]\right]$$
(4.9)

Now in order to incorporate the displacement due to excited modes, we introduce (4.5) into (4.9). The term

$$\sum_i m_i e^{-i\mathbf{k}\cdot\mathbf{x_i}} = \sum_i m_i e^{-i\mathbf{k}\cdot\mathbf{x}_{i,0}}e^{-i\mathbf{k}\cdot x_{\mathrm{zpf}}\hat{q}\,\mathbf{d}(\mathbf{x}_{i,0})}$$
(4.10)

assuming a single mode can be simplified by using $\mu(\mathbf{r}) = \sum_i m_i\delta(\mathbf{r} - \mathbf{x}_{i,0})$ which represents the mass localized at the lattice points.

$$\sum_i m_i e^{i\mathbf{k}\cdot\mathbf{x}_{i,0}}e^{ix_{zpf}\mathbf{k}\cdot\mathbf{d}(\mathbf{x}_{i,0})\,\hat{q}} = \int d^3r\,\mu(\mathbf{r})e^{i\mathbf{k}\cdot\mathbf{r}}e^{ix_{zpf}\mathbf{k}\cdot\mathbf{d}(\mathbf{r})\,\hat{q}}$$
(4.11)

We can now use this result to incorporate it into (4.9) to get

$$\mathscr{L}_{CSL}[\rho] = -\frac{(4\pi)^{3/2}\lambda r_c^3}{2m_0^2}\iint d^3r\,d^3r'\,\mu(\mathbf{r})\mu(\mathbf{r}')$$
$$\int \frac{d^3k}{(2\pi)^3}\,e^{-r_c^2 k^2}e^{i\mathbf{k}\cdot(\mathbf{r}-\mathbf{r}')}\left[e^{ix_{zpf}\mathbf{k}\cdot\mathbf{d}(\mathbf{r})\hat{q}}, \left[e^{-ix_{zpf}\mathbf{k}\cdot\mathbf{d}(\mathbf{r}')\hat{q}}, \rho\right]\right]$$
(4.12)

If we assume small displacements compared to the CSL length r_c we can taylor expand the exponential for small displacement $|\mathbf{k}| \cdot x_{\mathrm{zpf}}^2\langle\hat{q}\rangle/r_c \ll 1$

$$e^{ix_{zpf}\mathbf{k}\cdot\mathbf{d}(\mathbf{r})\hat{q}} = 1 + ix_{zpf}\mathbf{k}\cdot\mathbf{d}(\mathbf{r})\hat{q} + \mathcal{O}(x_{zpf}^2)$$
(4.13)

in terms of the zero point fluctuation x_{zpf} and finally obtain

$$\mathscr{L}_{CSL}[\rho] = -\lambda x_{zpf}^2 \kappa [\hat{q}, [\hat{q}, \rho]] \qquad (4.14)$$

with a new geometry factor

$$\kappa = \frac{(4\pi)^{3/2} r_c^3}{2m_0^2} \int \frac{d^3k}{(2\pi)^3} e^{-r_c^2 k^2} \left| \int d^3r\, e^{i\mathbf{k}\cdot\mathbf{r}} \mathbf{k}\cdot\mathbf{d}(\mathbf{r})\rho(\mathbf{r}) \right|^2 \qquad (4.15)$$

This deviates from the center of mass expression, in that it now contains the mode shape of the single mode j through the displacement function $d(r)$. Most importantly, although the contribution of the absolute value is always positive, the inside sum can also have negative components, similar to the correlation terms for varying densities. In this expression there is no need for a constant displacement $d = const.$ with regards to the mode or the center of mass. However, we can see that for constant displacement over the whole density, we can recover the same expression for the geometry factor as seen in the center of mass calculations. This implies that we have to treat non-COM motions according to the above equation. This is in contrast to the description in [16] where the mode is described as two separate center of mass motions. The addition of the mode shape however leads to a strongly oscillating integrand (with respect to r_c) effectively canceling out most of the contribution to the geometry factor. Explicitly, if we consider a mode with mode shape $\mathbf{d}(\mathbf{r}) = e_z \cdot \cos(k_0 z)$ and calculate the mode shape expression for a rod with radius r_0 and length L

$$\zeta = \int d^3r\, e^{i\mathbf{k}\cdot\mathbf{r}} \mathbf{k}\cdot\mathbf{d}(\mathbf{r})\mu(\mathbf{r})$$
$$= \int_0^{2\pi} d\phi \int_0^{r_0} dr \int_{-L/2}^{L/2} dz\, rk_z \cos(k_z z + k_r r) \cos(k_0 z)\mu_0 \quad (4.16)$$

we arrive at

$$\zeta = 2\pi\mu_0 k_z \left[\frac{sin\left((k_z - k_0)\frac{L}{2}\right)}{k_z - k_0} + \frac{sin\left((k_z + k_0)\frac{L}{2}\right)}{k_z + k_0} \right]$$
$$\left[\frac{1}{2}\left(\frac{\sin\left(\frac{k_r r_0}{2}\right)}{k_r/2} \right)^2 - r_0 \frac{\sin(k_r r_0)}{k_r} \right] \quad (4.17)$$

In this case, we can separate the axial and radial contributions, writing ζ as a composition of two functions $\zeta = 2\pi\mu_0 f_r(k_r, r_0) f_z(k_z, k_0, L)$. If we assume that we have a high frequency acoustic resonance $L \gg \frac{2\pi}{k_0}$ we can simplify the above equation and get the expression for κ to be

$$\kappa(r_c) \approx \frac{(4\pi)^{3/2} r_c^3}{2m_0^2} \frac{\hbar\pi k_0^2 \mu_0}{2\Omega} \frac{L\mu_0}{m_{\text{eff}}} e^{-k_0^2 r_c^2} \cdot \int_0^\infty dk_r k_r f_r^2(k_r, r_0) \qquad (4.18)$$

with m_{eff} the effective mass of our mode and $1/k_0$ the wavelength. We can see that for small wavelength of our acoustic mode, we get an exponential damping from the factor $e^{-k_0^2 r_c^2}$ while the effect itself is independent of the length of the rod L (a scaling of $L \propto m_0$) as long as we have $L \gg \frac{2\pi}{k_0}$. Therefore, any contributions from modes that are strongly oscillating (compared to r_c) become negligible along the base length of the cylinder.

4.3 BULK ACOUSTIC RESONATORS

Another effect of (4.18) is that it is independent of the length of the rod for $L \gg \frac{2\pi}{k_0}$. Surprisingly, this means that an increase in mass of the test mass does not lead to an increase of the collapse effect, in fact it can be detrimental. This can be seen by analyzing the following setup [27] for a bulk acoustic resonator with a given mode shape

$$s_{l,m} = \sin\left(\frac{l\pi z}{h}\right) J_0\left(\frac{2j_{0,m}r}{d}\right) \tag{4.19}$$

with $l = 503, m = 0$ and a frequency for the phonon mode of $\omega/2\pi = 6.65 \cdot 10^9 Hz$ with $Q = 7.1 \cdot 10^5$. The structure is a disc with diameter $d = 10^{-4}m$ and a height of $h = 4.2 \cdot 10^{-4}$. The effective mass of the mode is $m_{eff} = 8.77 \cdot 10^{-12}kg$ compared to its total mass of $m = 1.32 \cdot 10^{-9}kg$. We can directly calculate the effect of collapse heating by using the mode shape $|\mathbf{d}(r,z)| = s_{l,m}$ to get

$$\eta = \frac{(4\pi)^{3/2}\lambda r_c^3}{2m_0^2}\rho^2 x_{zpf}^2 2\pi \int_0^\infty \frac{f(k_z)}{(hk_z - \pi l)^2(hk_z + \pi l)^2} dk_z$$
$$\int_0^\infty e^{-2k^2 r_c^2} \frac{f(k_r)}{(d^2 k^2 - 4(j_{0,1})^2)^2} dk \tag{4.20}$$

with

$$f(k_z) = hk_z \left(4\pi^4 d^2 h^2 k_z^2 l^2 r_0^2 e^{-2k_z^2 r_c^2}\left(-2\cos(k_z z_0)\cos\left(\frac{\pi l z_0}{h}\right)\right.\right.$$
$$+ \cos^2\left(\frac{\pi l z_0}{h}\right) + 1\right)$$
$$\left.\left. + hk_z \sin^2\left(\frac{\pi l z_0}{h}\right) - 2\pi l \sin(k_z z_0)\sin\left(\frac{\pi l z_0}{h}\right)\right)\right) \tag{4.21}$$

$$f(k_r) = \left(d\, k J_1(kr_0) J_0\left(\frac{2r_0 j_{0,1}}{d}\right) - 2j_{0,1} J_0(kr_0) J_1\left(\frac{2r_0 j_{0,1}}{d}\right)\right)^2 \tag{4.22}$$

where J_i denote Bessel function of order i. Similar to the above simplified structure since $l = 503$ we again have the condition $z_0 \gg \frac{2\pi}{k_0}$ diminishing the collapse effect on our geometry factor. To make the notation more transparent, we define $\eta = \lambda x_{zpf}^2 \kappa$ to have κ only depend on the geometry of the probe mass. Evaluating the effect on κ of the mode shape gives a maximum value of $\kappa \approx 2.7 \cdot 10^3$ at $r_c \approx 2 \cdot 10^{-7}m$ fig:4.1.

We now want to extract the bound on the collapse rate λ. The total phonon number compared to the expected phonon number from thermal contributions can be written as

$$\left\langle m^\dagger m \right\rangle = \frac{\gamma n_B + \lambda x_{zpf}^2 \kappa}{\gamma} \tag{4.23}$$
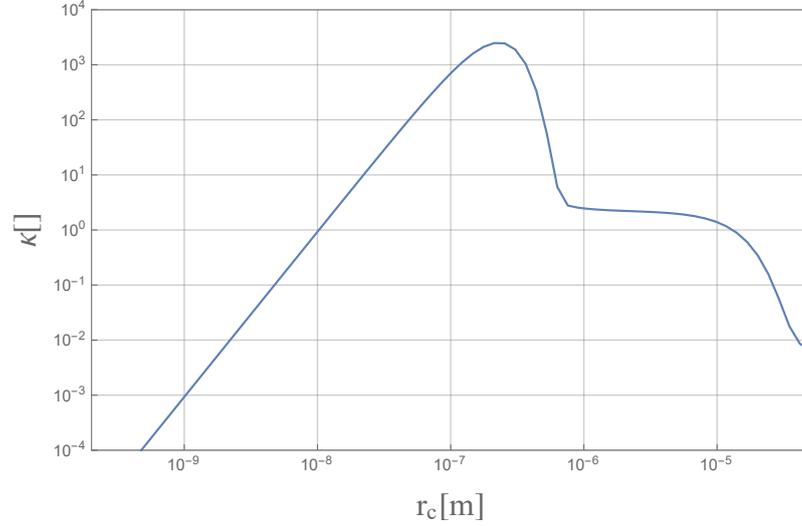
Figure 4.1: The unitless geometry factor κ as a function of the collapse parameter r_c with a maximum at $r_c \approx 2 \cdot 10^{-7} m$ of $\kappa \approx 2.7 \cdot 10^3$.

which immediately leads to

$$n_{add} = \frac{\hbar Q \lambda \kappa}{2 m_{eff} \omega^2} \tag{4.24}$$

where we used $\gamma = \omega / Q$. We can directly express λ as

$$\lambda = \frac{2 n_{add} m_{eff} \omega^2}{\hbar Q \kappa} \tag{4.25}$$

The maximum value for λ at a mean phonon occupation number of $n_{add} = 0.003$ in this setup at $r_c \approx 10^{-7} m$ is $\lambda \approx 0.72 Hz$ fig:4.2, which constitutes a very weak bound. From our theoretical analysis we already expected a diminished effect, since contributions from mode shapes of the type $\mathbf{d}(\mathbf{r}) = e_z \cdot \cos(k_o z)$ scale unfavorably. Another downside here is the relatively low Q-factor which is one of the main compensations for the high frequency regime.
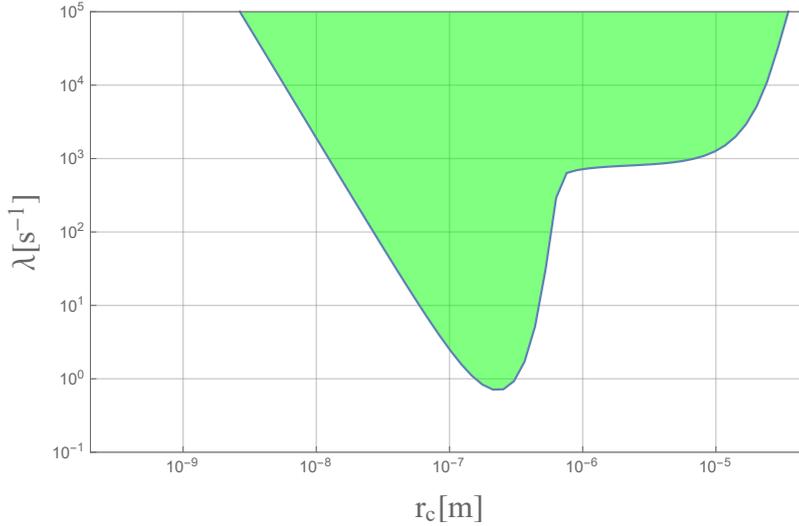
Figure 4.2: The exclusion region for the collapse parameters λ and r_c for the structure in [27]. The exclusion region is rather weak due to dominating anti correlations in the mode shape.

4.4 NEW EXPERIMENT WITH GIGAHERTZ STRUCTURES

Another system worth considering is the experiment described in [67]. An optomechanical crystal is used as a waveguide with optical and mechanical resonances localized on the region. The waveguide is made of silicon and is suspended on an integrated device. It features vertical, oval holes in the middle of the beam modifying the speed of light and sound within fig:4.3. The size of the holes varies over the length of the waveguide, resulting in a localization of the resonances of the optical and mechanical excitation. The mechanical vibration typically leak out of such a resonator configuration due to transforming into an anti-symmetric wave, which is not confined. To circumvent this phenomenon, the waveguide is embedded into an acoustic radiation shield. This acoustic radiation shield itself is a phononic crystal that has a bandgap around the resonance frequency of the waveguide, effectively isolating it from any acoustic environment. The resonator in question has a resonance frequency of $\omega/2\pi = 5.0 \cdot 10^9 Hz$, and an effective mass of $m_{eff} = 6.8 \cdot 10^{-17} kg$. The phonon excitation is induced by a photon with wavelength $\lambda \sim 1550 nm$. The quality factor of this device is a remarkable $Q = 4.9 \cdot 10^{10}$. The mean phonon occupation number is measured by comparing the stokes and anti-stokes scattering rates. If we can achieve an initial phonon occupation number with devices like [67] of $n \leq 10^{-3}$, the described setup becomes competitive for new bounds on collapse models. To get a first estimate, if we take $n = 0.001$ as the phonon number that can be at most attributed to a collapse effect compatible with CSL after measurement time, we can calculate an exclusion region for the parameter space.
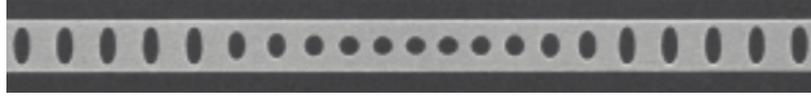
Figure 4.3: Picture of the waveguide. The oval holes are designed to act as a quasi cavity for both the acoustic and optical excitations. The phonon excitation has a resonance frequency of $\omega/2\pi = 5.0 \cdot 10^9 Hz$ with a Q-factor of $4.9 \cdot 10^{10}$.
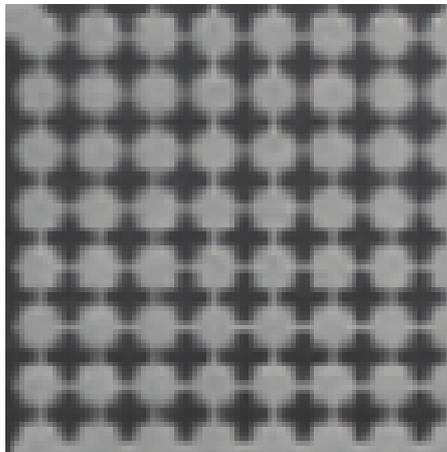
Figure 4.4: Picture of the acoustic shield. The cross structure exhibits an acoustic bandgap of $\Delta f = (6.5 - 3.5) \cdot 10^9 Hz$ centered around the resonance frequency of the waveguide.
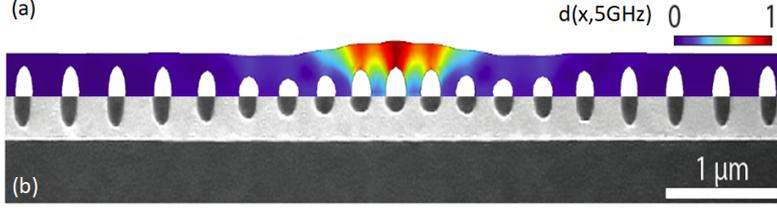
Figure 4.5: The simulated mode shape of the acoustic resonance at $\omega/2\pi = 5.0 \cdot 10^9 Hz$. The mode shape was simulated in COMSOL with a finite element method.

In order to evaluate the effect of CSL noise on the device, we obtain the mode shape through finite element simulation.

Evaluating

$$\xi = \int d^3r \, e^{i\mathbf{k}\cdot\mathbf{r}} \mathbf{k} \cdot \mathbf{d}(\mathbf{r})\rho(\mathbf{r}) \tag{4.26}$$

using the finite element method, as well as calculating the wavenumber integral

$$\int \frac{d^3k}{(2\pi)^3} e^{-r_c^2 k^2} |\xi|^2 \tag{4.27}$$

with the Monte Carlo method, we get the maximum value at $r_c \approx 10^{-7}m$ of $\kappa = 5.73(5) \cdot 10^5$. Compared to the previous experiment analyzed [27], we have an increased κ by two orders of magnitude. This is due to the specific mode shape in this experiment, only having one node in the center of the structure. The diminishing effect of an oscillating mode shape is avoided here. We can use the same calculational steps as before to determine possible bounds for the collapse rate λ. We can see that in this setup we have several relevant parameters improved compared to the previous analysis. The phonon occupation number here is about a factor 3 smaller, the Q-factor is increased by a factor 10^5, the effective mass is lower by another factor 10^5, while κ is also increased by two orders of magnitude. All in all, this amounts to a bound at $r_c \approx 10^{-7}m$ of $\lambda = 1.13 \cdot 10^{-9}Hz$. We did not take into account the induced phonon number from thermal excitations, instead attributed the total phonon number to an effect of CSL, giving a conservative upper bound.

An experimental verification of these initial phonon numbers as well as conclusive bounds are under investigation right now, and might even rule out the regime proposed by Adler to explain latent image formation. The proposed method is also within the validity for colored noise models if one assumes a cutoff at $\omega_\tau \gtrsim 10^{11} Hz$ (fig:3.9).

Using high frequency harmonic oscillators was also used in the proposal [36]. A more complete analysis of possible noise contributions
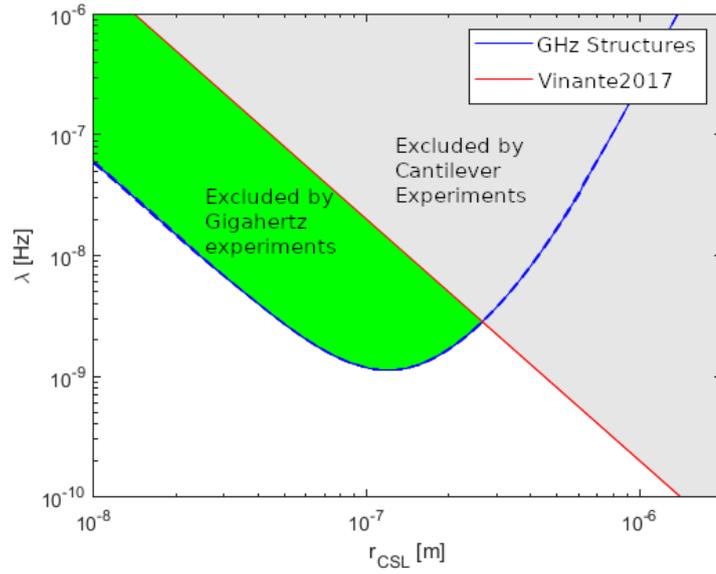
Figure 4.6: Comparison of the bound on the parameters λ and r_c for the experiment presented here (green), compared to the cantilever experiments [97, 98] (gray).
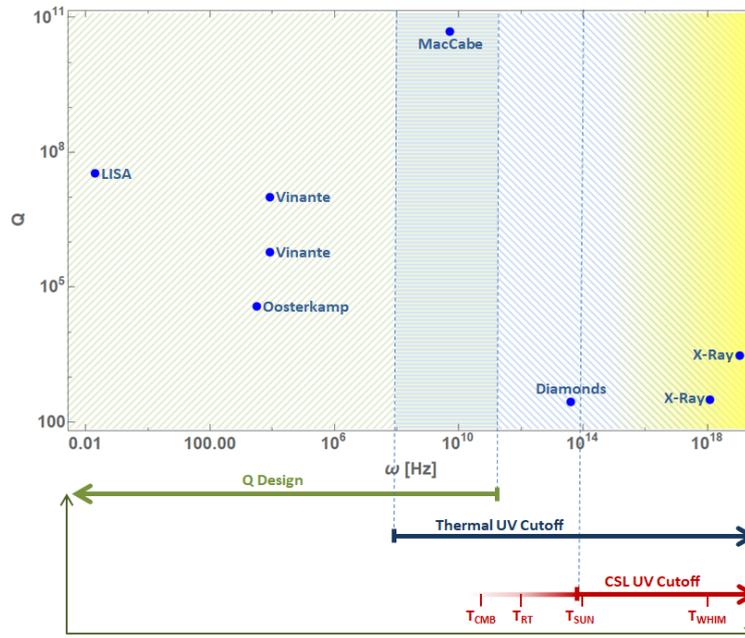
Figure 4.7: Comparison of various experiments with their Q-factors compared to their frequency regime. High quality factors benefit the heating effect of collapse models, while high frequencies enable a higher signal-to-noise ratio. If the proposed CSL UV cutoff is of cosmological origin, it leaves a window of frequencies to exploit. Another limitation is the design of devices, higher frequency devices need smaller manufacturing scales, creating a limitation at frequencies above $\omega \gtrsim 10^{11} Hz$.

was given where, alongside thermal noise, noise contributions due to probe photon leaking, measurement-induced phonons, coincidence dark counts and environmental vibrational noise were considered. The readout process here is done through coincidence counts by downconversion of the signal photon. This is done to reduce dark counts from the detectors. The full calculation of the incidence counts due to CSL can be found in the paper and amount to $R = \lambda \kappa \eta \approx 10^2 \lambda$ with the reduction of efficiency given by $\eta \approx 10^{-3}$. Similar to our above calculation, the sensitivity of such a setup would be competitive to test the Adler bound, since the coincidence counts due to other noise sources are of the order $R \approx 10^{-10}$. However, another issue pointed out in this work is the average signal time due to collapse which is given by $t = (\lambda \kappa \eta)^{-1} \approx 10^9 s$ or roughly ≈ 54 years. In order to reduce measurement time an array of devices could be used. The measurement time would scale inverse linear with the number of devices. At a device number of $N \approx 10^4$ the measurement time required would reduce to $t \approx 10^5 s$ or ≈ 2 days.

The employment of high frequency mechanical oscillators as test bed for collapse models seems to be a very promising avenue. Experiments are closing in on the potential parameter regions in which one would expect collapse models to become relevant. One of the advantages of optomechanical systems like the ones mentioned here is the operation close to a potential frequency cutoff due to colored noise. Contrary to the X-ray experiments [29] who operate in a frequency regime where the cutoff is expected, this approach would probe parameters beyond the Adler bound. In fact, varying the resonance frequencies of the device one could map the potential cutoff region.

CHAMELEON FIELDS AND TORSION PENDULUMS

As previously discussed in the theory section (chapter 2), a new class of scalar fields, chameleon fields, can be introduced to the standard model with unique properties. We discussed the theoretical side of this "screening" mechanism, camouflaging the effective force of these chameleons. However, the screening radius (2.255) becomes smaller and smaller for masses with given density but smaller and smaller radii. This makes chameleon fields and forces subject to test in tabletop experiments. One of the first analyzed setups is the Eöt-Wash experiment described in [55] and used for constraints of the chameleon field in [94, 95]. In this experiment two disks with 42 holes in them are placed parallel to each other. One acts as a torsion pendulum while the other is slowly rotated. Due to gravitational interaction the torsion pendulum disk aligns its holes with the second one, giving a torque that can be compared to the expected newtonian force. Initially, the experiment was devised to test the inverse square law of gravity with high precision. But Upadhye et. al. showed that such experiments can be used to put bounds on the chameleon parameters, thus testing chameleon predictions in tabletop experiments. In a follow up paper [94] the authors argue that the bounds on chameleon forces can be drastically improved in the regime of $\beta = 0.1$ (mass coupling $10^{-1}M_{Pl}$) and $n \geq 2$.

Another set of experiments proposed in [52] uses atom-interferometry to test constraints on the chameleon field. Here the difference in acceleration of the atom travelling through the two arms of the interferometer induces a phase shift. Measuring the interference pattern then allows to put constraints on the chameleon force. One of the challenges for such experiments is to determine the exact chameleon force in the setup. Since only very simple configurations have analytical solutions, numerical analysis becomes necessary. As was demonstrated in [35] a numerical analysis using the Gauss-Seidel method is viable.

We want to apply a similar analysis to a recently published experiment [102], which also uses a torsion pendulum method to measure the gravitational interaction between two small ($r \approx 1mm$) spheres comprising the smallest gravitational source mass in an experiment to date. In order to do so the source mass is mounted on a piezo arm, oscillating at a frequency of $f = 12.7mHz$. The test mass is mounted on a torsion pendulum brought close ($d \approx 2.5mm$ center to center). The readout is done through angular reflection from the pendulum. In order to detect the gravitational interaction, other forces influencing the setup have to be minimized. Specifically, charges on the spheres

could contribute a strong (relative to the gravitational interaction) force. The spheres are therefore discharged as best as possible, as well as separated by a gold coated aluminium membrane of thickness ($\Delta d \approx 150 \mu m$). In order to determine the chameleon contribution on such a setup, all components have to be taken into account.

We first need to define the expected minimum field in a typical experimental setup. In order to get an idea of the expected field at equilibrium in an empty chamber one might be tempted to use (2.248). However, care has to be taken. If the chamber is smaller than the expected Compton wavelength λ_c (2.249), the field will not equilibrate within its confines to the expected minimum. Instead we need to take the approximate chamber radius as new λ_c(e.g. $\lambda_c \approx r_{chamber}$) to get an educated guess for the minimum. The vacuum chamber size on the inside is $13.8cm \times 9cm \times 9cm$. We approximate the radius of the chamber as $r_{chamber} \approx 4.5cm$. Using the relation for the expected ϕ_{min} and the compton wavelength (2.249)

$$\frac{1}{n(n+1)\Lambda^{4+n}}\phi_{bg}^{n+2} \propto r_{chamber}^2 \tag{5.1}$$

$$\phi_{bg} = \xi \left(n(n+1)\Lambda^{4+n}r_{chamber}^2 \right)^{\frac{1}{n+2}} \tag{5.2}$$

we expect a minimum value at $\xi = 0.7 \pm 0.1$ as in [35, 52] giving $\phi_{bg} \approx (0.141 \pm 0.02)eV$. We then know all parameters to calculate the characteristic screening radius for a sphere embedded in ϕ_{min} using (2.255).

As can be seen from fig:5.1, the screening radius drops to zero for spheres of radius below $r_s \simeq 1.2mm$ in this approximation. However, the screening radius r_s is highly dependent on the minimum value of the field and the field geometry within the chamber. Since our geometry within the chamber contains two spheres plus a membrane, we still expect screening. On the other hand, since the sphere size in [102] is approximately $r_s \simeq 1mm$, we expect to see a small enough screening that the additional force might be resolvable.

When considering the full setup, the membrane has to be taken into account. This complicates the calculation for chameleon forces, since purely spherical approximations are not valid anymore. A numerical analysis of the setup is necessary. We will model the chamber in [102] as a cylinder with height $h = 13.8cm$ and diameter $d = 9cm$. This enables us to write the evolution equation as

$$\nabla^2\phi(h,d) = \frac{1}{M}\rho(h,d) - n\Lambda^{4+n}\phi(h,d)^{-(n+1)} \tag{5.3}$$

reducing it to a 2-dimensional problem. We can rescale this equation [81] by using $\phi/\Lambda \to \phi$, $\beta/\Lambda^3 \to \beta$, $\Lambda r \to r$ to arrive at

$$\nabla^2\phi = \frac{1}{M}\rho - n\phi^{-(n+1)} \tag{5.4}$$
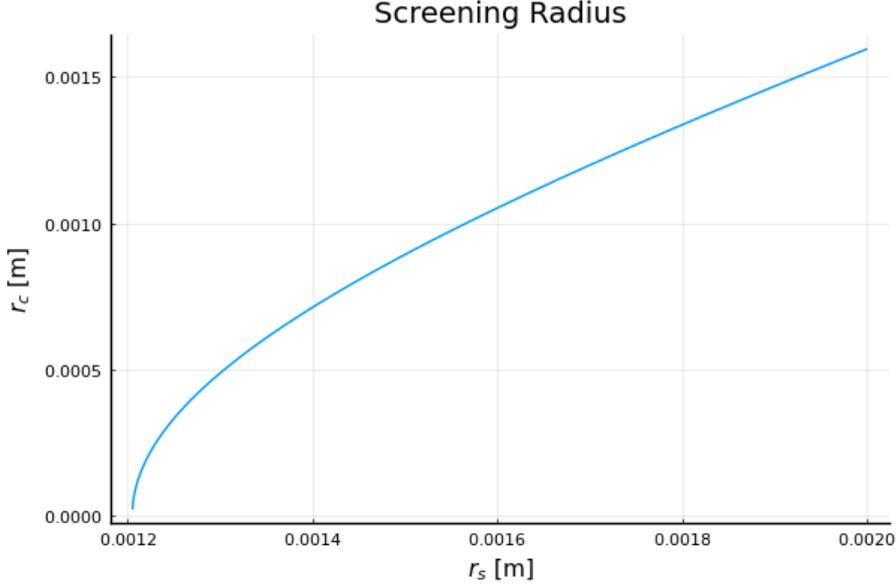
Figure 5.1: Screening radius as a function of sphere radius in a chameleon background ϕ_{bg}. If only one sphere is considered the screening radius is larger than the sphere size $r_s \approx 1mm$.

giving us unitless quantities for the involved parameters. We then use a discretization of the vacuum chamber and the spheres and membrane fig:5.2 for the density distribution in (5.4) where we break up the density into squares totalling #$cells = 1161^2$ initially.

The number of cells is chosen such that the shielding membrane in the middle is represented by one pixel, making the pixel sidelength $\Delta x = 150\mu m$. We use a Gauss-Seidel algorithm to solve for the given geometry. The discretized equation of (5.4) takes the form

$$\phi_{i,j} = w \cdot \left[\frac{1}{4} \left(\phi_{i+1,j} + \phi_{i-1,j} + \phi_{i,j+1} + \phi_{i,j-1} \right) \right.$$

$$\left. - \frac{\Delta x^2}{4} \left(\frac{1}{M} \rho_{i,j} - n\phi_{i,j}^{-(n+1)} \right) \right] + (1 - w) \cdot \phi_{i,j} \quad (5.5)$$

To avoid instabilities in the numerical calculation we use the same approach as in [35] where we introduce a parameter w to tame those instabilities. It turns out that a choice of $w = 0.3$ seems optimal in terms of convergence of the numerical simulation. The initial resolution is not high enough to determine the accelerations on the test mass. After sufficient convergence of the solution we increase the resolution of the density distribution to #$cells = 4644^2$. The increased number of cells gives us enough points per sphere to infer the total acceleration of the test mass. An increase to #$cells = 9288^2$ did not show a meaningful change of the calculated acceleration. We fix the parameters $\Lambda = 2.4 \cdot 10^{-3} eV$ and $n = 1$, as well as $M = M_{Pl}$ ($\beta = 1$).
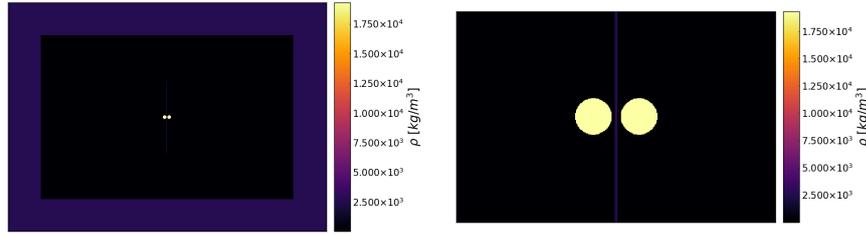
Figure 5.2: Density grid of the vacuum chamber with the two spheres and the thin membrane.

The total acceleration on the test mass is

$$a_h = - \int_{\Omega \in Sphere} \frac{1}{M} \partial_h \phi \, d\Omega \tag{5.6}$$

which is effectively the sum of the contributions of each cell within the test mass.

We first simulate an empty chamber fig:5 to see if our numerical results are matching the expected field strength as calculated with (5.2).

From here we move to the simulation of the setup in [102] with two spheres and a membrane in the middle. The spheres are made of gold with a density of $\rho_s = 19300 kg/m^3$ and at a mean COM distance of $\Delta d = 4.15mm$. The amplitude of the modulation was $\Delta d = 1.65mm$ giving a minimum distance $\Delta d_{min} = 2.5mm$ and a maximum distance $\Delta d_{max} = 5.8mm$. The membrane is made of aluminium with a density of $\rho_m = 2700 kg/m^3$. The distance is modulated through the source mass. In order to know the influence of the chameleon force, we simulate both extreme positions.

The potentials show a background field of $\phi_{bg} \approx 127meV$ with the potential landscape shown in fig:5.4. The screening mechanism is visible in a plot along the center line of the chamber, showing the screening effect more prominently within the sphere towards the center of the chamber (fig:5.5).

In order to extract the acceleration, we use (5.6). The accelerations within the chamber are shown in fig:5.6

Given our numerical simulations we can now give the fifth-force accelerations of the test mass with respect to the two evaluated positions. For the minimum distance $\Delta d = 2.5mm$, the acceleration of the test sphere is $a = 2.224 \cdot 10^{-11} m/s^2$. For the maximum distance we get $a = 1.341 \cdot 10^{-11} m/s^2$. This leaves us with an acceleration difference of $\Delta a = 8.84 \cdot 10^{-12} m/s^2$ (fig:5.7).
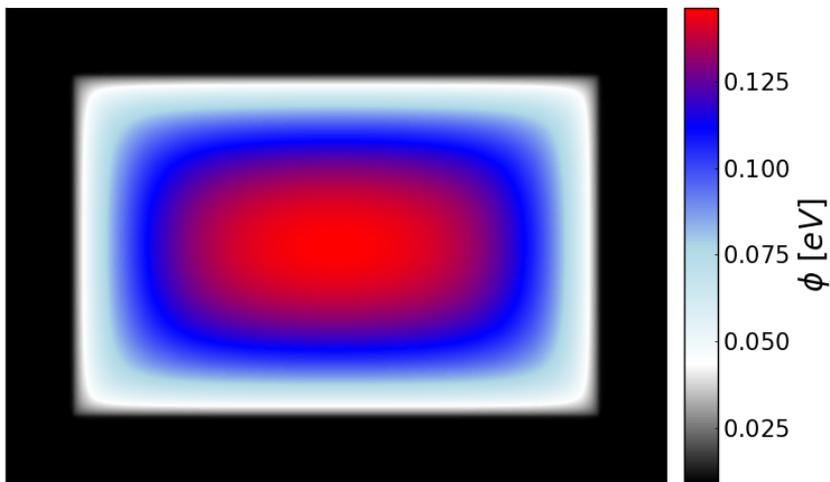
Figure 5.3: Empty chamber side view with $h = 13.8cm$ and $d = 9cm$. The field strength reaches a maximum at $\phi_{bg} = 146meV$, close to the predicted value from (5.2).

(a)

(b)

(c)

(d)
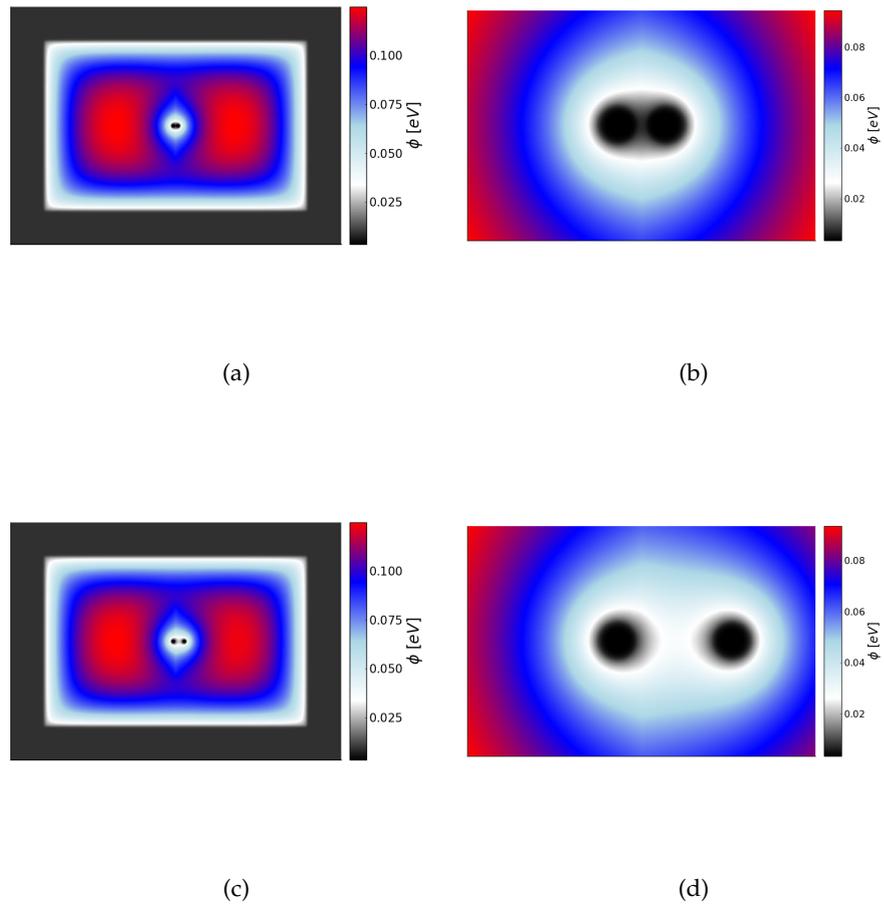
Figure 5.4: The chameleon potential within the vacuum chamber for sphere positions $\Delta d = 2.5mm$ (a),(b) and for sphere positions $\Delta d = 5.8mm$ (c),(d)
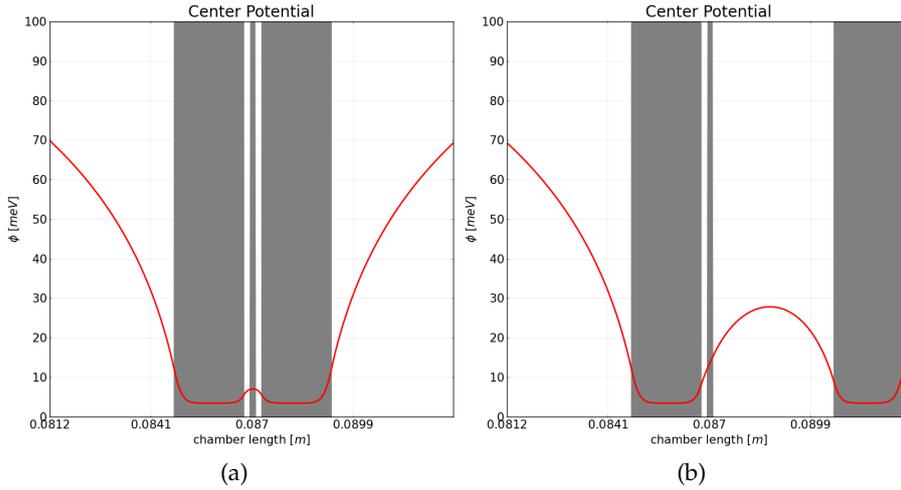
Figure 5.5: Plot of the potential along the centerline of the chamber for distances of the spheres of (a) $\Delta d = 2.5mm$ and (b) $\Delta d = 5.8mm$. The minimum of the potential inside the spheres is reached well before the centerpoint of the spheres, showing the screening effect.
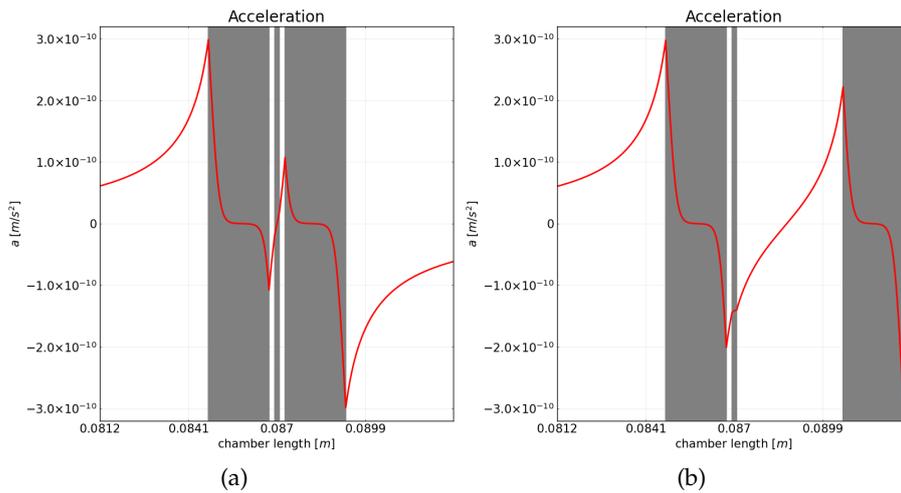
Figure 5.6: Pointwise fifth-force accelerations within the chamber for distances of the spheres of (a) $\Delta d = 2.5mm$ and (b) $\Delta d = 5.8mm$.
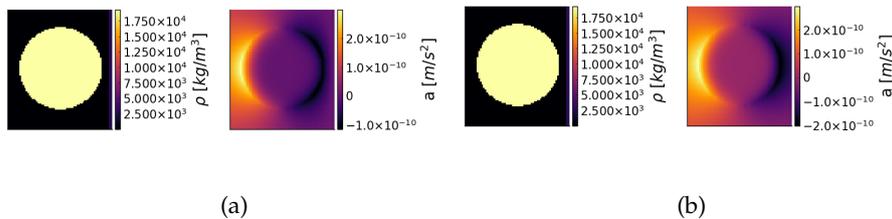
Figure 5.7: The pointwise fifth-force acceleration of the test mass for distances of the spheres of (a) $\Delta d = 2.5mm$ and (b) $\Delta d = 5.8mm$.
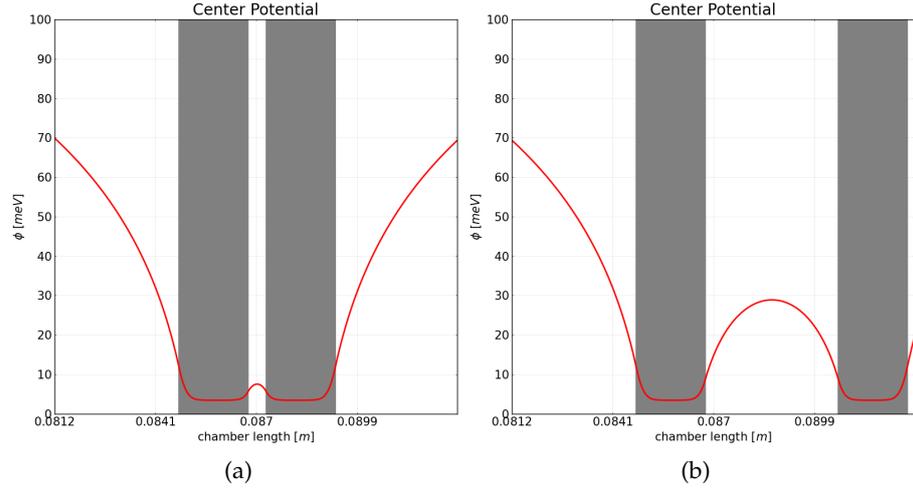
Figure 5.8: Plot of the potential along the centerline of the chamber for distances of the spheres of (a) $\Delta d = 2.5mm$ and (b) $\Delta d = 5.8mm$ without membrane in the middle. The minimum of the potential inside the spheres is reached well before the centerpoint of the spheres, showing the screening effect.

Comparing this result with the precision of measurement in [102] $\Delta a = (3 \cdot 10^{-10} \pm 3 \cdot 10^{-11})m/s^2$ shows that the chameleon effect can not be resolved as of yet, giving a contribution of about $\sim 2.5\%$ of the gravitational acceleration. However, a new iteration of the experiment is in preparation right now, making it feasible to use torsion pendulum experiments such as this to detect possible fifth force accelerations in the near future.

For completeness, we also simulated the same setup without the membrane in the middle for comparison. The results can be found in fig:5.8.

The accelerations without membrane are $a = 2.419 \cdot 10^{-11}m/s^2$, $a = 1.216 \cdot 10^{-11}m/s^2$ for the minimum and maximum distance and the acceleration difference is $\Delta a = 1.203 \cdot 10^{-11}m/s^2$. The influence of the membrane in this setup cannot be neglected, the relative acceleration is reduced by $\sim 26\%$.

In conclusion, torsion pendulum experiments have been shown to be viable test beds for measuring the gravitational force of small objects. Steady development will allow to detect gravity between masses as small as even the Planck mass. In this regime, models like the chameleon scalar field are expected to become comparable in strength to the gravitational interaction. We have demonstrated the feasibility of the above setup for searching for potential fifth forces, which could explain the accelerated expansion of our universe and the elusive origin of dark energy. Future iterations of this experiment will have higher precision and can potentially measure the gravitational

interaction of even smaller masses (down to the Planck mass), giving a greater contribution of the predicted chameleon force.

CONCLUSIONS & OUTLOOK

In this work, we explored novel decoherence phenomena, induced by either the introduction of time dilation, gravitational wave background or modifications of quantum mechanics. Be it gravitational in origin, or due to the attempt to describe a quantum to classical transition, these decoherence signatures could give new insight into the connection of quantum mechanics and general relativity. We characterized multiple different forms of decoherence, being either introduced naturally due to gravitational phenomena or added artificially to accommodate a transition from a microscopic- to a macroscopic/classical description. The gravitational decoherence can be divided into two approaches. Decoherence due to a time dilation of degrees of freedom predicts decoherence of superposition under the influence of a general relativistic action, a novel effect, that can only be attributed to the peculiar properties of general relativistic proper time. This effect is not universal in the sense that it only appears if the superposition has a clock degree of freedom, keeping track of the proper time difference. In the case of massive superpositions in a gravitational field, the effect only manifests if there is a height difference in the superposition perpendicular to the source of gravity. The effect becomes relevant in macroscopic systems, where a superposition of size $\delta x \approx 10^{-3}m$ with gram scale masses produces decoherence times of $\tau \approx 10^{-6}s$. Reaching meaningful decoherence for experiments however seems unfeasible for the moment.

The second approach is to consider the influence of gravitational waves as a stochastic background. The origin of the background is assumed to be gravitational wave sources like binary star systems in our galaxy or beyond. In the low frequency regime, this background takes the form of a gaussian stochastic field, modeled as brownian motion. These stochastic background effects could be measured via sagnac interferometry picking up a phase uncertainty. For space based interferometers the effect is rather small though, making a detection in such systems unlikely in the near future.

Another candidate for additional decoherence effects is modifications of quantum mechanics. One of the most prominent classes of theories here are collapse models, predicting a nonlinear collapse of superpositions to definite position states. This collapse strength is dependent on the mass of the system, leading to an effective quantum to classical transition, suppressing macroscopic superpositions. Since collapse models are phenomenological models, the exact transition is encoded in two free parameters, the collapse rate and collapse length.

In order to enable quantum mechanics in microscopic system, as well as account for classical behavior in macroscopic systems, theoretical bounds on the parameters are given, however there is still a large parameter space to be probed. We analyzed multiple approaches to accomplish this, including interferometry and taking advantage of the stochastic nature of collapse models to infer bounds through an additional heating intrinsic to these models.

We proposed in this work a new way of testing this parameter space with high frequency oscillators, exploiting the phonon occupation of a breathing mode. This is in contrast to previous proposals, only aimed at center of mass degrees of freedom to probe a heating effect. For a low phonon occupation number these new systems become competitive to test collapse models with unprecedented accuracy potentially even ruling out theoretical bounds from Adler to account for latent image formation. Our new approach is also insensitive to a proposed frequency cutoff of cosmological origin due to a colored noise collapse field, as well as avoid dissipative extensions of the model. A possible experimental setup as in [67] could be used to probe this regime in the future to confirm the unitarity of quantum mechanics or to open up a door to new phenomena.

We also developed a numerical algorithm to test arbitrary geometries for possible fifth forces and applied it to an experimental setup used for sensing gravitational forces with a torsion pendulum [102]. Our code allows us to test the strength of the chameleon force corrections and enables us to predict the influence of additional parts, like separating membranes on the force strength. We could show that the corrections to the measured gravitational force might become relevant in future iterations of the experiment.

Part I

APPENDIX

A

SCHRÖDINGER NEWTON SIMULATION

The Mathematica code to simulate the free evolution of a gaussian wave packet with the Schrödinger Newton equation. The initial values can be input through the parameters a, m, NN, TT with a being the width of the gaussian wave packet, m the mass and NN, TT the mesh values in time and position. The initial parameters then get rescaled to allow for a comparison to the value $aa = 5 \cdot 10^{-7} m$. The interval sizes are determined by

$$\Delta r = \frac{a}{200} \tag{A.1}$$

$$\Delta t = \frac{a^2 m}{2TT\hbar} \tag{A.2}$$

The scaling parameter is determined from a as follows

$$\mu = \left(\frac{aa}{a}\right)^{1/3} \tag{A.3}$$

and the rescaled parameters are $\Delta rr = \mu^3 \Delta r, \Delta tt = \mu^5 \Delta t, mm = \mu^{-1} m$. The algorithm uses the Crank-Nicholson method to calculate the time evolution.

```mathematica
ψdisc = Table[
          1
    ──────────────────── , {j, 1, NN}];
          (j Δrr)²
    (π aa²)^(3/4) e^(─────)
                    2 aa²

ψdisc = Developer`ToPackedArray[Transpose@List[ψdisc]];

    (i ℏ) Δtt
β = - ──────────── ;
    (8 mm) Δrr²

    (i π G) mm² Δtt Δrr²
γ = ──────────────────────── ;
              ℏ

spar = SparseArray[

    {Band[{1, 2}] → Developer`ToPackedArray[

        Flatten[{6 β, Table[ β (j + 1)
                             ──────────── , {j, 1, NN - 2}]}]]],
                                 j

        Band[{2, 1}] → Developer`ToPackedArray[Table[ β (j - 1)
                                                      ──────────── , {j, 1, NN - 1}]]]}, NN];
                                                           j

im = Developer`ToPackedArray[Table[i, {i, 1, NN}]];

iimC = Compile[{{nn, _Integer}}, Block[{mm},

    mm = Table[0., {i, 1, nn}, {j, 1, nn}];

    Do[If[i < j - 1, mm[[j, i]] = i²
                                  ────── ;, mm[[j, i]] = i;], {i, 1, nn}, {j, 2, nn}];
                                  j - 1

    mm
    ]];

iim = Developer`ToPackedArray[iimC[NN]];

SN[ψ_] := Block[{absψ, g, trid},

    absψ = Abs[ψ]^2;

    g = ReplacePart[( 1
                      ── - 2 β - γ #1.absψ &)@iim[[1 ;; NN]], {1, 1} → ( 1
                      2                                                  ── - 6 β - γ im.absψ)[[1]]];
                                                                         2

    trid = SparseArray[{i_, i_} ⧴ g[[i, 1]], Length@g] + spar;

    LinearSolve[trid, ψ] - ψ];

out = Block[{n = TT}, Monitor[NestList[(n = n - 1;

        SN[#]) &, ψdisc, TT], n]]; // AbsoluteTiming
```

BIBLIOGRAPHY

[1] BP Abbott et al. "LIGO: the laser interferometer gravitational-wave observatory." In: *Reports on Progress in Physics* 72.7 (2009), p. 076901 (cit. on p. 89).

[2] Benjamin P Abbott et al. "GW170817: observation of gravitational waves from a binary neutron star inspiral." In: *Physical Review Letters* 119.16 (2017), p. 161101 (cit. on p. 18).

[3] Stephen L. Adler. "Lower and Upper Bounds on CSL Parameters from Latent Image Formation and IGM Heating." In: *Journal of Physics A: Mathematical and Theoretical* 40.12 (2006), pp. 2935–2958. ISSN: 1751-8113. DOI: 10 . 1088 / 1751 - 8113 / 40 / 12 / S0310 . 1088 / 1751 - 8121 / 40 / 44 / C01. arXiv: quant - ph/0605072 [quant-ph] (cit. on pp. 59, 61, 79).

[4] Stephen L Adler and Angelo Bassi. "Collapse models with non-white noises." In: *Journal of Physics A: Mathematical and Theoretical* 40.50 (2007), pp. 15083–15098. ISSN: 1751-8113. DOI: 10 . 1088 / 1751 - 8113 / 40 / 50 / 012. URL: http : / / stacks . iop . org / 1751 - 8121 / 40 / i = 50 / a = 012 ? key = crossref . 01d3454a705aa21b365cb7f03fde0dd3 (cit. on pp. 29, 56, 59, 95).

[5] Stephen L Adler and Angelo Bassi. "Collapse models with non-white noises: II. Particle-density coupled noises." In: *Journal of Physics A: Mathematical and Theoretical* 41.39 (2008), p. 395308. ISSN: 1751-8113. DOI: 10.1088/1751-8113/41/39/395308. URL: http://stacks.iop.org/1751-8121/41/i=39/a=395308?key=crossref.a8d3eeb5878e4a636d5731bb906c5dfd (cit. on p. 95).

[6] Stephen L. Adler and Fethi M. Ramazanoğlu. "Photon-emission rate from atomic systems in the CSL model." In: *Journal of Physics A: Mathematical and Theoretical* 40.44 (2007), pp. 13395–13406. ISSN: 1751-8113. DOI: 10.1088/1751-8113/40/44/017 (cit. on pp. 53, 54).

[7] Stephen L. Adler and Andrea Vinante. "Bulk heating effects as tests for collapse models." In: *Physical Review A* 97.5 (2018), p. 052119. ISSN: 2469-9926. DOI: 10.1103/PhysRevA.97.052119. arXiv: 1801.00509 (cit. on pp. 53–57).

[8] Michele Armano et al. "Sub-femto-g free fall for space-based gravitational wave observatories: LISA pathfinder results." In: *Physical review letters* 116.23 (2016), p. 231101 (cit. on p. 89).

[9] Ludwig Arnold. "Stochastic differential equations." In: *New York* (1974) (cit. on p. 39).

[10]   Lorenzo Asprea, Giulio Gasbarri, and Angelo Bassi. "Gravitational decoherence: a general non relativistic model." In: *arXiv* (2019). arXiv: 1905.01121 (cit. on p. 24).

[11]   M. Bahrami et al. "Proposal for a Noninterferometric Test of Collapse Models in Optomechanical Systems." In: *Physical Review Letters* 112.21 (2014), p. 210404. ISSN: 0031-9007. DOI: 10.1103/PhysRevLett.112.210404 (cit. on p. 86).

[12]   Mohammad Bahrami et al. "The Schrödinger–Newton equation and its foundations." In: *New Journal of Physics* 16.11 (2014), p. 115007 (cit. on p. 32).

[13]   Angelo Bassi, Detlef Dürr, and Günter Hinrichs. "Uniqueness of the Equation for Quantum State Vector Collapse." In: *Physical Review Letters* 111.21 (2013), p. 210401. ISSN: 0031-9007. DOI: 10.1103/PhysRevLett.111.210401. arXiv: 1303.4284 (cit. on pp. 34, 42).

[14]   Angelo Bassi and GianCarlo Ghirardi. "Dynamical reduction models." In: *Physics Reports* 379.5-6 (2003), pp. 257–426. ISSN: 0370-1573. DOI: 10.1016/S0370-1573(03)00103-0. arXiv: quant-ph/0302164 [quant-ph] (cit. on pp. 12, 39, 42).

[15]   Angelo Bassi et al. "Models of wave-function collapse, underlying theories, and experimental tests." In: *Reviews of Modern Physics* 85.2 (2013), pp. 471–527. ISSN: 0034-6861. DOI: 10.1103/RevModPhys.85.471. arXiv: 1204.4325 (cit. on pp. 12, 39, 42).

[16]   Sebastiano Belli et al. "Entangling macroscopic diamonds at room temperature: Bounds on the continuous-spontaneous-localization parameters." In: *Physical Review A* 94.1 (2016), p. 012108. ISSN: 2469-9926. DOI: 10.1103/PhysRevA.94.012108 (cit. on p. 105).

[17]   Iwo Bialynicki-Birula and Jerzy Mycielski. "Nonlinear wave mechanics." In: *Annals of Physics* 100.1-2 (1976), pp. 62–93. ISSN: 0003-4916. DOI: 10.1016/0003-4916(76)90057-9. URL: https://www.sciencedirect.com/science/article/pii/0003491676900579?via{\%}3Dihub (cit. on p. 25).

[18]   M. P. Blencowe. "Effective Field Theory Approach to Gravitationally Induced Decoherence." In: *Physical Review Letters* 111.2 (2013), p. 021302. ISSN: 0031-9007. DOI: 10.1103/PhysRevLett.111.021302 (cit. on p. 23).

[19]   Philippe Brax et al. "Detecting Dark Energy in Orbit – the Cosmological Chameleon." In: *Phys.Rev.D70:123518,2004* (Aug. 2004). DOI: 10.1103/PhysRevD.70.123518. arXiv: astro-ph/0408415 [astro-ph] (cit. on p. 63).

[20]   L. De Broglie. "Non-linear Wave Mechanics." In: *Elsevier, Amsterdam* (1960) (cit. on p. 25).

[21] Clare Burrage, Edmund J. Copeland, and E. A. Hinds. "Probing Dark Energy with Atom Interferometry." In: *JCAP 03 (2015) 042* (Aug. 6, 2014). DOI: 10.1088/1475-7516/2015/03/042. arXiv: 1408.1409 [astro-ph.CO] (cit. on pp. 65–67).

[22] P A Bushev et al. "Single electron relativistic clock interferometer." In: *New Journal of Physics* 18.9 (2016), p. 093050. ISSN: 1367-2630. DOI: 10.1088/1367-2630/18/9/093050. URL: http://stacks.iop.org/1367-2630/18/i=9/a=093050?key=crossref.df1621f572cb387c250ad06f8c5803ac (cit. on p. 70).

[23] Matteo Carlesso, Luca Ferialdi, and Angelo Bassi. "Colored collapse models from the non-interferometric perspective." In: *The European Physical Journal D* 72.9 (2018), p. 159 (cit. on p. 95).

[24] Matteo Carlesso, Andrea Vinante, and Angelo Bassi. "Multilayer test masses to enhance the collapse noise." In: (2018). arXiv: 1805.11037 (cit. on pp. 93, 94).

[25] Matteo Carlesso et al. "Experimental bounds on collapse models from gravitational wave detectors." In: *Physical Review D* 94.12 (2016), p. 124036. ISSN: 2470-0010. DOI: 10.1103/PhysRevD.94.124036 (cit. on pp. 89, 91).

[26] Steve Carlip. "Is quantum gravity necessary?" In: *Classical and Quantum Gravity* 25.15 (2008), p. 154010 (cit. on pp. 28, 31).

[27] Yiwen Chu et al. "Quantum acoustics with superconducting qubits." In: *Science (New York, N.Y.)* 358.6360 (2017), pp. 199–202. ISSN: 1095-9203. DOI: 10.1126/science.aao1511. URL: http://www.ncbi.nlm.nih.gov/pubmed/28935771 (cit. on pp. 96, 107, 109, 111).

[28] R Colella, A. W. Overhauser, and SA Werner. "Observation of gravitationally induced quantum interference." In: *Physical Review Letters* 34 (1975), pp. 1472–1474. URL: http://www.atomwave.org/rmparticle/aorefs/aifmrefssortedbytopic/inertialsensingrefs/gravity/COW75neutrongravity.pdf (cit. on pp. 12, 14).

[29] C. Curceanu et al. "Spontaneously Emitted X-rays: An Experimental Signature of the Dynamical Reduction Models." In: *Foundations of Physics* 46.3 (2016), pp. 263–268. ISSN: 0015-9018. DOI: 10.1007/s10701-015-9923-4 (cit. on pp. 81, 113).

[30] Lajos Diosi. "Gravitation and quantum-mechanical localization of macro-objects." In: *Physics Letters A* 105.4 (1984), pp. 199–202. URL: http://www.sciencedirect.com/science/article/pii/0375960184903979 (cit. on p. 29).

[31]   Lajos Diosi. "A universal master equation for the gravitational violation of quantum mechanics." In: *Physics Letters A* 120.8 (1987), pp. 377–381. ISSN: 0375-9601. DOI: 10.1016/0375-9601(87)90681-5. URL: http://adsabs.harvard.edu/abs/1987PhLA..120..377D (cit. on p. 48).

[32]   Lajos Diosi. "Continuous quantum measurement and Ito formalism." In: *Physics Letters A* 129.8-9 (1988), pp. 419–423 (cit. on p. 42).

[33]   Lajos Diosi. "Models for universal reduction of macroscopic quantum fluctuations." In: *Physical Review A* 40.3 (1989), pp. 1165–1174. ISSN: 0556-2791. DOI: 10.1103/PhysRevA.40.1165 (cit. on pp. 42, 48).

[34]   Sandra Eibenberger et al. "Matter–wave interference of particles selected from a molecular library with masses exceeding 10000 amu." In: *Physical Chemistry Chemical Physics* 15.35 (2013), pp. 14696–14700 (cit. on p. 77).

[35]   Benjamin Elder et al. "Chameleon Dark Energy and Atom Interferometry." In: *Phys. Rev. D 94, 044051 (2016)* (Mar. 2016). DOI: 10.1103/PhysRevD.94.044051. arXiv: 1603.06587 [astro-ph.CO] (cit. on pp. 115–117).

[36]   Stefan Forstner et al. "Nanomechanical test of quantum linearity." In: *Optica* 7.10 (2020), p. 1427. ISSN: 2334-2536. DOI: 10.1364/optica.391671. arXiv: 1909.01608 (cit. on p. 111).

[37]   Andor Frenkel. "A Tentative Expression of the Karolyhazy Uncertainty of the Space-Time Structure Through Vacuum Spreads in Quantum Gravity." In: *Foundations of Physics* 32.5 (2002), pp. 751–771. ISSN: 0015-9018. DOI: 10.1023/A:1016057026165 (cit. on p. 44).

[38]   C. C. Gan, C. M. Savage, and S. Z. Scully. "Optomechanical tests of a Schrödinger-Newton equation for gravitational quantum mechanics." In: *Physical Review D* 93.12 (2016), p. 124049. ISSN: 2470-0010. DOI: 10.1103/PhysRevD.93.124049 (cit. on p. 74).

[39]   Crispin Gardiner. *Stochastic methods*. Vol. 4. Springer Berlin, 2009 (cit. on p. 34).

[40]   Stefan Gerlich et al. "Quantum interference of large organic molecules." In: *Nature Communications* 2.1 (2011). ISSN: 2041-1723. DOI: 10.1038/ncomms1263 (cit. on p. 69).

[41]   Gian Carlo Ghirardi, Renata Grassi, and Fabio Benatti. "Describing the macroscopic world: closing the circle within the dynamical reduction program." In: *Foundations of Physics* 25.1 (1995), pp. 5–38 (cit. on p. 59).

[42] GianCarlo Ghirardi, Renata Grassi, and Alberto Rimini. "Continuous-spontaneous-reduction model involving gravity." In: *Physical Review A* 42.3 (1990), pp. 1057–1064. ISSN: 1050-2947. DOI: 10.1103/PhysRevA.42.1057 (cit. on pp. 34, 42, 51, 52, 59).

[43] GianCarlo Ghirardi, A Rimini, and T Weber. "Unified dynamics for microscopic and macroscopic systems." In: *Physical review D: Particles and fields* 34.2 (1986), pp. 470–491. ISSN: 0556-2821. URL: http://www.ncbi.nlm.nih.gov/pubmed/9958098 (cit. on pp. 34, 42, 52, 59).

[44] GianCarlo Ghirardi, Alberto Rimini, and Tobias Weber. *Quantum Probability and Applications II*. Vol. 1136. Lecture Notes in Mathematics. Berlin, Heidelberg: Springer Berlin Heidelberg, 1985. ISBN: 978-3-540-15661-1. DOI: 10.1007/BFb0074453 (cit. on pp. 34, 42).

[45] N. Gisin. "Quantum Measurements and Stochastic Processes." In: *Physical Review Letters* 52.19 (1984), pp. 1657–1660. ISSN: 0031-9007. DOI: 10.1103/PhysRevLett.52.1657 (cit. on pp. 26, 39).

[46] N. Gisin. "Weinberg's non-linear quantum mechanics and supraluminal communications." In: *Physics Letters A* 143.1-2 (1990), pp. 1–2. ISSN: 0375-9601. DOI: 10.1016/0375-9601(90)90786-N. URL: https://www.sciencedirect.com/science/article/pii/037596019090786N?via{\%}3Dihub (cit. on p. 26).

[47] Domenico Giulini and André Großardt. "Gravitationally induced inhibitions of dispersion according to the Schrödinger–Newton equation." In: *Classical and Quantum Gravity* 28.19 (2011), p. 195026. ISSN: 0264-9381. DOI: 10.1088/0264-9381/28/19/195026. arXiv: 1105.1921 (cit. on p. 31).

[48] André Großardt. "Approximations for the free evolution of self-gravitating quantum particles." In: *Physical Review A* 94.2 (2016), p. 022101. ISSN: 2469-9926. DOI: 10.1103/PhysRevA.94.022101. arXiv: 1503.02622 (cit. on p. 29).

[49] André Großardt. "Newtonian self-gravity in trapped quantum systems and experimental tests." In: *Journal of Physics: Conference Series* 880.1 (2017), p. 012019. ISSN: 1742-6588. DOI: 10.1088/1742-6596/880/1/012019. URL: http://stacks.iop.org/1742-6596/880/i=1/a=012019?key=crossref.73bffb19d945d0fe94588e24cfbc1380 (cit. on p. 29).

[50] André Großardt et al. "Effects of Newtonian gravitational self-interaction in harmonically trapped quantum systems." In: *Scientific Reports* 6.1 (2016), p. 30840. ISSN: 2045-2322. DOI: 10.1038/srep30840. URL: http://www.nature.com/articles/srep30840 (cit. on pp. 29, 74).

[51] André Großardt et al. "Optomechanical test of the Schrödinger-Newton equation." In: *Physical Review D* 93.9 (2016), p. 096003. ISSN: 2470-0010. DOI: 10.1103/PhysRevD.93.096003 (cit. on pp. 29, 75).

[52] Paul Hamilton et al. "Atom-interferometry constraints on dark energy." In: *Science, 349, 849-851 (2015)* (Feb. 2015). DOI: 10.1126/science.aaa8883. arXiv: 1502.03888 [physics.atom-ph] (cit. on pp. 115, 116).

[53] Richard Harrison, Irene Moroz, and KP Tod. "A numerical study of the Schrödinger–Newton equations." In: *Nonlinearity* 16.1 (2002), p. 101 (cit. on pp. 29, 30).

[54] Bassam Helou et al. "LISA pathfinder appreciably constrains collapse models." In: *Physical Review D* 95.8 (2017), p. 084054. ISSN: 2470-0010. DOI: 10.1103/PhysRevD.95.084054 (cit. on p. 89).

[55] C. D. Hoyle et al. "Sub-millimeter Tests of the Gravitational Inverse-square Law." In: *Phys.Rev.D70:042004,2004* (May 2004). DOI: 10.1103/PhysRevD.70.042004. arXiv: hep-ph/0405262 [hep-ph] (cit. on p. 115).

[56] Hannes Hübel et al. "High-fidelity transmission of polarization encoded qubits from an entangled source over 100 km of fiber." In: *Optics Express* 15.12 (2007), p. 7853. ISSN: 1094-4087. DOI: 10.1364/oe.15.007853. arXiv: 0801.3620 (cit. on p. 70).

[57] Marc-Thierry Jaekel et al. "Quantum decoherence and gravitational waves." In: *arXiv* (2008), pp. 1–7. arXiv: 0806.2541 (cit. on pp. 18, 20).

[58] Caitlin Jones, Giulio Gasbarri, and Angelo Bassi. "Mass-coupled relativistic spontaneous collapse models." In: *arXiv* (2020). ISSN: 2331-8422. arXiv: 2012.02627 (cit. on p. 62).

[59] Caitlin Jones, Tommaso Guaita, and Angelo Bassi. "On the (im)possibility of extending the GRW model to relativistic particles." In: *arXiv* im (2019). ISSN: 2331-8422. arXiv: 1907.02370 (cit. on p. 62).

[60] F Karolyhazy. "Gravitation and quantum mechanics of macroscopic objects." In: *Il Nuovo Cimento A* 41.1 (1966). DOI: 10.1007/BF02717926 (cit. on p. 44).

[61] F Karolyhazy. "Gravitation and the quantum mechanics of macroscopic bodies." In: *Magyar Fizikai Folyoirat* 22 (1974), pp. 23–85 (cit. on p. 44).

[62] Justin Khoury and Amanda Weltman. "Chameleon Cosmology." In: *Phys.Rev.D69:044026,2004* (Sept. 2003). DOI: 10.1103/PhysRevD.69.044026. arXiv: astro-ph/0309411 [astro-ph] (cit. on p. 63).

[63] Justin Khoury and Amanda Weltman. "Chameleon Fields: Awaiting Surprises for Tests of Gravity in Space." In: *Phys.Rev.Lett.93:171104,2004* (Sept. 2003). DOI: 10 . 1103 / PhysRevLett . 93 . 171104. arXiv: astro - ph / 0309300 [astro-ph] (cit. on pp. 63, 65).

[64] E. Komatsu et al. "FIVE-YEAR WILKINSON MICROWAVE ANISOTROPY PROBE OBSERVATIONS: COSMOLOGICAL INTERPRETATION." In: *The Astrophysical Journal Supplement Series* 180.2 (2009), pp. 330–376. DOI: 10.1088/0067-0049/180/2/330 (cit. on p. 62).

[65] B. Lamine, M.-T. Jaekel, and S. Reynaud. "Gravitational decoherence of atomic interferometers." In: *The European Physical Journal D* 20.2 (2002), pp. 165–176. ISSN: 1434-6060. DOI: 10.1140/epjd/e2002-00126-y (cit. on pp. 18, 21).

[66] D. Larson et al. "SEVEN-YEAR WILKINSON MICROWAVE ANISOTROPY PROBE (WMAP) OBSERVATIONS: POWER SPECTRA AND WMAP -DERIVED PARAMETERS." In: *The Astrophysical Journal Supplement Series* 192.2 (2011), p. 16. DOI: 10.1088/0067-0049/192/2/16 (cit. on p. 62).

[67] Gregory S. MacCabe et al. "Phononic bandgap nano-acoustic cavity with ultralong phonon lifetime." In: (2019). arXiv: 1901.04129 (cit. on pp. 96, 109, 126).

[68] Michele Maggiore. "Gravitational wave experiments and early universe cosmology." In: *Physics Report* 331.6 (2000), pp. 283–367. ISSN: 0370-1573. DOI: 10.1016/S0370-1573(99)00102-7. arXiv: 9909001 [gr-qc] (cit. on p. 19).

[69] Christian Møller et al. "Les théories relativistes de la gravitation." In: *Colloques Internationaux CNRS* 91.1 (1962) (cit. on p. 28).

[70] Irene M Moroz, Roger Penrose, and Paul Tod. "Spherically-symmetric solutions of the Schrödinger-Newton equations." In: *Classical and Quantum Gravity* 15.9 (1998), p. 2733 (cit. on p. 29).

[71] Peter J. Mosley et al. "Heralded generation of ultrafast single photons in pure quantum states." In: *Physical Review Letters* 100.13 (2008), pp. 1–4. ISSN: 0031-9007. DOI: 10 . 1103 / PhysRevLett.100.133601. arXiv: 0711.1054 (cit. on p. 70).

[72] Stefan Nimmrichter, Klaus Hornberger, and Klemens Hammerer. "Optomechanical Sensing of Spontaneous Wave-Function Collapse." In: *Physical Review Letters* 113.2 (2014), p. 020405. ISSN: 0031-9007. DOI: 10.1103/PhysRevLett.113.020405. arXiv: 1405.2868 (cit. on pp. 85, 86).

[73] Stefan Nimmrichter et al. "Concept of an ionizing time-domain matter-wave interferometer." In: *New Journal of Physics* 13.7 (2011), p. 075002 (cit. on p. 77).

[74]   Stefan Nimmrichter et al. "Testing spontaneous localization theories with matter-wave interferometry." In: *Physical Review A - Atomic, Molecular, and Optical Physics* 83.4 (2011), pp. 8–11. ISSN: 1050-2947. DOI: 10.1103/PhysRevA.83.043621. arXiv: 1103.1236 (cit. on p. 79).

[75]   J. Nobakht et al. "Unitary unravelling for the Dissipative Continuous Spontaneous Localization model: application to optomechanical experiments." In: *arXiv* (2018). arXiv: 1808.01143 (cit. on p. 97).

[76]   A. D. O'Connell et al. "Quantum ground state and single-phonon control of a mechanical resonator." In: *Nature* 464.7289 (2010), pp. 697–703. ISSN: 0028-0836. DOI: 10.1038/nature08967. URL: http://www.nature.com/articles/nature08967 (cit. on pp. 76, 77).

[77]   A. W. Overhauser and R. Colella. "Experimental Test of Gravitationally Induced Quantum Interference." In: *Physical Review Letters* 33.20 (1974), pp. 1237–1239. ISSN: 0031-9007. DOI: 10.1103/PhysRevLett.33.1237 (cit. on pp. 13, 69).

[78]   Philip Pearle. "Ways to describe dynamical state-vector reduction." In: *Physical Review A* 48.2 (1993), pp. 913–923. ISSN: 1050-2947. DOI: 10.1103/PhysRevA.48.913 (cit. on p. 56).

[79]   Roger Penrose. "On Gravity's role in Quantum State Reduction." In: *General Relativity and Gravitation* 28.5 (1996), pp. 581–600. ISSN: 0001-7701. DOI: 10.1007/BF02105068 (cit. on pp. 48, 50).

[80]   Roger Penrose. "Quantum computation, entanglement and state reduction." In: *Philosophical Transactions of the Royal Society of London. Series A: Mathematical, Physical and Engineering Sciences* 356.1743 (1998), pp. 1927–1939 (cit. on p. 29).

[81]   Martin Pernot-Borras et al. "Fifth force induced by a chameleon field on nested cylinders." In: vol. 101. 12. American Physical Society (APS), Apr. 17, 2020, p. 124056. DOI: 10.1103/physrevd.101.124056. arXiv: 2004.08403 [gr-qc] (cit. on p. 116).

[82]   Achim Peters, Keng Yeow Chung, and Steven Chu. "Measurement of gravitational acceleration by dropping atoms." In: *Nature* 400.6747 (1999), p. 849 (cit. on p. 14).

[83]   Igor Pikovski et al. "Universal decoherence due to gravitational time dilation." In: *Nature Physics* 11.8 (2015), pp. 668–672. ISSN: 1745-2473. DOI: 10.1038/nphys3366. arXiv: 1311.1095 (cit. on pp. 14, 16, 17).

[84]   Joseph Polchinski. "Weinberg's nonlinear quantum mechanics and the Einstein-Podolsky-Rosen paradox." In: *Physical Review Letters* 66.4 (1991), pp. 397–400. ISSN: 0031-9007. DOI: 10.1103/PhysRevLett.66.397 (cit. on p. 26).

[85] Helmut Rauch, Wolfgang Treimer, and Ulrich Bonse. "Test of a single crystal neutron interferometer." In: *Physics Letters A* 47.5 (1974), pp. 369–371 (cit. on p. 12).

[86] Leon Rosenfeld. "On quantization of fields." In: *Nuclear Physics* 40 (1963), pp. 353–356 (cit. on p. 28).

[87] Ariel G. Sánchez et al. "The clustering of galaxies in the SDSS-III Baryon Oscillation Spectroscopic Survey: cosmological implications of the large-scale two-point correlation function." In: *Monthly Notices of the Royal Astronomical Society* 425.1 (2012), pp. 415–437. DOI: 10.1111/j.1365-2966.2012.21502.x. arXiv: 1203.6616 [astro-ph.CO] (cit. on p. 62).

[88] Maximilian Schlosshauer. *Decoherence and the quantum-to-classical transition. The Frontiers Collection.* Springer, 2007 (cit. on p. 5).

[89] Bernard F Schutz. "Gravitational wave astronomy." In: *Classical and Quantum Gravity* 16.12A (1999), A131 (cit. on p. 18).

[90] Andrea Smirne and Angelo Bassi. "Dissipative Continuous Spontaneous Localization (CSL) model." In: *Scientific Reports* 5.1 (2015), p. 12518. ISSN: 2045-2322. DOI: 10.1038/srep12518. URL: http://www.nature.com/articles/srep12518 (cit. on pp. 57, 97).

[91] Andrea Smirne, Bassano Vacchini, and Angelo Bassi. "Dissipative extension of the Ghirardi-Rimini-Weber model." In: *Physical Review A* 90.6 (2014), p. 062135. ISSN: 1050-2947. DOI: 10.1103/PhysRevA.90.062135 (cit. on p. 57).

[92] N. Suzuki et al. "THEHUBBLE SPACE TELESCOPECLUSTER SUPERNOVA SURVEY. V. IMPROVING THE DARK-ENERGY CONSTRAINTS ABOVEz 1 AND BUILDING AN EARLY-TYPE-HOSTED SUPERNOVA SAMPLE." In: *The Astrophysical Journal* 746.1 (2012), p. 85. DOI: 10.1088/0004-637x/746/1/85 (cit. on p. 62).

[93] Marko Toroš and Angelo Bassi. "Bounds on quantum collapse models from matter-wave interferometry: calculational details." In: *Journal of Physics A: Mathematical and Theoretical* 51.11 (2018), p. 115302. ISSN: 1751-8113. DOI: 10.1088/1751-8121/aaabc6. arXiv: 1601.02931. URL: http://stacks.iop.org/1751-8121/51/i=11/a=115302?key=crossref.c447f7c27c5e6c94ad0f98a8b44d1250 (cit. on pp. 77, 79).

[94] Amol Upadhye. "Dark energy fifth forces in torsion pendulum experiments." In: *Physical Review D* 86.10 (Sept. 2, 2012), p. 102003. DOI: 10.1103/PhysRevD.86.102003. arXiv: 1209.0211 [hep-ph] (cit. on pp. 63, 115).

[95]   Amol Upadhye, Steven S. Gubser, and Justin Khoury. "Unveiling Chameleons in Tests of Gravitational Inverse-Square Law." In: *Phys.Rev. D74 (2006) 104024* (Aug. 2006). DOI: `10.1103/PhysRevD.74.104024`. arXiv: `hep-ph/0608186 [hep-ph]` (cit. on p. 115).

[96]   O. Usenko et al. "A superconducting quantum interference device based read-out of a subattonewton force sensor operating at millikelvin temperatures." In: *Applied Physics Letters* 98.13 (2011), p. 133105. ISSN: 0003-6951. DOI: `10.1063/1.3570628` (cit. on p. 86).

[97]   A. Vinante et al. "Upper Bounds on Spontaneous Wave-Function Collapse Models Using Millikelvin-Cooled Nanocantilevers." In: *Physical Review Letters* 116.9 (2016), p. 090402. ISSN: 0031-9007. DOI: `10.1103/PhysRevLett.116.090402`. arXiv: `1510.05791` (cit. on pp. 85–88, 96, 112).

[98]   A. Vinante et al. "Improved Noninterferometric Test of Collapse Models Using Ultracold Cantilevers." In: *Physical Review Letters* 119.11 (2017), p. 110401. ISSN: 0031-9007. DOI: `10.1103/PhysRevLett.119.110401` (cit. on pp. 88, 94, 96, 112).

[99]   Steven Weinberg. "Photons and gravitons in perturbation theory: Derivation of Maxwell's and Einstein's equations." In: *Physical Review* 138.4B (1965), B988 (cit. on p. 18).

[100] Steven Weinberg. *Gravitation and cosmology: principles and applications of the general theory of relativity*. Vol. 1. Wiley New York, 1972 (cit. on p. 14).

[101] Steven Weinberg. "Testing quantum mechanics." In: *Annals of Physics* 194.2 (1989), pp. 336–386. ISSN: 0003-4916. DOI: `10.1016/0003-4916(89)90276-5`. URL: `https://www.sciencedirect.com/science/article/pii/0003491689902765?via{\%}3Dihub` (cit. on p. 25).

[102] Tobias Westphal et al. "Measurement of Gravitational Coupling between Millimeter-Sized Masses." In: *Nature* 591.7849 (Sept. 2020), pp. 225–228. DOI: `10.1038/s41586-021-03250-7`. arXiv: `2009.09546 [gr-qc]` (cit. on pp. 67, 115, 116, 118, 122, 126).

[103] Huan Yang et al. "Macroscopic Quantum Mechanics in a Classical Spacetime." In: *Physical Review Letters* 110.17 (2013), p. 170401. ISSN: 0031-9007. DOI: `10.1103/PhysRevLett.110.170401` (cit. on pp. 33, 73, 74).

[104] Michael Zawisky et al. "Testing the world's largest monolithic perfect crystal neutron interferometer." In: *Nuclear Instruments and Methods in Physics Research Section A: Accelerators, Spectrometers, Detectors and Associated Equipment* 481.1-3 (2002), pp. 406–413 (cit. on p. 14).

[105] Magdalena Zych et al. "Quantum interferometric visibility as a witness of general relativistic proper time." In: *Nature Communications* 2.1 (2011), p. 505. ISSN: 2041-1723. DOI: 10 . 1038/ncomms1498. URL: http://www.nature.com/articles/ncomms1498 (cit. on p. 14).

[106] Magdalena Zych et al. "General relativistic effects in quantum interference of photons." In: *Classical and Quantum Gravity* 29.22 (2012), p. 224010. ISSN: 0264-9381. DOI: 10 . 1088 / 0264 - 9381 / 29 / 22 / 224010. URL: http : / / stacks . iop . org / 0264 - 9381 / 29 / i = 22 / a = 224010 ? key = crossref . 2f0ce0eae7965ebd6d0ecf12d07a557b (cit. on pp. 14, 69).